

Quantum Annealing With Trigger Hamiltonian

Vrinda Mehta

Chapter 1

Theoretical Background

1.1 Quantum Computing

Analogous to the digital bits used for classical computation, a quantum computer requires quantum bits, more commonly known as qubits, as the fundamental register. However, unlike the classical bits which can acquire the value of either a 0 or a 1, a qubit state can be a linear superposition of the states $|0\rangle$ and $|1\rangle$, where $|\rangle$ represents a quantum state in the Dirac notation, i.e.,

$$|\psi\rangle = a_0 |0\rangle + a_1 |1\rangle, \quad (1.1)$$

where a_0 and a_1 are the complex amplitudes such that $|a_1|^2 + |a_0|^2 = 1$. According to the principles of quantum mechanics, a measurement of the qubit state then yields either $|0\rangle$, with probability $|a_0|^2$ or $|1\rangle$, with probability $|a_1|^2$.

In its simplest form, a qubit is therefore a two-level system. A spin-1/2 particle with its two levels being the up spin and the down spin, can naturally be used as a qubit. In this notation, it is conventional to associate state $|0\rangle$ with $|\uparrow\rangle$, and state $|1\rangle$ with $|\downarrow\rangle$. The three components of the Pauli matrices corresponding to the spin-1/2 operator \mathbf{S} spanned by these states are:

$$\sigma_x = \begin{pmatrix} 0 & 1 \\ 1 & 0 \end{pmatrix}, \sigma_y = \begin{pmatrix} 0 & -i \\ i & 0 \end{pmatrix}, \sigma_z = \begin{pmatrix} 1 & 0 \\ 0 & -1 \end{pmatrix},$$

which are then used as the fundamental elements of quantum computing.

For N such qubits, the basis state is a tensor product of the single-qubit basis states. Since each single state constitutes two basis vectors, the N -qubit state comprises of $L = 2^N$ basis vectors. This constitutes of the computational basis - $|00\dots0\rangle, |00\dots1\rangle, \dots, |11\dots1\rangle$. Therefore, a general N -qubit state can be represented as

$$|\psi\rangle = a_0 |00\dots0\rangle + a_1 |00\dots1\rangle + \dots + a_L |11\dots1\rangle, \quad (1.2)$$

which requires L complex amplitudes for its description.

The computational basis can be more conveniently notated as $|00\dots0\rangle = |0\rangle, |00\dots1\rangle = |1\rangle, \dots, |11\dots1\rangle = |L\rangle$. In this representation, eq. (1.2) thus becomes

$$|\psi\rangle = a_0 |0\rangle + a_1 |1\rangle + \dots + a_L |L\rangle. \quad (1.3)$$

Therefore, the Hilbert space spanned by N qubits is an L -dimensional space.

Since Pauli matrices, together with the identity operator I , form a complete basis for a vector in 2×2 space, any gate acting on a qubit can be expressed as a linear combination of Pauli matrices [Quantum Walks and search algorithms, Renato Portugal]. The action of a Pauli matrix, σ^α , where $\alpha \in \{x, y, z\}$ on the j^{th} of the N bits of the basis vector is represented as σ_j^α . Thus, the Pauli operator σ_j^α acting on the general state $|\psi\rangle$, given in eq. (1.2), just acts on the j^{th} bit of the basis vector, altering the coefficients a_0, a_1, \dots, a_L . The other bits of the basis vector remain unchanged as a result of being acted upon by identity matrices $I = \begin{pmatrix} 1 & 0 \\ 0 & 1 \end{pmatrix}_{i \neq j}$.

1.2 Optimization Problems and Quantum Annealing

Mathematically, an optimization problem comprises of a cost function, $f_0(\mathbf{x})$ involving N variables $x_1, x_2, x_3, \dots, x_N$, such that $\mathbf{x} = (x_1, \dots, x_N)$. The goal is then to find the solution \mathbf{x}_0 that minimises (or maximises) the cost function. In the computing language the cost function is written as a Boolean expression in the form of conjunction (a Boolean AND operation) of r clauses, where each clause is a disjunction (a Boolean OR operation) of k variables or their negations (k -SAT problems)[Convex Optimization, Stephen Boyd (book)], [Ting Hsu et. al]. A 2-SAT instance is thus formulated as a Boolean expression where each clause is a disjunction of two literals. The literals, $L_{i,j}$, are Boolean variables or their negations. The task is then to find a truth assignment to the Boolean variables that makes the formula $G = (L_{1,1} \vee L_{1,2}) \wedge (L_{2,1} \vee L_{2,2}) \wedge \dots \wedge (L_{r,1} \vee L_{r,2})$ true. If $G=1$ then the 2-SAT instance is satisfiable.

Many physically inspired approaches have also been adopted to find the solution for the optimization problems. One of the widely used techniques is to encode the problem into the couplings of Ising Hamiltonians [Nonstoquastic Hamiltonians]. The ground state of this Hamiltonian, corresponding to the state of the minimum energy, then represents the optimal solution of the problem. At low enough temperatures, the system state should eventually relax to the ground state, yielding the required solution.

For finding the optimal solution, the whole spectrum of the cost function needs to be explored. This requires that the system should be able to escape from a local minimum, if it gets trapped in one, during the course. The presence of multiple local minima thus makes the determination of the optimal solution harder [Optimization using quantum mechanics: quantum annealing through adiabatic evolution: Santoro and Tosatti].

The method of simulated annealing was therefore utilised for [Kirkpatrick S, Gelatt C D Jr and Vecchi M P 1983 Science 220 671], where adding thermal fluctuations to the cost function, keeps the system from getting trapped in the local minima. Yet if the barrier potential diverges or becomes very high, this approach can no longer be helpful. It was in this spirit that the technique of quantum annealing was first employed by B.Apolloni, C.Carvalho and D.de Falco in 1988 [Quantum stochastic optimization, Appoloni, Carvalho, de Falco], wherein quantum fluctuations were used in place of thermal fluctuations. By making use of the quantum tunnelling effect, this approach can still allow for the search of global minima as the system state can tunnel through the poor local minima.

The cost function is mapped on to the Ising model of spins, making use of the external magnetic field h_i^z and the spin couplings J_{ij}^z of the model, and thus has the following form:

$$H_P = - \sum_{i=1}^N h_i^z \sigma_i^z - \sum_{\langle i,j \rangle} J_{ij}^z \sigma_i^z \sigma_j^z, \quad (1.4)$$

where σ_i^z denotes the z component of Pauli-spin matrix acting on the i^{th} spin, and the set $\langle i,j \rangle$ represents the set of pairwise couplings.

The recipe for the annealing algorithm consists of starting with an initial Hamiltonian H_I , whose ground state can be easily determined and realised. Most commonly used is the transverse field Hamiltonian:

$$H_I = - \sum_{i=1}^N h_i^x \sigma_i^x. \quad (1.5)$$

The ground state for H_I is therefore the uniform superposition state:

$$|\psi\rangle = \frac{1}{(\sqrt{2})^N} (|0\rangle + |1\rangle)_1 * (|0\rangle + |1\rangle)_2 * \dots * (|0\rangle + |1\rangle)_N. \quad (1.6)$$

The Hamiltonian is then slowly swept towards the problem Hamiltonian, with the means of an annealing parameter, say s , defined as $s = t/T_A$, where t is the instantaneous time, and T_A is the total annealing time. The Hamiltonian, $H(t)$, corresponding to the most straightforward annealing scheme, is then given by:

$$H(t) = (1 - s(t))H_I + s(t)H_P. \quad (1.7)$$

Therefore, the Hamiltonian transitions from the initial Hamiltonian, $H(t = 0) = H_I$ to the final Hamiltonian, $H(t = T_A) = H_P$.

According to the **quantum adiabatic theorem**, the instantaneous state of the system stays close to the ground state of Hamiltonian $H(t)$, if one starts with ground state of the initial Hamiltonian and if the driving from the initial Hamiltonian to the problem Hamiltonian is slow enough, which is determined by the minimum energy gap, Δ_{min} , between the ground state and the first excited state of the Hamiltonian $H(t)$ during the course of annealing. [ADIABATIC QUANTUM COMPUTATION, Enej Ilievsk]. Mathematically, adiabatic theorem of evolution holds when

$$T_A \propto \Delta_{min}^{-2}, \quad (1.8)$$

where T_A is the total annealing time. [Perspectives of quantum annealing: Methods and implementations]. Therefore, the performance of quantum annealing depends strongly on the minimum energy gap.

Thus, the problem of finding the optimal solution reduces to the problem of solving the time dependent Schrödinger equation for the resulting $H(t)$ (see eq. 1.7):

$$i \frac{\partial}{\partial t} |\psi\rangle = H(t) |\psi\rangle. \quad (1.9)$$

However, the process of evolution, starting from the trivial ground state of the initial Hamiltonian and going to a non-trivial ground state of the problem Hamiltonian, is accompanied by a quantum phase transition. Such a transition is characterized by a vanishing energy gap in the thermodynamic limit. For the problems which are considered to be difficult, the minimum gap is found to close exponentially as a function of the system size, i.e., $\Delta_{min} \propto e^{-cN}$, for a positive constant c and N number of spins. This suggests that the annealing time required to ascertain that the evolution is adiabatic also grows exponentially, $T_A \propto e^{2cN}$. On the other hand, if the gap closes polynomially ($\Delta_{min} \propto N^{-l}$, for a positive constant l), the computation time is also polynomial, $T_A \propto N^{2l+1}$, and the problem is considered easy [Perspectives, Nishimori].

Therefore, the dependence of the minimum energy gap on the size of the system determines the annealing time required to make the evolution of the state of the system to be adiabatic. Thus, one method of improving the performance of quantum annealers is by controlling the closing of the gap. Altering the annealing scheme is believed to be one of the ways in which this can be achieved [Perspectives of quantum annealing: Methods and implementations, Adiabatic quantum computation: Tameem Albash, Quantum Adiabatic Evolution Algorithms with Different Paths: Farhi, Different strategies for Optimization Using the Quantum Adiabatic Algorithm: Farhi, Nonstoquastic Hamiltonians and quantum annealing of an Ising spin glass]. In this work we aim to achieve the same by including a third Hamiltonian, the Trigger Hamiltonian - H_T in the time dependent Hamiltonian $H(t)$ (see eq. 1.7)[Farhi-Goldstein, Farhi (Different), Review, Non-stoquastic]. The trigger Hamiltonian should vanish at both the start and end of the annealing process, so that one can still start with the easily realizable ground state of the initial Hamiltonian, and the resulting state of the problem Hamiltonian remains unaffected. The Hamiltonian thus takes the form:

$$H(t) = (1-s)H_I + gs(1-s)H_T + sH_P, \quad (1.10)$$

where parameter g controls the strength of the added trigger.

Furthermore, for this thesis we deal with two types of trigger Hamiltonians - The ferromagnetic trigger (F) and the anti-ferromagnetic trigger (A)[Nonstoquastic...], given as

$$H_T^F = - \sum_{\langle i,j \rangle} \sigma_i^x \sigma_j^x, \quad (1.11)$$

and

$$H_T^A = + \sum_{\langle i,j \rangle} \sigma_i^x \sigma_j^x, \quad (1.12)$$

with the same pairwise coupling set $\langle i,j \rangle$ as for the problem Hamiltonian. The trigger can also be chosen to have the form $\pm \sum_{\langle i,j \rangle} \sigma_i^y \sigma_j^y$. As will be seen in the following chapters, adding these triggers alters the energy spectrum considerably, which in turn affects the overlap of the final state with the ground state in different ways.

The following sections focus on two approaches that have been used in this work to solve the time-dependent Schrödinger equation. The Suzuki-Trotter product formula has been adopted to track the evolution of the state, and to compute the overlap of the final state with the already determined ground state of the problem Hamiltonian. The full diagonalization method, on the other hand, has been used to calculate the errors involved in using the Suzuki-Trotter approximation, and to determine the energy spectra and minimum gaps for $H(t)$ for $t \in [0, T_A]$, where T_A is the total annealing time.

1.3 Exact Diagonalization

This method consists of determining the eigenvalues and eigenvectors of the Hamiltonian matrix, which is an $L \times L$ ($2^N \times 2^N$) matrix, at each time step.

For constructing the Hamiltonian matrix at time step $t \in [0, T_A]$, all the basis vectors in the computational basis are acted upon by the instantaneous Hamiltonian, given by eq. (1.10). The action of the Hamiltonian on the i^{th} basis vector corresponds to the i^{th} column of the Hamiltonian matrix, e.g. for $|\psi\rangle = (1, 0, \dots, 0)^T$, $H|\psi\rangle$ gives the first column of the Hamiltonian matrix.

The resulting matrix is then diagonalized to obtain the eigenvalues Λ , and unitary matrix of the eigenvectors, V . Since $V^\dagger HV = \Lambda$, the unitary evolution operator $U(t) = e^{-itH} = Ve^{-it\Lambda}V^\dagger$.

This approach, however, has some serious limitations. Firstly, the memory requirement to store the Hamiltonian matrix grows exponentially with the number of qubits ($\mathcal{O}(2^{2N})$). Additionally, full diagonalization takes $\mathcal{O}(2^{3N})$ floating-point operations [Kristel-Hans paper]. Therefore, this method is rendered impractical for solving the time dependent Schrödinger equation for systems more than 20 qubits.

1.4 Suzuki-Trotter Product Formula

For solving the time dependent Schrödinger eq.(1.9), one needs to evaluate the unitary matrix exponentials of the evolution operator, $U(t)$ given as:

$$U(t) = e^{-itH} = e^{-it(H_1 + \dots + H_K)} = \lim_{m \rightarrow \infty} \left(\prod_{k=1}^K e^{-itH_k/m} \right)^m. \quad (1.13)$$

In this work, the Lie-Trotter-Suzuki product formula is employed to construct unitary approximations to the evolution operator. Defining τ as t/m , to be the time step at which the evolution operator is applied, a repeated application of $U(\tau)$ yields $U(t)$. For a sufficiently small time step τ , the first order approximation for $U(t)$ in eq. (1.13) is

$$\tilde{U}_1(\tau) = e^{-i\tau H_1} \dots e^{-i\tau H_K}, \quad (1.14)$$

which holds good for $\tau \|H\| << 1$.

For an improved accuracy, a second order approximation is made to $U(t)$ in eq. (1.13), using $\tilde{U}_1(\tau)$ from eq. (1.14):

$$\tilde{U}_2(\tau) = \tilde{U}_1^\dagger(-\tau/2)\tilde{U}_1(\tau/2) = e^{-i\tau H_K/2} \dots e^{-i\tau H_1/2} e^{-i\tau H_1/2} \dots e^{-i\tau H_K/2}. \quad (1.15)$$

Since $\tilde{U}_1(\tau)$ is unitary, as all H_k in eq. (1.13) are Hermitian , $\tilde{U}_2(\tau)$ is also unitary. Thus the measure of error, calculated using the absolute difference between $U(\tau)$ and $\tilde{U}_2(\tau)$, grows cubically in τ [Kristel-Hans paper, 62 from there], i.e.

$$\|U(\tau) - \tilde{U}_2(\tau)\| \leq c\tau^3 \quad (1.16)$$

for a positive constant c . Since the whole annealing process requires m such time steps, the involved error becomes

$$\|U(m\tau) - \tilde{U}_2(m\tau)\| \leq m^3 c \tau^3. \quad (1.17)$$

Since $m\tau = t$, (1.17) is equivalent to

$$\|U(m\tau) - \tilde{U}_2(m\tau)\| \leq cm^2 t \tau^2 = c_2 t \tau^2, \quad (1.18)$$

where $c_2 = cm^2$.

The Hamiltonian $H(t)$ is then decomposed as follows:

$$H = H_{single} + H_x + H_Y + H_z, \quad (1.19)$$

where $H_{single} = -(1-s) \left(\sum_{i=1}^N h_i^x \sigma_i^x \right) - s \left(\sum_{i=1}^N h_i^z \sigma_i^z \right)$, $H_x = \mp(1-s) \left(\sum_{\langle i,j \rangle} J_{i,j}^x \sigma_i^x \sigma_j^x \right)$, $H_y = \mp(1-s) \left(\sum_{\langle i,j \rangle} J_{i,j}^y \sigma_i^y \sigma_j^y \right)$,

and $H_z = -s \left(\sum_{\langle i,j \rangle} J_{i,j}^z \sigma_i^z \sigma_j^z \right)$. In general,

$$e^{i\mathbf{v}\cdot\boldsymbol{\sigma}} = \cos(v)I + i\frac{\sin(v)}{v}\mathbf{v}\cdot\boldsymbol{\sigma}, \quad (1.20)$$

where I represents the identity matrix, and $v = \sqrt{v_x^2 + v_y^2 + v_z^2}$. Then,

$$e^{-itH_{\text{single}}} = \prod_{i=1}^N e^{it[(1-s)\sum_i h_i^x \sigma_i^x + s \sum_i h_i^z \sigma_i^z]} = \prod_{i=1}^N \begin{pmatrix} \cos(th_i) + i \frac{sh_i^z}{h_i} \sin(th_i) & i \frac{(1-s)h_i^x}{h_i} \sin(th_i) \\ i \frac{(1-s)h_i^x}{h_i} \sin(th_i) & \cos(th_i) - i \frac{sh_i^z}{h_i} \sin(th_i), \end{pmatrix} \quad (1.21)$$

$$\text{where } h_i = \sqrt{(1-s(t))^2 h_i^{x2} + s(t)^2 h_i^{z2}}.$$

The computational basis states are the eigenstates of the Pauli-z operator, σ_i^z . Thus e^{-itH^z} is a diagonal matrix in the computational basis, and its action on the input state changes the phase of each of the basis vectors. As H^z is a sum of pair interactions, it is trivial to implement this operation as a sequence of multiplications by 4×4 diagonal matrices [Kristel-Hans paper].

The same approach can be adopted for implementing H_x operations as well, by using the rotation operators Y_j as follows. Writing $Y = \prod_{i=1}^N Y_i$, we obtain

$$e^{-itH^x} = \bar{Y} Y e^{-itH^x} \bar{Y} Y = \bar{Y} e^{it \sum_{i,j} J_{ij}^x \sigma_i^z \sigma_j^z} Y. \quad (1.22)$$

Chapter 2

Landau-Zener Tunnelling

The Landau-Zener model describes the response of the magnetization of a 2-level spin system, under the action of a slowly reversing external magnetic field at zero temperature [Hans Landau-Zener paper]. Consider, the following single spin- $\frac{1}{2}$ Hamiltonian as an example:

$$H_{LZ}(t) = -\Gamma\sigma_x - ct\sigma_z, \quad (2.1)$$

where Γ sets the scale of the splitting between the two energy levels, and c is the sweep rate of the applied magnetic field, i.e $H(t)=ct$. Thus for a field switching its value from $-H_0$ to H_0 in time T , $c = \Delta H/T = 2H_0/T$.

Now, for large negative times t , and $|H(t)| \geq |\Gamma|$, $H_{LZ}(t) \approx ct\sigma_z$. Thus, the spin-down state, $|\downarrow\rangle$, is close to the ground state of the Hamiltonian, as $ct\sigma_z|\downarrow\rangle = -ct|\downarrow\rangle$. As t goes to infinity, $H_{LZ}(t) \approx -ct\sigma_z$, so that the ground state now lies close to the spin up state, $|\uparrow\rangle$, as $-ct\sigma_z|\uparrow\rangle = -ct|\uparrow\rangle$. According to quantum adiabatic theorem the state of the system should always lie close to the instantaneous ground state of the Hamiltonian $H(t)$, if one starts with the ground state and if the field is changed slowly enough. However, there is a finite probability that the state transits to a higher excited level during the sweep. The probability, p' , for this nonadiabatic transition (Landau-Zener tunnelling), as given by the Landau-Zener formula, is

$$p' = \exp\left(\frac{-\pi\Gamma^2}{c}\right). \quad (2.2)$$

Therefore, the probability, p , that the state of the system follows instantaneous ground state of the Hamiltonian adiabatically, by changing the magnetization state of the system, in accordance to the reversing field, $H(t)$, is

$$p = 1 - p' = 1 - \exp\left(\frac{-\pi\Gamma^2}{c}\right). \quad (2.3)$$

If the energy splitting between the ground state and the first excited state of the Hamiltonian at the anticrossing is denoted by ΔE , then it can be observed that $\Delta E = 2\Gamma$. Thus, in terms of ΔE , eq. (2.4) becomes

$$p = 1 - \exp\left(\frac{-\pi\Delta E^2}{4c}\right). \quad (2.4)$$

The deviation from the ground state occurs at $H \approx 0$, with a probability p' , and is accompanied by a step in the magnetization. This step depends on both the

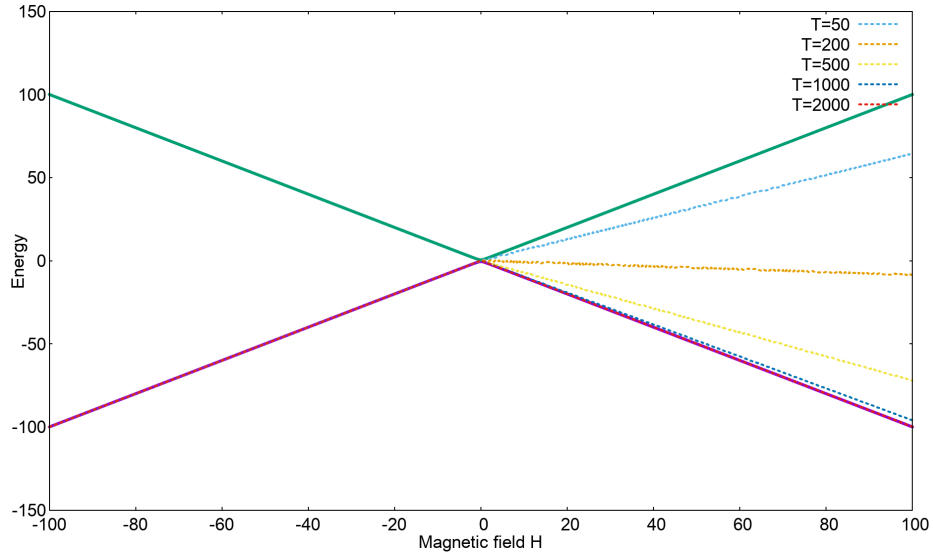


Figure 2.1: Energy spectrum for single qubit Hamiltonian in equation (2.1), with energy expectation values of the instantaneous state of the system with different sweeping times. $\Gamma = 0.5$, $H_0 = 100$.

energy splitting Γ , and the sweep rate c [Hans, On Quantum Simulators and Adiabatic Quantum Algorithms: Sarah Mostame?].

For a simple 2-level system where Γ is chosen to be 0.5 and the field is swept from a value from -100 to 100, fig. (2.1) gives the energy spectra for the Hamiltonian in eq. (2.1). Fig. (2.1) also shows the energy expectation values corresponding to the instantaneous state of the system for different times T chosen for sweeping the field. As is evident from the figure, the probability of the state of the system staying close to the ground state increases with decreasing speed (increasing T), as expected from eq. (2.3). For a sweeping time of $T=500$, fig. (2.2) shows the instantaneous magnetization state of the system.

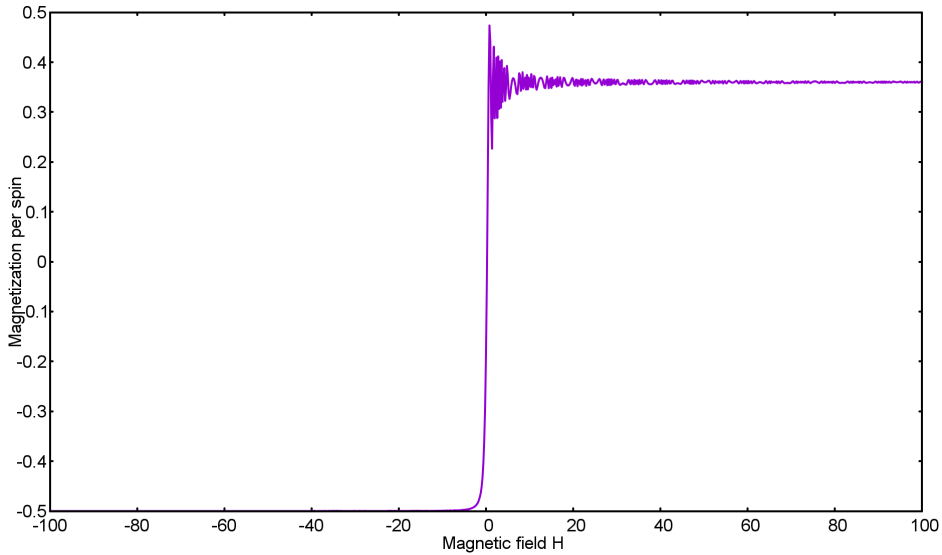


Figure 2.2: Instantaneous magnetization of the system state for $\Gamma = 0.5$, $H_0 = 100$ and $c=0.4$.

Comparing figs. (2.1) and (2.2), it can be observed that the step in the magnetization corresponds to the position of the anti-crossing between the ground state and the first excited state in the energy spectrum.

For verifying eq. (2.3), the overlap of the resulting state was computed with the ground state of the Hamiltonian, for different sweeping times. Fig. (2.3) shows the result obtained.

From eq. (2.3), $p = 1 - e^{-\frac{\pi\Gamma^2}{2H_0}T} = 1 - e^{-aT}$, where $a = \frac{\pi\Gamma^2}{2H_0}$. For the chosen parameters, a was calculated to be 3.926×10^{-3} . This value was found to be in agreement with the value 3.198×10^{-3} , obtained for the fitting parameter in fig. (2.3).

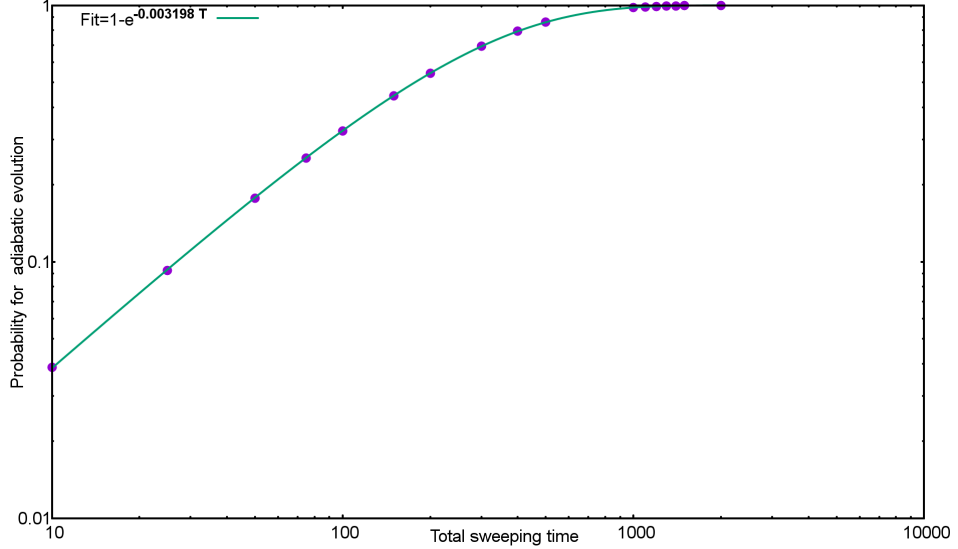


Figure 2.3: Probability for adiabatic evolution as a function of different sweep times for $\Gamma = 0.5$.

Although in both Quantum annealing and Landau-Zener model one deals with time dependent Hamiltonians, and the main task consists of studying the evolution of the state of the system under its action, there are two major points of difference. Landau-Zener formula is applicable to 2-level systems, and the process of reversing the magnetic field is ideally carried over an infinite amount of time. On the other hand, the Ising Hamiltonian considered for quantum annealing generally consists of more than two energy levels, and the evolution is carried out for a limited time, i.e. from $s=0$ to $s=1$ in terms of the annealing parameter: $s=t/T_A$, where T_A is the total annealing time.

Despite these differences, the Landau-Zener formula can be used to predict the probability of an adiabatic evolution for an Ising model, by making use of some approximations. The Ising model in a transverse field involving N variables is one of the simplest microscopic models for uniaxial magnets. Consider, for example, the Hamiltonian

$$H = -J \sum_{\langle i,j \rangle} \sigma_i^z \sigma_j^z - \Gamma \sum_i \sigma_i^x - H(t) \sum_i \sigma_i^z, \quad (2.5)$$

where set $\langle i,j \rangle$ defines the interactions between pairs of spins in the cluster. For a uniaxial magnet, only the lowest two levels are important for the adiabatic motion of the ground state. The scattering from the ground state to the first excited state occurs only when these levels come close, at the point of anti-crossing, i.e. around $H=0$. The dependence of energy on H around the anti-crossing is expected to be approximately expressed as the eigenvalue of the two level system:

$$(M_0 H \sigma^z - \Gamma \sigma^x) |\psi\rangle = E(H) |\psi\rangle, \quad (2.6)$$

where M_0 is a saturated magnetization at high field. In the case of strong uniaxial magnet, $M_0 = N$. The probability for the system state to follow the ground state adiabatically then becomes

$$p_N = 1 - \exp\left(\frac{-\pi \Delta E^2}{4Nc}\right). \quad (2.7)$$

Choosing a two spin system, with $\Gamma = 0.5$, $J = 3$, and $H_0 = 100$, fig. (2.4) shows the energy spectrum as a function of the magnetic field.

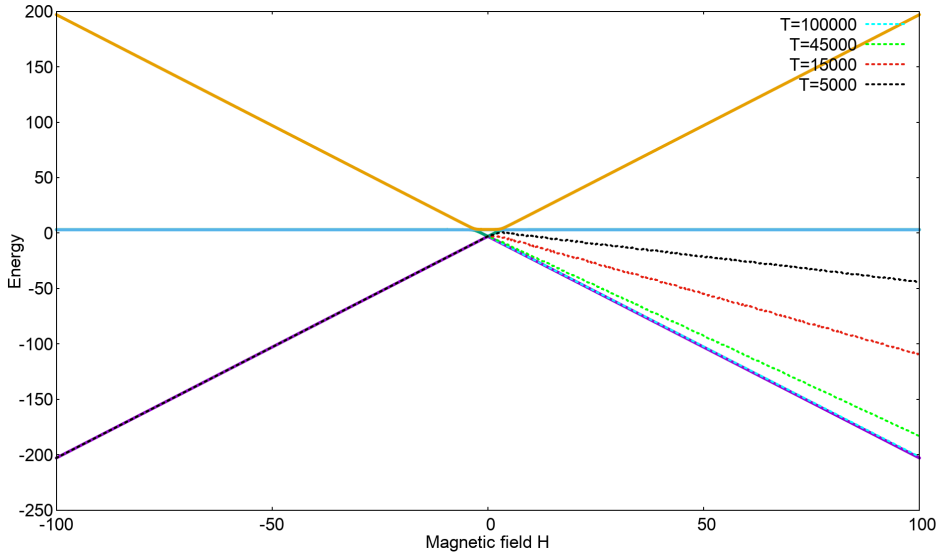


Figure 2.4: Energy spectrum for two spin Hamiltonian in equation (2.5), with energy expectation value of the instantaneous state of the system with different sweeping times. $\Gamma = 0.5$, $J = 3$, $H_0 = 100$.

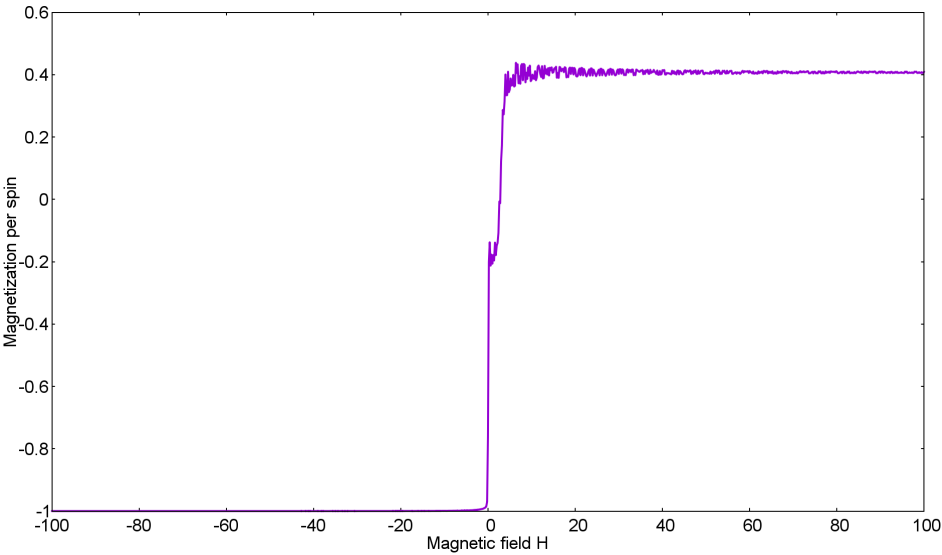


Figure 2.5: Instantaneous magnetization of the system state for $\Gamma = 0.5$, $H_0 = 100$ and $c=0.02$.

Figs. (2.5) and (2.6) show the instantaneous magnetization values for two different speeds. Similar to the case of a single spin Hamiltonian, the steps in the magnetization values correspond to the position of anticrossing between the energy levels of the spectrum, in this case as well. Other than the first step in the magnetization at $H \approx 0$, in this case, the second step corresponds to the value of H where energy levels become nearly degenerate.

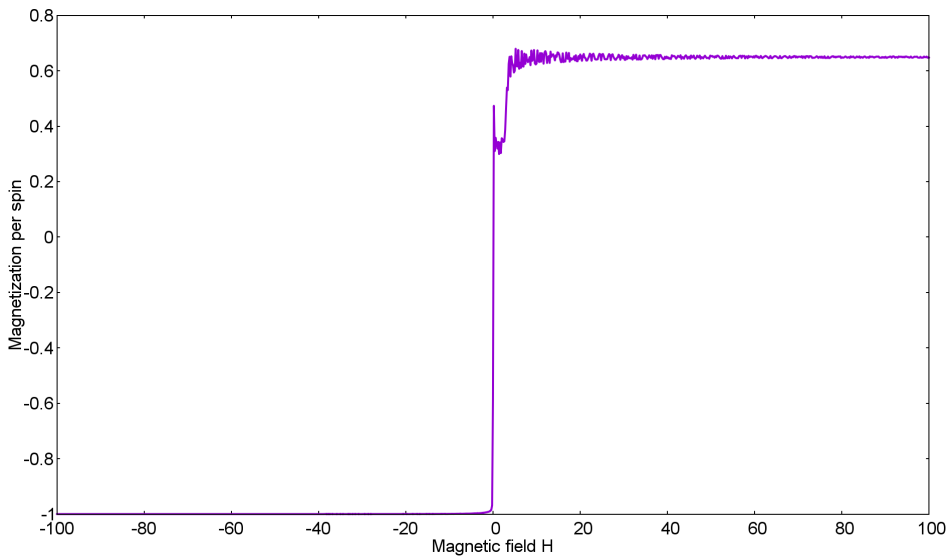


Figure 2.6: Instantaneous magnetization of the system state for $\Gamma = 0.5$, $H_0 = 100$ and $c=0.01$.

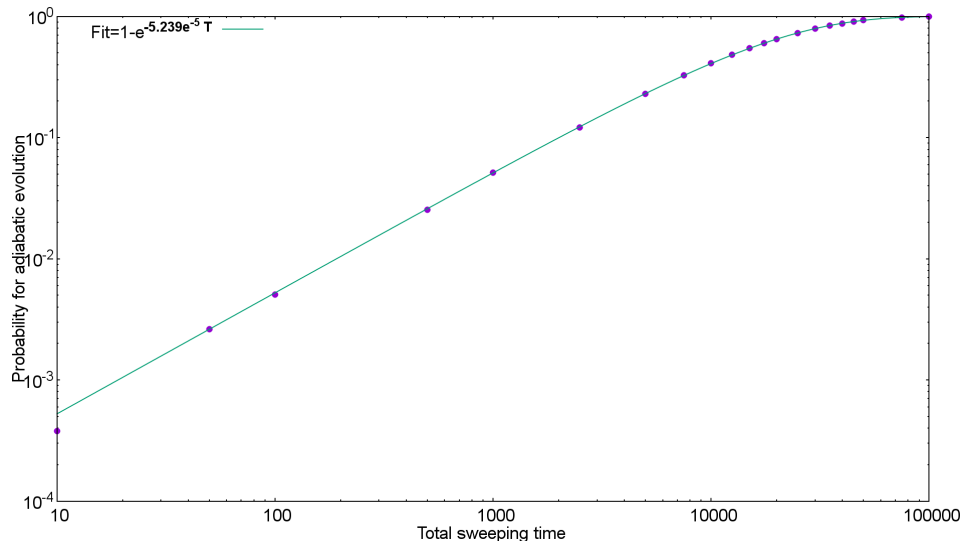


Figure 2.7: Probability for adiabatic evolution as a function of different sweep times for $\Gamma = 0.5$ and $J = 3$.

On increasing the total time for sweeping the field, i.e. decreasing the sweeping speed, the probability of staying in the ground state, by changing the state of magnetization should increase. This can be confirmed by comparing figs. (2.5) and (2.6).

Finally, for verifying eq. (2.7) the overlap of the resulting state with the ground state is computed for different times. Results obtained are shown in fig. (2.7).

The value of minimum gap, ΔE obtained was 0.162, which results in $a = \frac{\pi \Delta E^2}{8 \Delta H} = 5.182 \times 10^{-5}$. The value of the fitting function obtained in fig. (2.7) is 5.239×10^{-5} . Thus, the Landau-Zener formula can be extended to the N-spin Ising Hamiltonian with the approximations.

Eq. (2.7) will be used again as a check for adiabatic evolution in the subsequent chapters.

Chapter 3

Results with Original Hamiltonian

3.1 Second order

Since the Suzuki-Trotter product formula is only an approximation to solve the time dependent Schrödinger equation, the error involved depends on the time interval τ - the time step at which the evolution is computed (see Eq. 1.17).

Thus, for checking if the evolution using the Suzuki-Trotter product formula is indeed second order, the dependence of the error should be verified to be quadratic in τ , in accordance with Eq. (1.18).

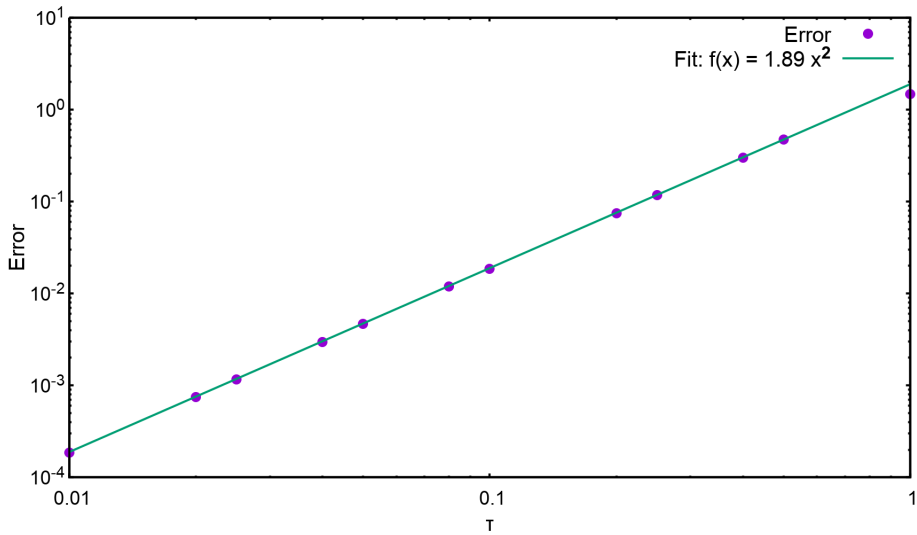


Figure 3.1: The error in Suzuki-Trotter formula relative to the full diagonalization method. The involved error grows quadratically in τ .

Since the dependence of the error on τ can be approximated to be linear in the log scale, as shown in Fig. (??), the simulation implementing TDSE can be trusted to be following the second order Suzuki-Trotter product formula.

For the course of this thesis, we worked with 8 spin and 12 spin 2-local problems. The first set had 91 unique problems, while the second set had 1000 such problems. All the problems had a predetermined unique ground state, and only one avoided crossing between the ground and the first excited state. The 8 spin problems had 9 pair-wise couplings, while the 12 spin problems had 13 such couplings. The success probability was then obtained by calculating the overlap between the known ground state and the final state resulting from the code performing product evolution. Furthermore, for determining the energy spectra for specific problems, exact diagonalization method was employed.

This chapter focusses on the results obtained for original Ising Hamiltonian, i.e. in the absence of any triggers.

For every problem belonging to the set, three annealing times were chosen to calculate the success probability. These correspond to $T_A \in \{10, 100, 1000\}$. For a given T_A , the resulting success probability is a function of the

minimum energy gap, Δ_{min} , between the ground and the first excited state. For a fixed T_A , the success probability is expected to decrease with decreasing Δ_{min} , if the evolution of the state is adiabatic. Thus, the hardness of a problem can be estimated by its minimum energy gap.

As the first example, considered here is problem number 733, that was noted to have high success probability, i.e., $p = 0.9944$ for $T_A = 100$. Fig. (??), shows the energy spectrum for this problem. Δ_{min} was found to be 0.4407 in this case. Also plotted in the figure are the energy expectation values for the instantaneous state obtained for the three different annealing times.

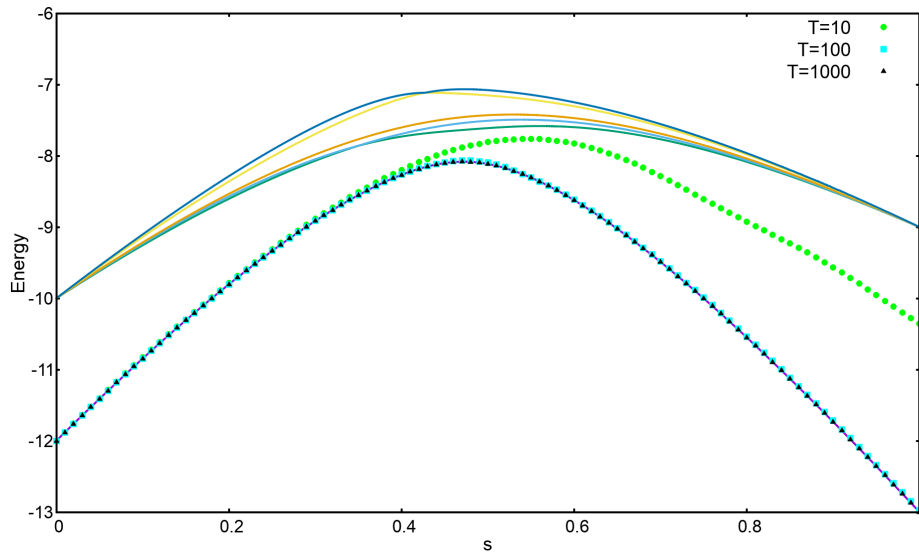


Figure 3.2: The energy spectrum for problem 733, with energy expectation values for the instantaneous state, corresponding to three annealing times. For $T_A=100$, p was found to be 0.9944, while $\Delta_{min} = 0.4407$.

As expected, the overlap of the final state with the ground state of the problem Hamiltonian increases on increasing the total annealing time in Fig. (??).

Secondly, problem number 950, with small success probability, $p = 0.0146$ at $T_A = 100$, was chosen. Fig. (??) shows the energy spectrum and the energy expectation values for the instantaneous state corresponding to three annealing times, for this problem. It should be noted, that the minimum gap in this is much smaller than in problem 733, and has a value of $\Delta_{min} = 0.0312$. This explains the decrease in success probability for the same annealing times.

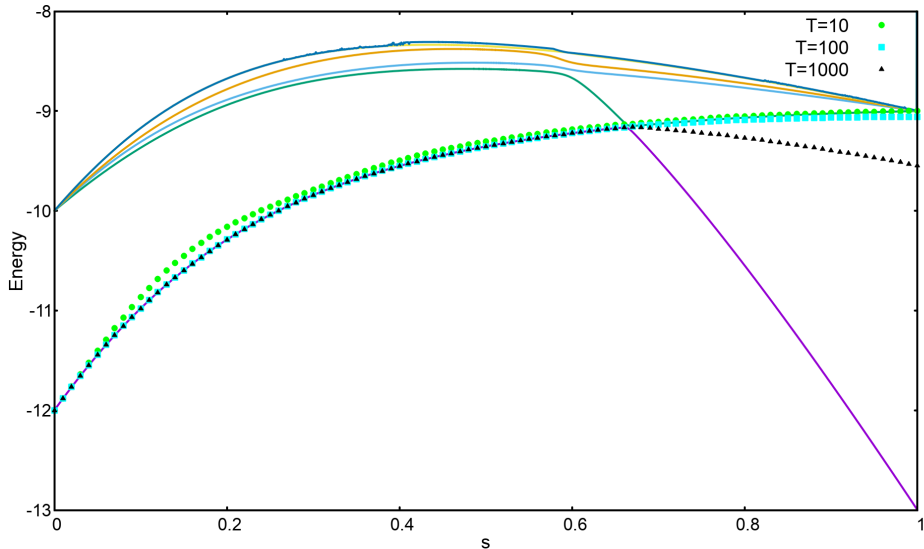


Figure 3.3: The energy spectrum for problem 950, with energy expectation values for the instantaneous state, corresponding to three annealing times. For $T_A=100$, p was found to be 0.0146, while $\Delta_{min} = 0.0312$.

As the third case, problem number 528, with an intermediate success probability of $p = 0.5199$ at $T_A = 100$ was studied. For this case too, the energy spectrum and the energy expectation values for the instantaneous state, corresponding to the three annealing times were determined, as is shown in Fig. (??). The value of minimum gap was $\Delta = 0.1573$ for this problem, which is intermediate to the above two cases.

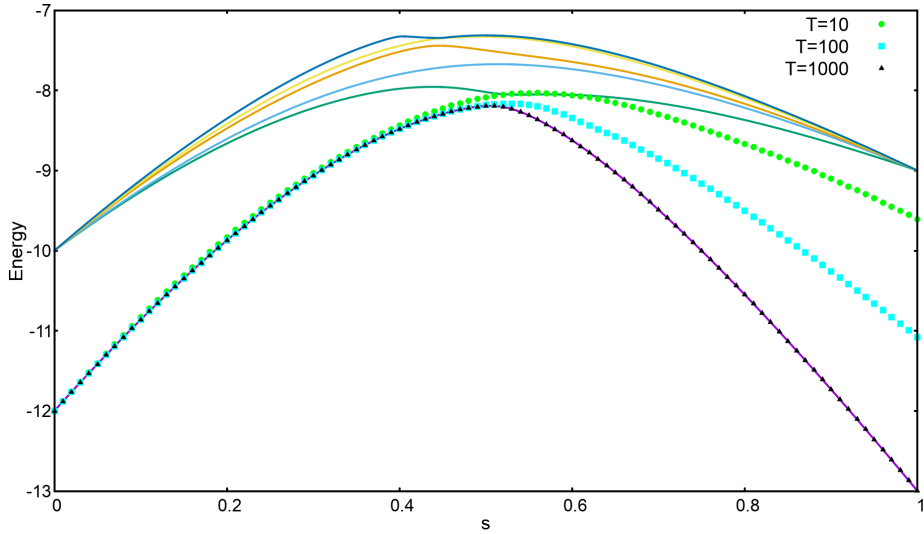


Figure 3.4: The energy spectrum for problem 528, with energy expectation values for the instantaneous state, corresponding to three annealing times. For $T_A=100$, p was found to be 0.5199, while $\Delta = 0.1573$.

To obtain a rough estimate of the spread of the difficulty of the problems considered in this work, Fig. (??) shows a plot of the distribution of the success probabilities for $T_A = 100$, for all the problems in the set. The range of the success probability spreads from 0.014 for the most difficult cases, to approximately 1 for the relatively easier cases. The mode of the distribution was found to be 0.141 and 0.199, while the mean success probability was found to be 0.208.

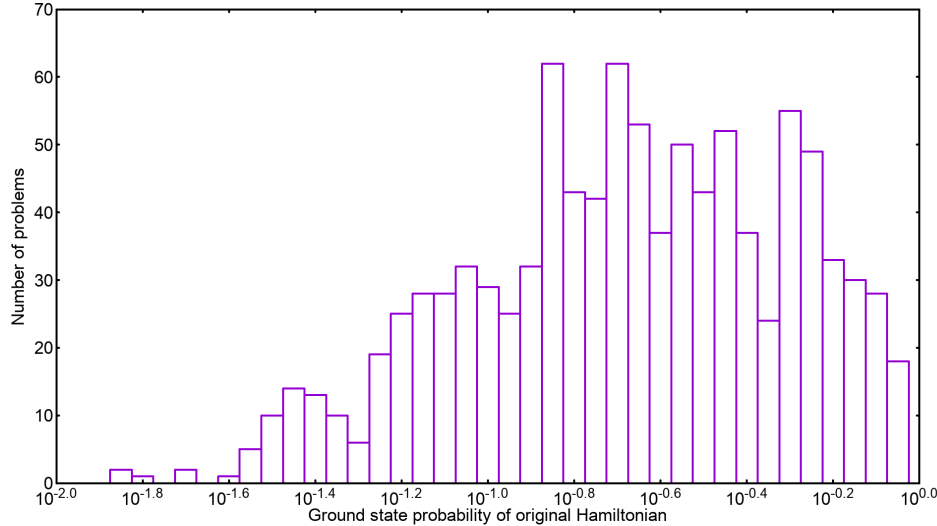


Figure 3.5: Histogram for success probability of the Hamiltonians without any triggers for 1000 12-spin problems for $T_A=100$.

Finally, to check if the sweeping from the initial Hamiltonian to the final Hamiltonian is adiabatic, the success probability of all the 12-spin problems has been plotted in Fig. (??).

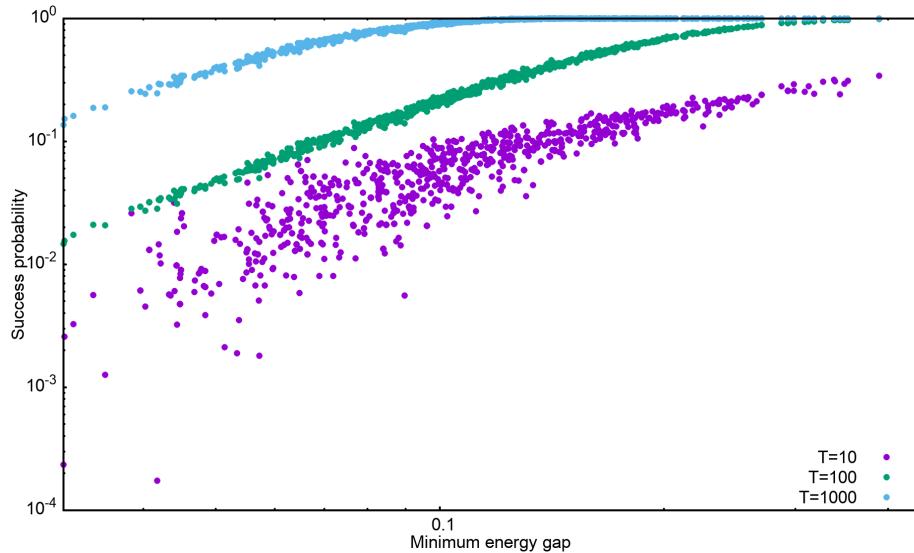


Figure 3.6: Success probability Versus minimum energy gaps for all the 12-spin problems for annealing times of 10,100 and 1000.

From Eq. (2.4), the probability of ending in a state close to the ground state of the problem Hamiltonian should follow the Landau-Zener dependence on the minimum energy gap between the ground and first excited state of the Hamiltonian, if the evolution of the state is adiabatic. Since different problems belonging to the set correspond to different values of Δ_{min} , the success probability for each problem, plotted against the respective minimum energy gap for a fixed annealing time, can give an estimate of the fraction of cases undergoing adiabatic evolution. More the scattering in the resulting curve, smaller is the fraction of problems following the adiabatic theorem. It can therefore be noted in Fig. (??) that for $T_A=10$, the scattering is significantly larger than in the other two cases. It should additionally be observed that as the annealing time is increased, the success probability for a specific problem becomes successively larger. This suggests that as the annealing time is increased, the evolution of the state becomes adiabatic for more number of problems.

Chapter 4

Results with Ferromagnetic Trigger

As mentioned in the first chapter, there are two trigger Hamiltonians that were studied in the course of this thesis. This chapter focuses on the performance of quantum annealing on adding the ferromagnetic trigger, H_T^F to the Ising Hamiltonian.

For the same transverse-field initial Hamiltonian, and each problem from the set of problem Hamiltonians, ferromagnetic trigger was added with three different strengths, i.e. the strength parameter, g in eq. (??) was chosen to be 0.5, 1 and 2.

In the subsequent segments, the effects of adding the ferromagnetic trigger with different strengths will be discussed. For studying the dynamics during the evolution, the same cases have been chosen as in the previous chapter.

We therefore start by problem 733. Figs. (4.1),(4.2) and (4.3) show the energy spectra for this problem upon adding the ferromagnetic trigger with strengths 0.5, 1 and 2 respectively. The corresponding energy expectation values for the instantaneous state have also been included in these plots.

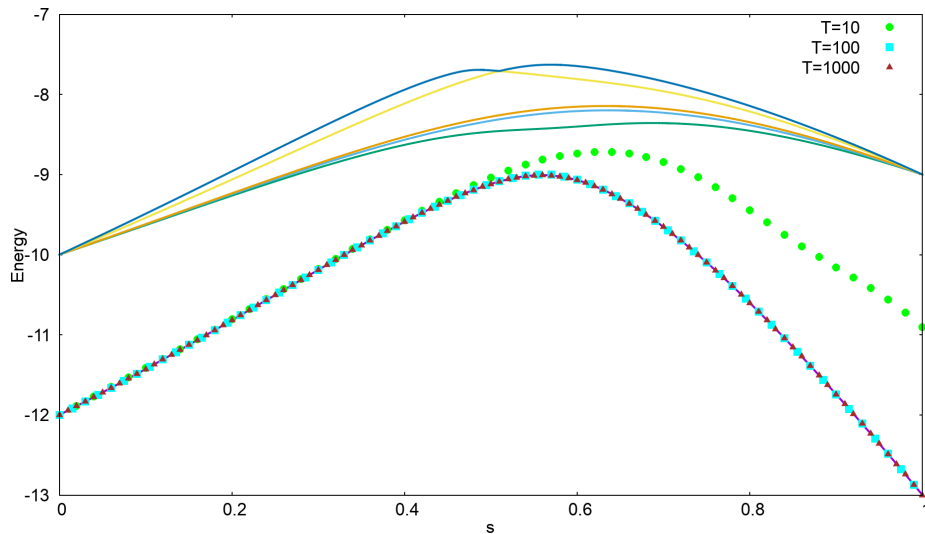


Figure 4.1: The energy spectrum and energy expectation values for the instantaneous state of problem 733, after adding the ferromagnetic trigger with $g=0.5$, for the three annealing times. Δ_{min} was found to be 0.5779, while $p=0.9996$ for $T_A=100$.

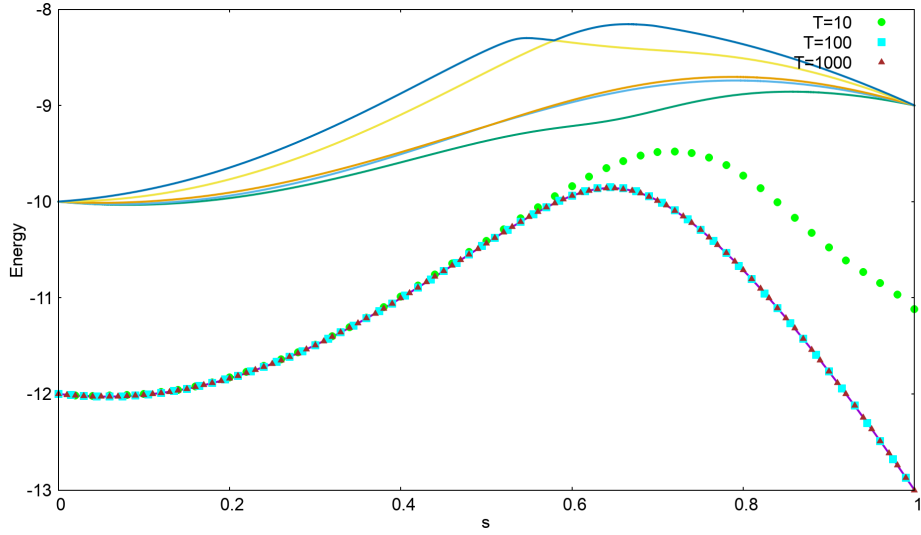


Figure 4.2: The energy spectrum and energy expectation values for the instantaneous state of problem 733, after adding the ferromagnetic trigger with $g=1$, for the three annealing times. Δ_{min} was found to be 0.6908, while $p=0.9998$ for $T_A=100$.

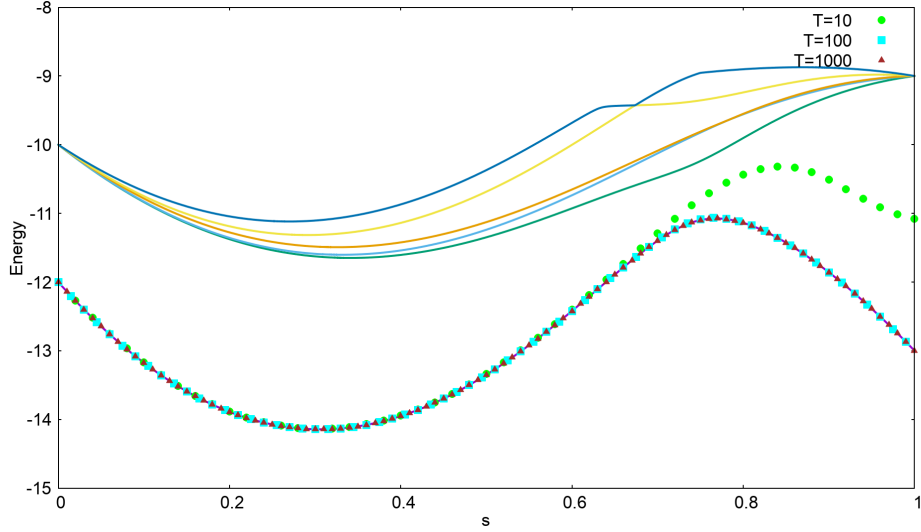


Figure 4.3: The energy spectrum and energy expectation values for the instantaneous state of problem 733, after adding the ferromagnetic trigger with $g=2$, for the three annealing times. Δ_{min} was found to be 0.8333, while $p=0.9997$ for $T_A=100$.

From these figures, it can be noted that compared to the original Hamiltonian, the minimum gap, Δ_{min} has increased for all the three case. Furthermore, the Δ_{min} becomes larger as the strength of the trigger Hamiltonian is increased from 0.5 to 2.

Secondly, the position of Δ_{min} is shifted more towards the right upon increasing the strength. Additionally, the concavity of the energy levels of the spectrum also increases with it. Finally, all the success probabilities upon adding the trigger are larger than the success probability of the original case, owing to the increase in the the minimum gaps. In general, the success probability also increases with increasing the strength of the trigger, though the final overlap also depends on the the exact energy spectrum.

Tab. (4.1) shows a comparison of the minimum energy gaps and success probabilities for problem 733, before and after adding the trigger.

Problem 733	Original Hamiltonian	Trigger=F, g=0.5	Trigger=F, g=1	Trigger=F, g=2
Δ_{min}	0.4407	0.5779	0.6908	0.8333
p	0.9944	0.9996	0.9998	0.9997
s value at Δ_{min}	0.459	0.552	0.629	0.733

Table 4.1: A comparison of the minimum energy gaps and the success probabilities for $T_A=100$, between the original Hamiltonian for problem 733 and that after adding the ferromagnetic trigger (F) with different strengths. The minimum gaps become larger as the strength of the ferromagnetic trigger is increased. The success probabilities are increased as a result. The value of s corresponding to the position of the minimum gap also becomes larger.

Next, we focus on problem 950, which had a small success probability for the original Hamiltonian. Figs. (4.4), (4.5), (4.6) show the energy spectra and the energy expectation values for the instantaneous state, upon adding the ferromagnetic trigger with $g= 0.5, 1$ and 2 respectively.

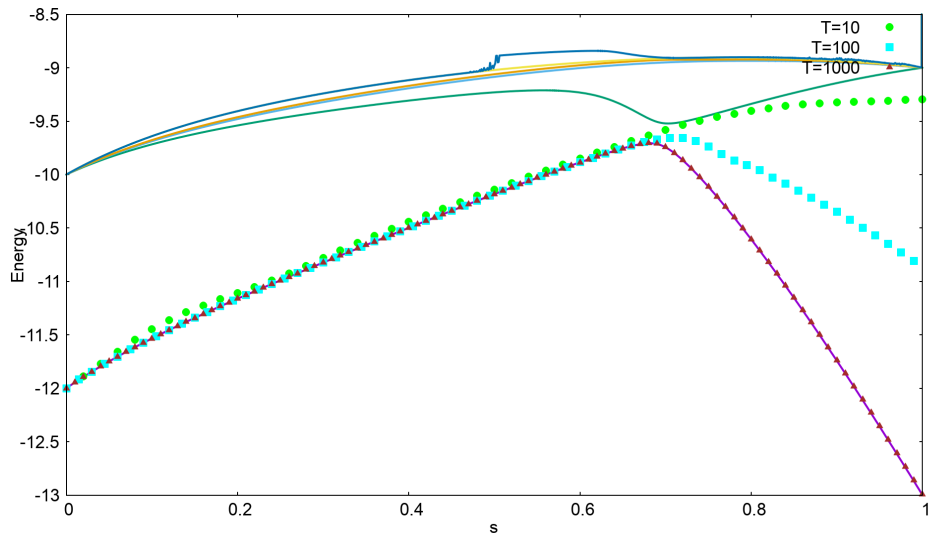


Figure 4.4: The energy spectrum and energy expectation values for the instantaneous state of problem 950, after adding the ferromagnetic trigger with $g=0.5$, for the three annealing times. Δ_{min} was found to be 0.2074, while $p=0.4650$ for $T_A=100$.

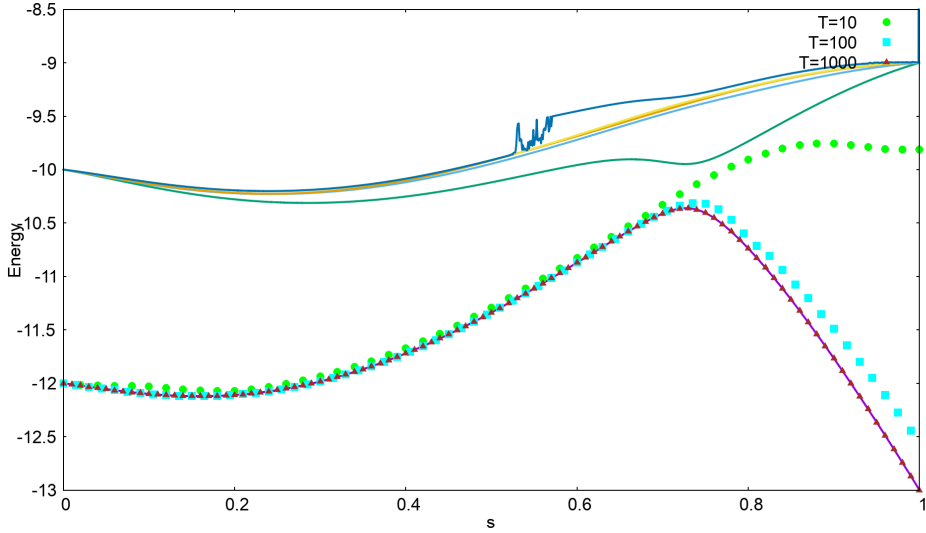


Figure 4.5: The energy spectrum and energy expectation values for the instantaneous state of problem 950, after adding the ferromagnetic trigger with $g=1$, for the three annealing times. Δ_{min} was found to be 0.4129, while $p=0.8889$ for $T_A=100$.

For this case too, the minimum energy gaps were found to have increased, leading to an improvement in the success probabilities. The improvements can be seen to become larger with increasing strengths of the trigger. The position of the minimum gap was again found to shift more rightwards in terms of the annealing parameter s upon increasing the strength, while the concavity of the energy levels increased.

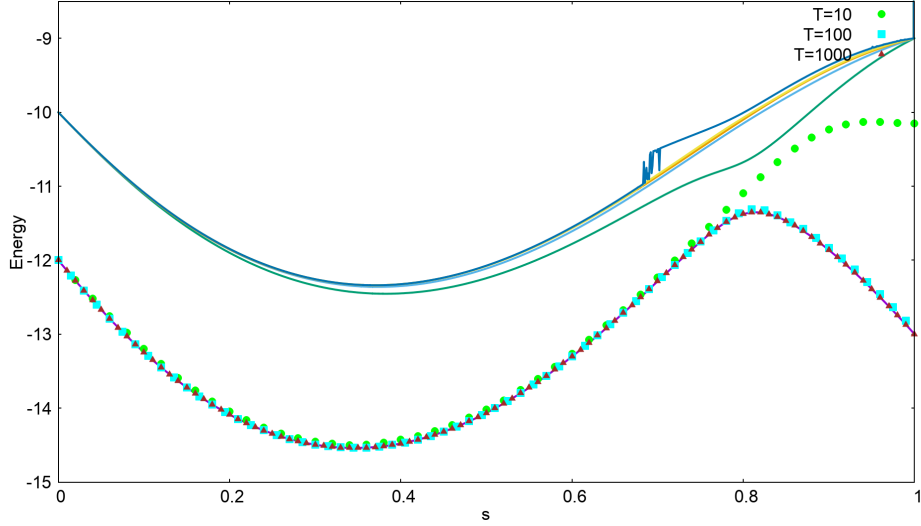


Figure 4.6: The energy spectrum and energy expectation values for the instantaneous state of problem 950, after adding the ferromagnetic trigger with $g=2$, for the three annealing times. Δ_{min} was found to be 0.6943, while $p=0.9870$ for $T_A=100$.

However, compared to the improvement in the success probability after adding the ferromagnetic trigger to problem 733, the improvement in problem 950 is significantly larger. Defining the relative success probability as the ratio of the success probability of a particular problem after adding the trigger (p^F) to the original success probability (p^o), for problem 733, the relative success probability at $T_A=100$ is 1.005 for $g=2$, while that for problem 950 is 67.6. In terms of the ratio of the minimum energy gaps, for problem 733, $\frac{\Delta_{min}^F}{\Delta_{min}^o}=1.89$, while for problem

950, it was found to be $\frac{\Delta_{min}^F}{\Delta_{min}^O}=22.2$. This can be understood as follows. For the original Hamiltonian for problem 733 and $T_A=100$, the system state always stays close to the ground state of the Hamiltonian (see Fig. ??), because of the large minimum energy gap. Therefore, even as adding the ferromagnetic trigger enlarges the minimum gap, there is not much scope of improvement for further increasing the overlap with the ground state. On the other hand, the original minimum energy gap in problem 950 is rather small. This causes the state of the system to shift most of its amplitude to the first excited state, thereby decreasing the overlap with ground state. Since the ferromagnetic trigger widens the minimum energy gap considerably in this case, the overlap with the ground state increases, resulting in a much larger relative success probability.

Tab. (4.2) gives a comparison of the minimum energy gaps and success probabilities for problem 950, before and after adding the trigger.

Problem 950	Original Hamiltonian	Trigger=F, g=0.5	Trigger=F, g=1	Trigger=F, g=2
Δ_{min}	0.0312	0.2074	0.4129	0.6943
p	0.0146	0.4650	0.8889	0.9870
s value at Δ_{min}	0.665	0.691	0.727	0.793

Table 4.2: A comparison of the minimum gaps and the success probabilities for $T_A=100$ between the original Hamiltonian for problem 950 and that after adding the ferromagnetic trigger with different strengths. The minimum gaps become larger as the strength of the ferromagnetic trigger (F) is increased. The success probabilities are increased as a result. The value of s corresponding to the position of the minimum gap also becomes larger.

Next, we consider problem 528 with intermediate success probability with original Hamiltonian. Figs. (4.7), (4.8) and (4.9) show the energy spectra and the energy expectation values for the instantaneous state after adding the ferromagnetic trigger with strengths 0.5, 1 and 2 respectively.

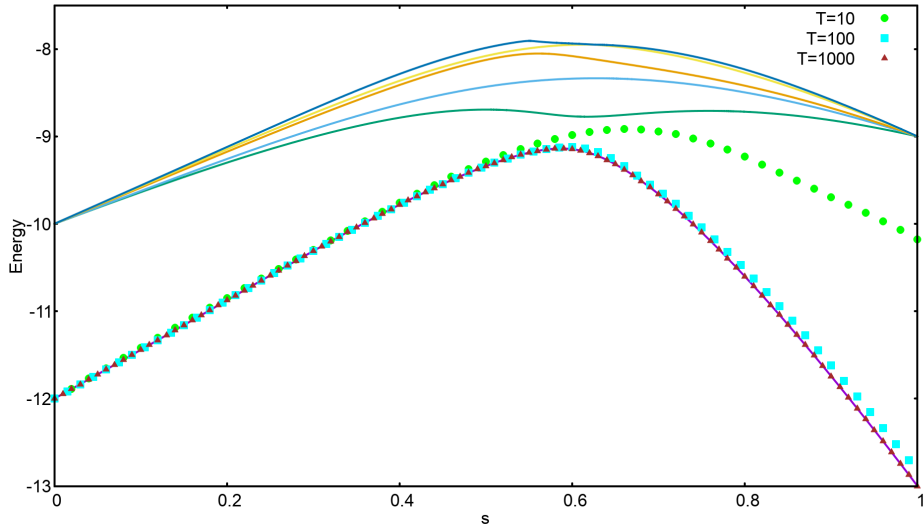


Figure 4.7: The energy spectrum and energy expectation values for the instantaneous state of problem 528, after adding the ferromagnetic trigger with $g=0.5$, for the three annealing times. Δ_{min} was found to be 0.3748, while $p=0.9577$ for $T_A=100$.

For this case too, the minimum energy gaps were found to have increased, leading to an improvement in the success probabilities. The improvements can be seen to become larger with increasing strengths of the trigger. The position of the minimum gap was again found to shift more rightwards in terms of the annealing parameter s upon increasing the strength, while the concavity of the energy levels of the spectrum increased.

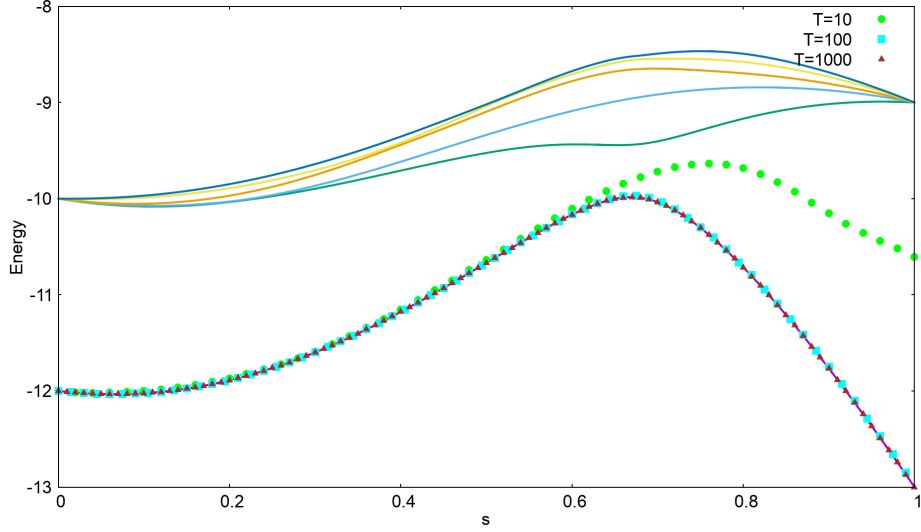


Figure 4.8: The energy spectrum and energy expectation values for the instantaneous state of problem 528, after adding the ferromagnetic trigger with $g=1$, for the three annealing times. Δ_{min} was found to be 0.5439, while $p=0.9945$ for $T_A=100$.

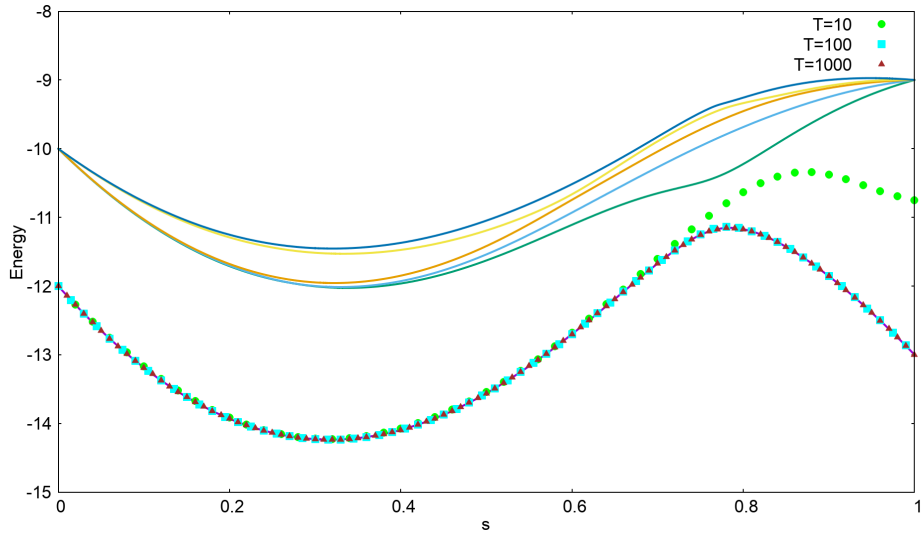


Figure 4.9: The energy spectrum and energy expectation values for the instantaneous state of problem 528, after adding the ferromagnetic trigger with $g=2$, for the three annealing times. Δ_{min} was found to be 0.7512, while $p=0.9981$ for $T_A=100$.

The relative success ratio for this case, $=1.91$, while $\frac{\Delta_{min}^F}{\Delta_{min}^O}=4.77$ at $g=2$. These values are also intermediate to those for problems 733 and 950. Tab. (4.3) shows a comparison of the success probabilities and the minimum gaps, between the original Hamiltonian and the Hamiltonian after adding the ferromagnetic trigger with different strengths.

Problem 528	Original Hamiltonian	Trigger=F, g=0.5	Trigger=F, g=1	Trigger=F, g=2
Δ_{min}	0.1573	0.3748	0.5439	0.7512
p	0.5199	0.9577	0.9945	0.9981
s value at Δ_{min}	0.514	0.595	0.665	0.760

Table 4.3: A comparison of the minimum energy gaps and the success probabilities for $T_A=100$, between the original Hamiltonian for problem 528 and that after adding the ferromagnetic trigger (F) with different strengths. The minimum gaps become larger as the strength of the ferromagnetic trigger is increased. The success probabilities are increased as a result. The value of s corresponding to the position of the minimum gap also becomes larger.

Next, the minimum energy gaps and the success probabilities were computed for all the 12-spin problems, before and after adding the ferromagnetic trigger, with $g \in \{0.5, 1, 2\}$, for $T_A \in \{10, 100, 1000\}$.

Fig. (4.10) shows the scatter plot of the minimum energy gaps after adding the ferromagnetic trigger with different strengths against the original minimum energy gaps, for all the problems of the set.

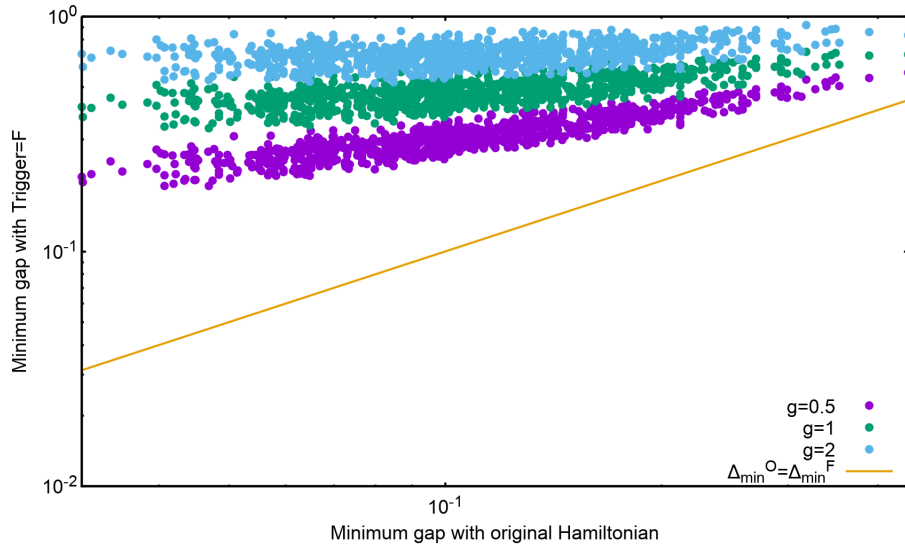


Figure 4.10: Scatter plot of the minimum gaps upon adding the ferromagnetic trigger with $g \in \{0.5, 1, 2\}$ against the original minimum energy gaps. The solid line represents the limit where the minimum gap remains unchanged.

With ferromagnetic trigger, all the minimum energy gaps were found to have increased, for all the values of g . Furthermore, for all the problems, the gaps became even larger as the ferromagnetic trigger became stronger. It can also be noted that the enhancement in the minimum energy gaps is larger in cases with relatively small original minimum gaps, as was also seen by calculating $\frac{\Delta_{min}^F}{\Delta_{min}^O}$ for the three chosen problems (733, 950 and 528).

For gauging the performance of the quantum annealing algorithm after adding the ferromagnetic trigger, scatter plots of the success probabilities after adding the ferromagnetic trigger against the original success probabilities have been shown in Figs. (4.11), (4.12) and (4.13) corresponding to $g= 0.5, 1$ and 2 respectively.

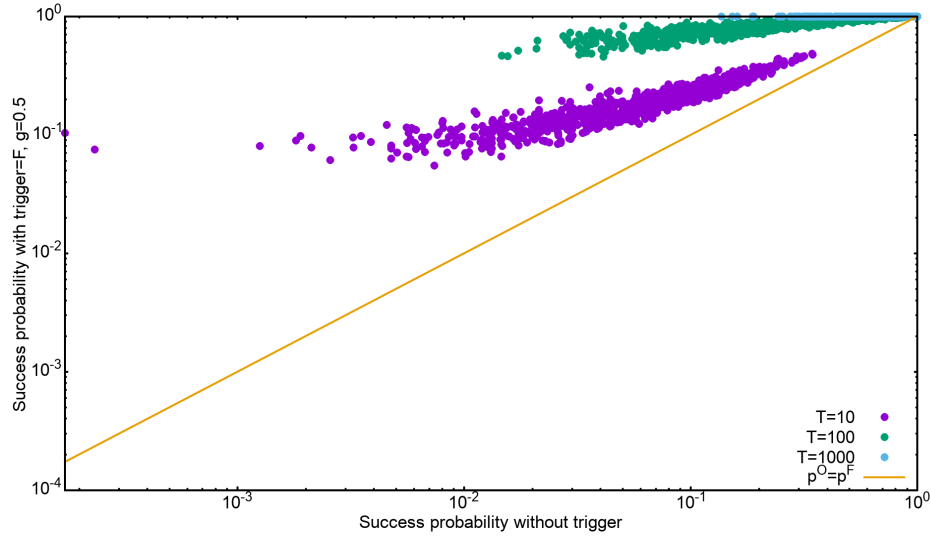


Figure 4.11: Scatter plot for the success probability after adding ferromagnetic trigger with $g=0.5$ against the success probability of the original Hamiltonian, for annealing time $T_A \in \{10, 100, 1000\}$. The solid line represents the limit where the success probability remains unchanged.

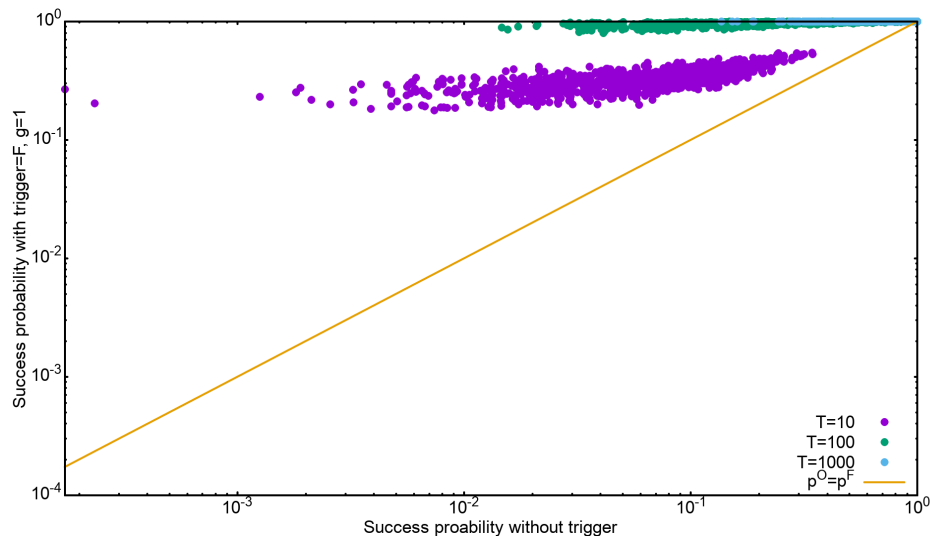


Figure 4.12: Scatter plot for the success probability after adding ferromagnetic trigger with $g=1$ against the success probability of the original Hamiltonian, for annealing time $T_A \in \{10, 100, 1000\}$. The solid line represents the limit where the success probability remains unchanged.

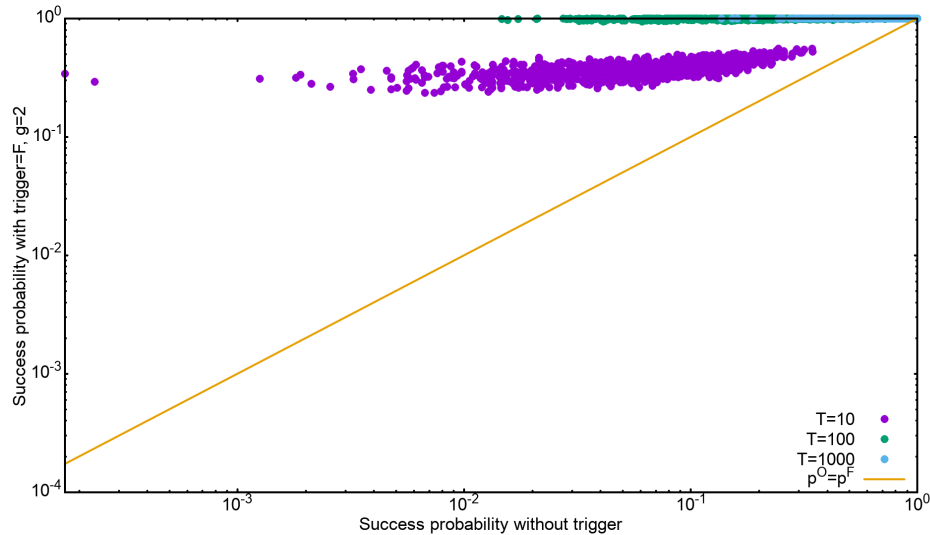


Figure 4.13: Scatter plot for the success probability after adding ferromagnetic trigger with $g=2$ against the success probability of the original Hamiltonian, for annealing time $T_A \in \{10, 100, 1000\}$. The solid line represents the limit where the success probability remains unchanged.

For all the three cases, and all the problems in the set, the success probability after adding the trigger was found to be greater than the success probability of the original Hamiltonian. Since in the adiabatic regime, the overlap of the final state with the ground state increases with increasing the annealing times, the success probability of the original Hamiltonians with long annealing times ($T_A=1000$) is already large (≈ 1). Adding the ferromagnetic trigger can therefore not improve the success probability too much. This explains the confinement of the points representing the success probability for $T_A=1000$ close to the solid line ($p^O = p^F$) on the upper right corner for all the three values of the strength parameter. Owing to the same reason, the points corresponding to the success probability for $T_A=10$ have a much larger spread. For the easy cases (larger p^O), the success probability upon adding the trigger (p^F) has a similar value. Such points lie close to the line. On the other hand, for more difficult cases (smaller p^O) the improvement can be larger, and such points lie away from the line.

Furthermore, since for a given problem, increasing the strength of the ferromagnetic trigger makes the minimum gaps larger, the success probability for that case also becomes larger. This explains the distribution of the points getting successively more flat with increasing strength of the trigger, for all annealing times (see Figs. 4.11, 4.12 and 4.13).

Finally, we look at the dynamics of the evolution. According to Eq. (2.4), for an adiabatic evolution of the state of the system, the success probability, p , i.e. the measure of the overlap of the final state with the ground state of the Hamiltonian, is related to the minimum energy gap, Δ_{min} as follows:

$$p = 1 - \exp(-C\Delta_{min}^2), \quad (4.1)$$

for some constant C . Since different problems in the problem set correspond to different minimum energy gaps, a plot of the success probability with these gaps should follow Eq. (2.4) if the evolution of the state for a problem is adiabatic. Moreover, adding the trigger changes the energy spectra, and thereby the minimum energy gaps of these problems. Fig. (4.14) shows the success probability versus the minimum energy gap plot for all the problems upon adding the ferromagnetic trigger with three different strengths (0.5, 1 and 2), and for three annealing times (10, 100 and 1000).

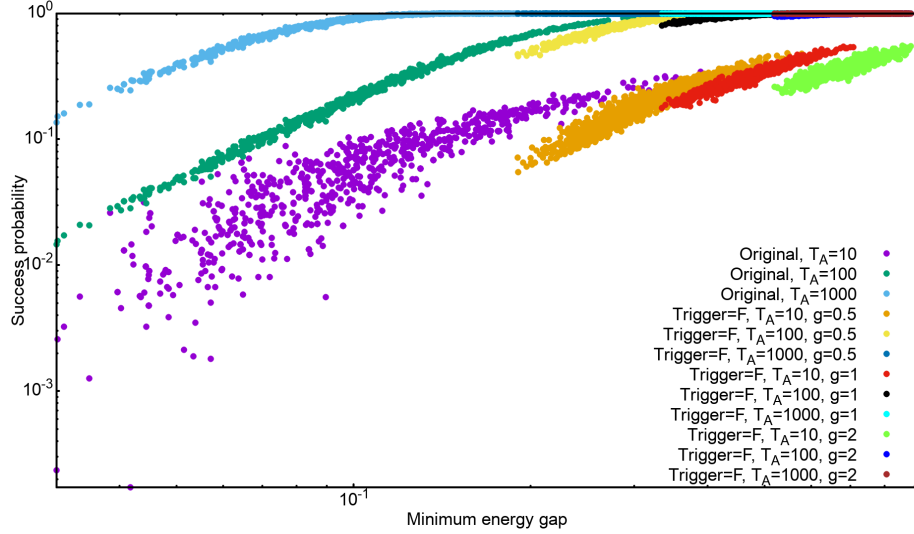


Figure 4.14: Plot of the success probability versus minimum energy gaps for all the problems belonging to the set. The plot shows the effect of adding ferromagnetic trigger to the original Hamiltonian with strengths 0.5, 1 and 2, while the annealing time is chosen to 10, 100 and 1000.

From the Fig.(4.14) it can be noted that all the curves roughly follow the Landau-Zener dependence (see Eq. (2.4)) of the success probability on the minimum energy gaps. However, for the original Hamiltonian, and $T_A=10$, the scattering is larger compared to the other curves. The scattering of the curves decreases on increasing the annealing times, suggesting that longer annealing times ascertain the evolution of the state to be adiabatic. Since adding the ferromagnetic trigger enlarges the minimum energy gaps, the curves are shifted to the right upon adding the trigger and increasing their strength.

Chapter 5

Results with Anti-ferromagnetic Trigger

This chapter will focus on the effects on the performance of quantum annealing algorithm upon adding the second trigger, namely the anti-ferromagnetic trigger, to the original Hamiltonian. Unlike in the case of the ferromagnetic trigger, for anti-ferromagnetic trigger the strength parameter, g in equation (1.10) plays a more decisive role than merely controlling the extent by which the minimum gap is enlarged. The anti-ferromagnetic trigger alters the energy spectra, the minimum energy gaps, and the number of anti-crossings between the ground and first excited energy state of the Hamiltonian, depending on the strength with which the trigger is added, as well as on the problem itself. We shall begin by observing the effects of adding the anti-ferromagnetic trigger to the original Hamiltonian, for the three chosen problems. The following sections will then showcase the role that the strength parameter - g plays.

The chosen problems

Let us begin by considering the first chosen case, with largest success probability.

Figures (5.1), (5.2) and (5.3) show the energy spectra and the instantaneous energy values after adding the anti-ferromagnetic trigger to the first chosen case, with strengths 0.5, 1 and 2 respectively.

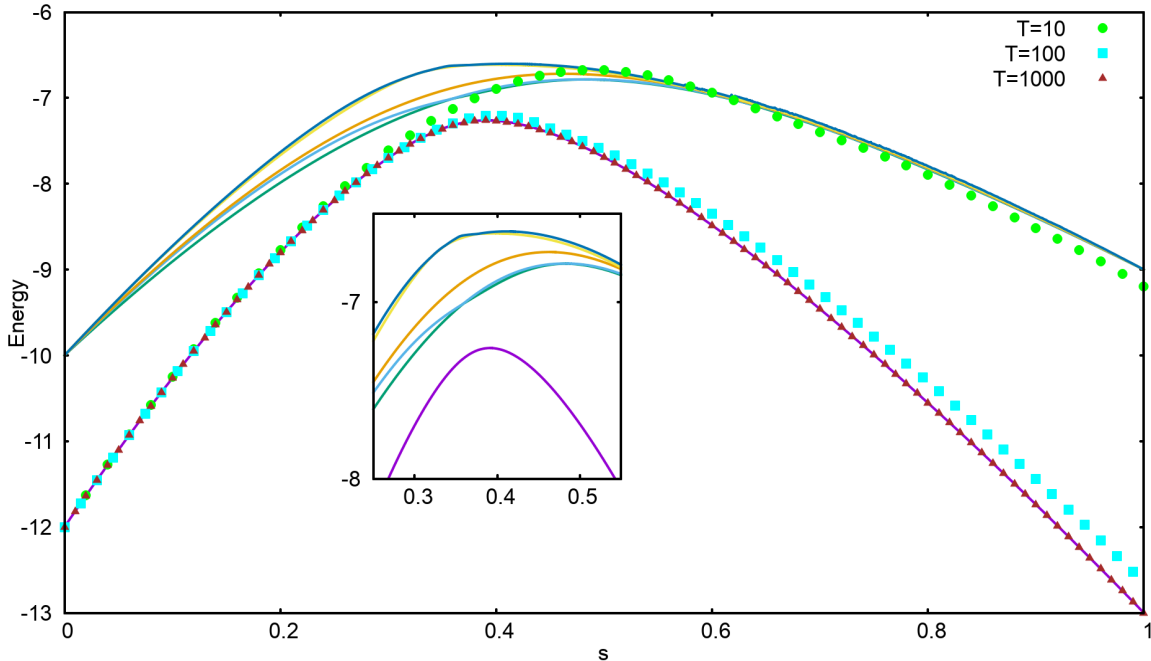


Figure 5.1: The energy spectrum for the first problem, with instantaneous energy values corresponding to three annealing times, with Anti-ferromagnetic trigger, and $g=0.5$. Δ_{min} was found to be 0.3070, while $p=0.9117$ for $T_A=100$.

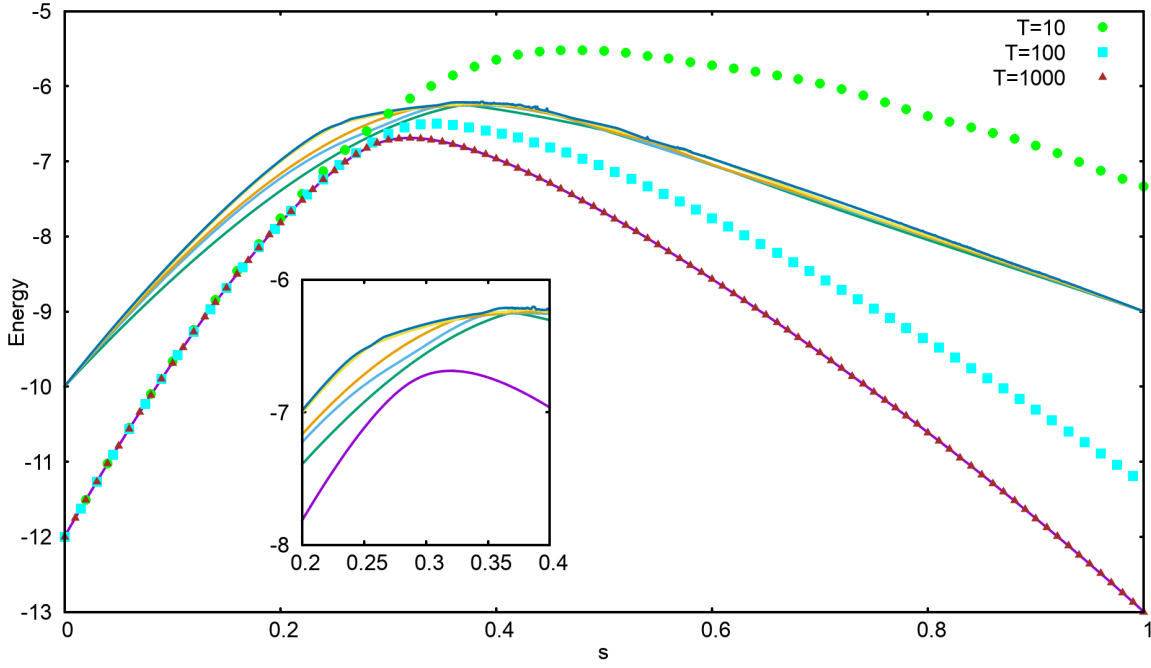


Figure 5.2: The energy spectrum for the first problem, with instantaneous energy values corresponding to three annealing times, with Anti-ferromagnetic trigger, and $g=1$. Δ_{min} was found to be 0.1349, while $p=0.5747$ for $T_A=100$.

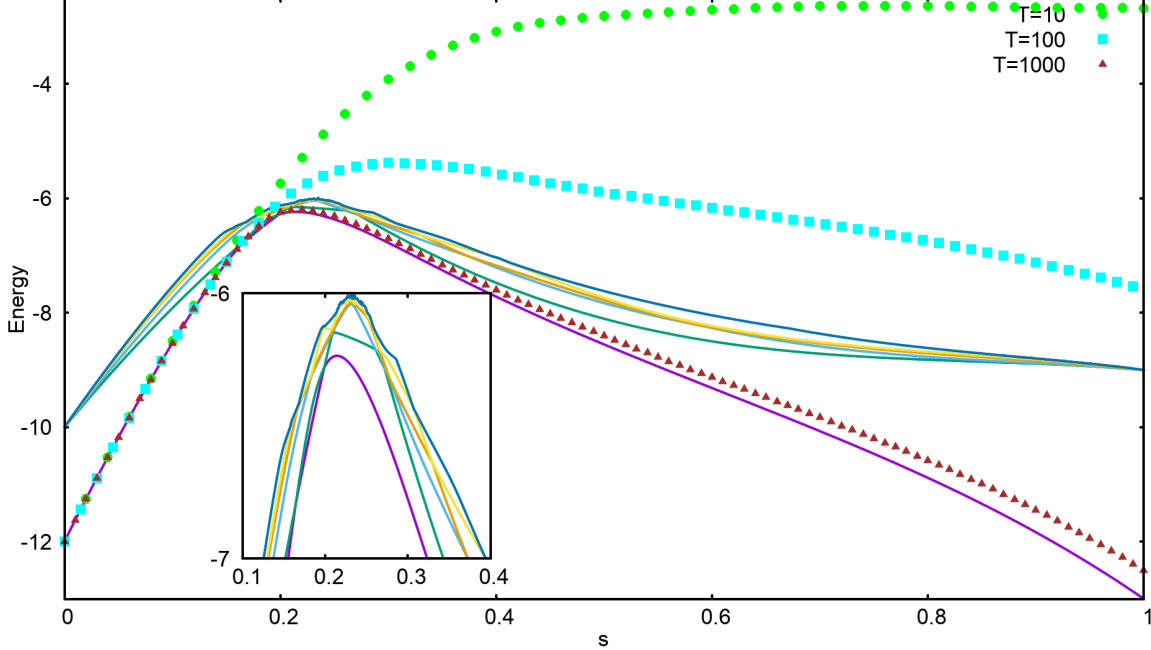


Figure 5.3: The energy spectrum for the first problem, with instantaneous energy values corresponding to three annealing times, with Anti-ferromagnetic trigger, and $g=2$. Δ_{min} was found to be 0.0020, while $p=0.0273$ for $T_A=100$.

Table (5.1) shows a comparison of the success probabilities - p , and minimum energy gaps - Δ_{min} between the original Hamiltonian and the Hamiltonian after adding the anti-ferromagnetic triggers with different strengths.

CASE 1	Original Hamiltonian	Trigger=A, g=0.5	Trigger=A, g=1	Trigger=A, g=2
Δ_{min}	0.4407	0.3070	0.1349	0.0020
$p(T_A=10)$	0.3444	0.1446	0.0279	1.271×10^{-4}
$p(T_A=100)$	0.0044	0.9117	0.5747	0.0273
$p(T_A=1000)$	0.9999	0.9999	0.9999	0.8761
s value at Δ_{min}	0.459	0.367	0.282	0.254
Number of anti-crossings	1	2	1	4

Table 5.1: A comparison of the minimum gaps and the success probabilities for the first chosen case, between the original Hamiltonian and and the Hamiltonian with anti-ferromagnetic trigger (A) of different strengths. The minimum gaps become successively smaller as the strength of the anti-ferromagnetic trigger is increased. The success probabilities are decreased as a result. The value of s corresponding to the position of the minimum gap also becomes smaller.

As can be noted from the table above, the minimum energy gap decreases upon adding the ferromagnetic trigger, and this decrease becomes larger as the strength of the trigger is increased. Consequently, the success probabilities (after adding the trigger) are found to be decreasing as well. The value of annealing parameter - s also become smaller with increasing strength of the trigger. A new feature observed after adding the anti-ferromagnetic trigger is the change in the number of anti-crossings between the ground and the first energy state. For strengths g=0.5 and g=2, the number of energy anti-crossings increase to 2 and 4 respectively, while for g=1 it remains unchanged. Moreover, when the anti-ferromagnetic trigger is added with strength 2, the energy spectrum changes quite drastically in comparison to the original spectrum (??), as can be more clearly seen in the inset of figure (5.3).

Next, let us consider the second chosen problem that had small success probability in absence of any triggers. Figures (5.4), (5.5), and (5.6) show the energy spectrum and the instantaneous energy values corresponding to three annealing times.

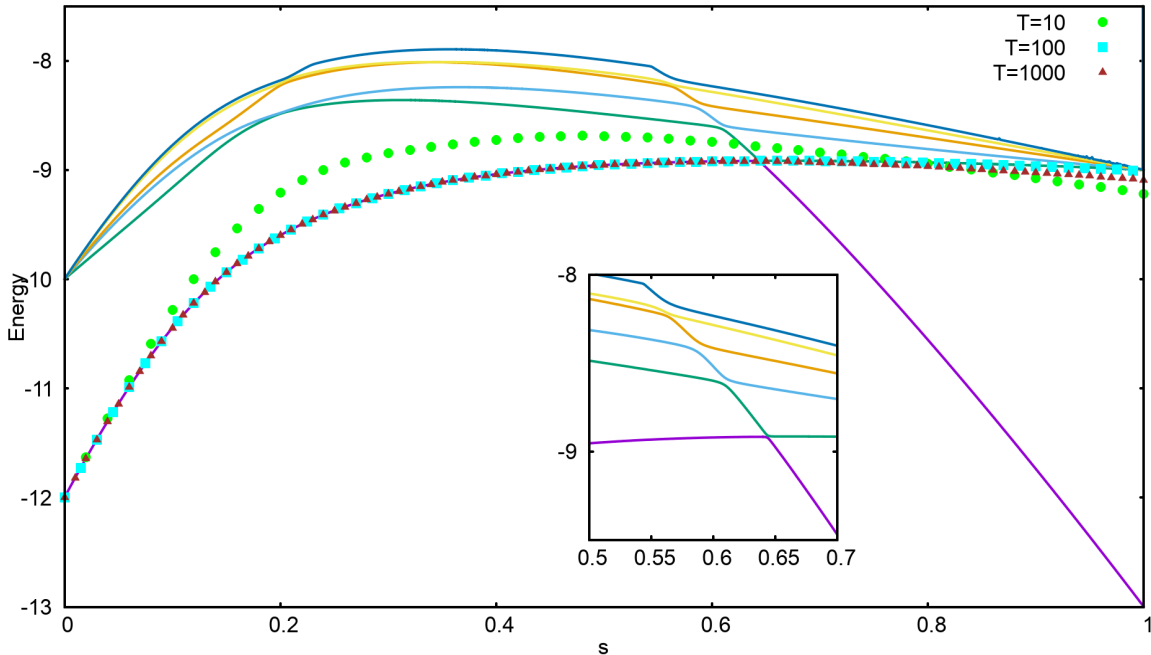


Figure 5.4: The energy spectrum for the second problem, with instantaneous energy values corresponding to three annealing times, with Anti-ferromagnetic trigger, and $g=0.5$. Δ_{min} was found to be 0.0130, while $p=0.0022$ for $T_A=100$.

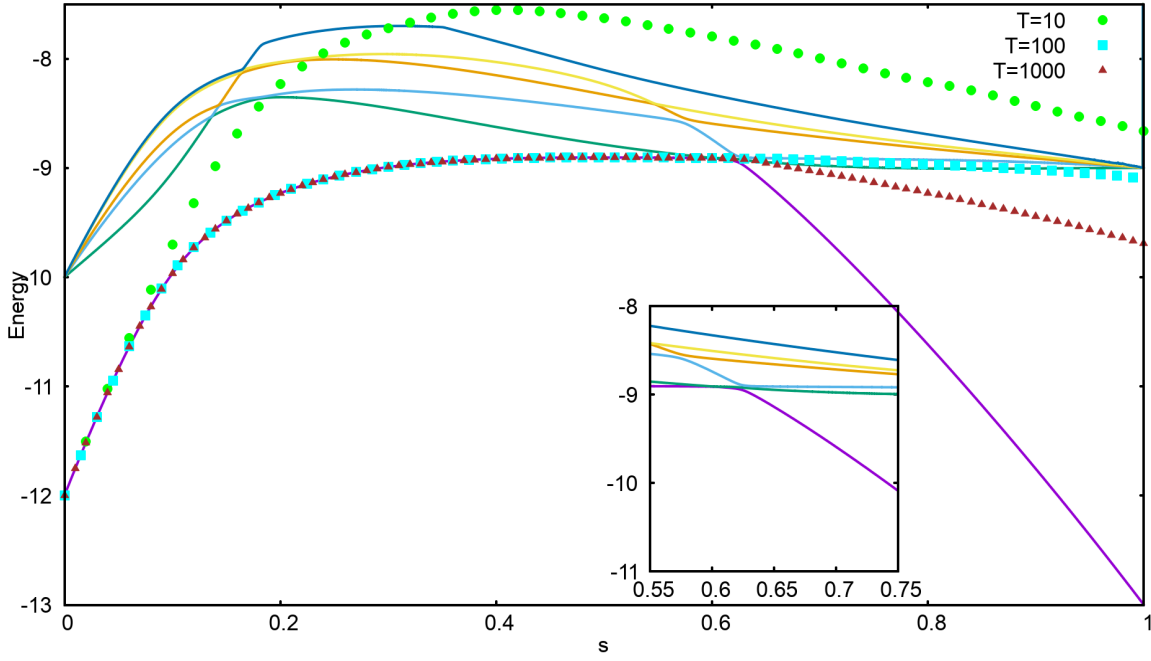


Figure 5.5: The energy spectrum for the second problem, with instantaneous energy values corresponding to three annealing times, with Anti-ferromagnetic trigger, and $g=1$. Δ_{min} was found to be 0.0019, while $p=0.0239$ for $T_A=100$.

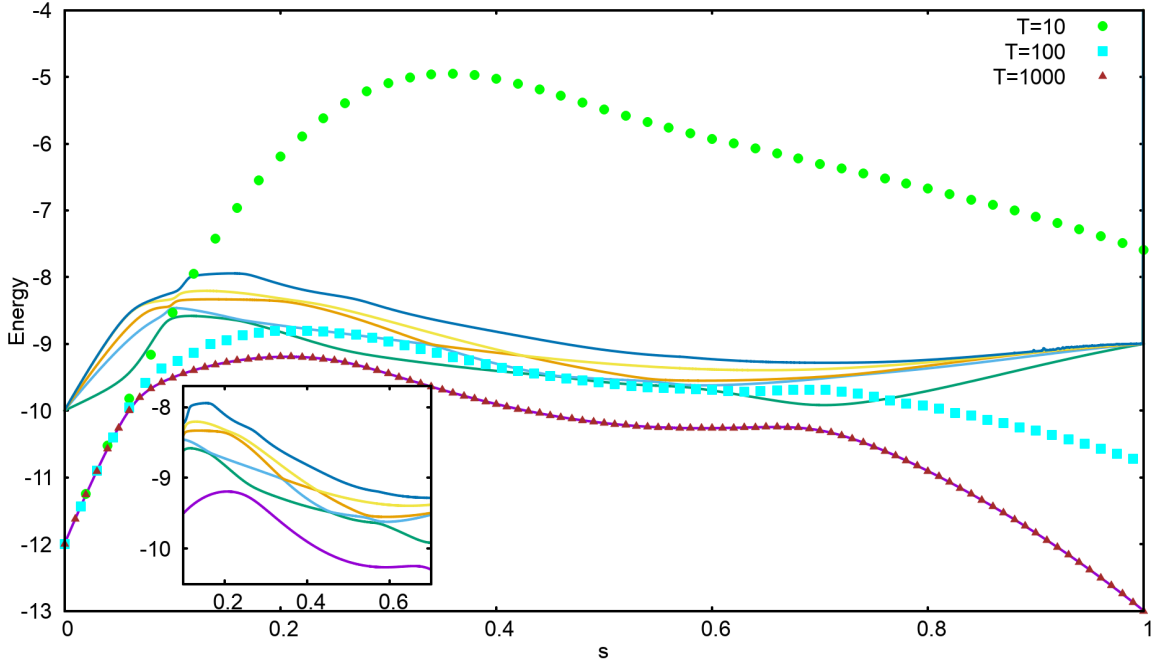


Figure 5.6: The energy spectrum for the second problem, with instantaneous energy values corresponding to three annealing times, with Anti-ferromagnetic trigger, and $g=2$. Δ_{min} was found to be 0.1784, while $p=0.4468$ for $T_A=100$.

For this case, table (5.2) shows a comparison of the minimum energy gaps, and success probabilities (corresponding to different annealing times) between the original Hamiltonian and the Hamiltonian upon adding the anti-ferromagnetic trigger with different strengths.

CASE 2	Original Hamiltonian	Trigger=A, g=0.5	Trigger=A, g=1	Trigger=A, g=2
Δ_{min}	0.0312	0.0130	0.0019	0.1784
$p(T_A=10)$	2.343×10^{-4}	0.0567	0.0017	0.0071
$p(T_A=100)$	0.0146	0.0022	0.0239	0.4468
$p(T_A=1000)$	0.1362	0.0228	0.1729	0.9999
s value at Δ_{min}	0.665	0.644	0.601	0.263
Number of anti-crossings	1	1	2	3

Table 5.2: A comparison of the minimum gaps and the success probabilities for the second chosen case, between the original Hamiltonian and and the Hamiltonian with anti-ferromagnetic trigger (A) of different strengths. The minimum gap becomes small for $g=0.5$, and even smaller for $g=1$, while it becomes even larger than the original minimum energy gap for $g=2$. The value of s corresponding to the position of the minimum gap becomes smaller with increasing strength of the trigger.

The minimum energy gaps decrease with respect to the original energy gaps upon adding the trigger with strengths 0.5, and 1. However, the success probability at $T_A=10$ for anti-ferromagnetic trigger with $g=0.5$ and $g=1$ is larger compared to that of the original Hamiltonian, owing to different reasons.

Since upon adding the anti-ferromagnetic trigger with strength 0.5, the minimum energy gap becomes smaller, the annealing time of $T_A=10$ is so short that the state of the system transits to the first excited state even before the minimum gap anti-crossing. Upon approaching the minimum gap anti-crossing the system state shifts some of the amplitude back to the ground state, increasing the success probability in this case (figure 5.4). However, for the original Hamiltonian the gap is large enough for an annealing time of 10 for the state to not shift to the first excited state before the minimum energy gap (figure ??). The state therefore stays close to the first excited state after passing the anti-crossing. Furthermore, for annealing times $T_A=100$ and $T_A=1000$, the system state transitions only at the minimum gap anti-crossing and closely follows the second and first excited states respectively. The overlap with the ground state decreases, and therefore the success probability in both these cases also reduces.

For the other case - with anti-ferromagnetic trigger with strength 1, the number of energy anti-crossings increases to 2. The first energy anti-crossing is small enough for just $T_A=10$ to shift the system state to the first excited state. Quickly after transitioning to the first excited state, the system state shifts to higher energy levels (figure 5.5). Since the state of the system is a superposition of many energy eigenstates, the present state of system has small, yet finite overlap with the ground state. In the original Hamiltonian, however, the system state shifts to the first excited state at the only energy anti-crossing, and therefore the overlap with the ground state becomes negligible (figure ??).

By choosing the strength to be 2, the minimum energy gap of this problem becomes larger than the original minimum energy gap, while the number of anti-crossings between the ground and the first excited state increases to 3. The success probability in this case is always larger than the original success probability for all annealing times. For $T_A=10$, the state of the system shifts to the first excited state at first energy anti-crossing, and then quickly shifts to a superposition state with the higher energy states. This results in a larger overlap with the ground state compared to the case of the state closely following the first excited state after reaching the only energy anti-crossing in case of the original problem (??).

For $T_A=100$, the state starts transitioning to the first excited state only as it approaches the second energy anti-crossing. The state does further shift to higher energy levels, but comes back to the first excited state before the third energy anti-crossing. After passing by the third anti-crossing some of the amplitude of the wave function shifts to the ground state again, and therefore the success becomes larger than the original problem.

Finally, for $T_A=1000$, the annealing time and the minimum energy gap is large enough for the system to always stay close to the ground state, hence the larger success probability.

Lastly, figures (5.7), (5.8) and (5.9) show the energy spectra and instantaneous energy values for the third problem, after adding the anti-ferromagnetic trigger with strengths 0.5, 1 and 2 respectively.

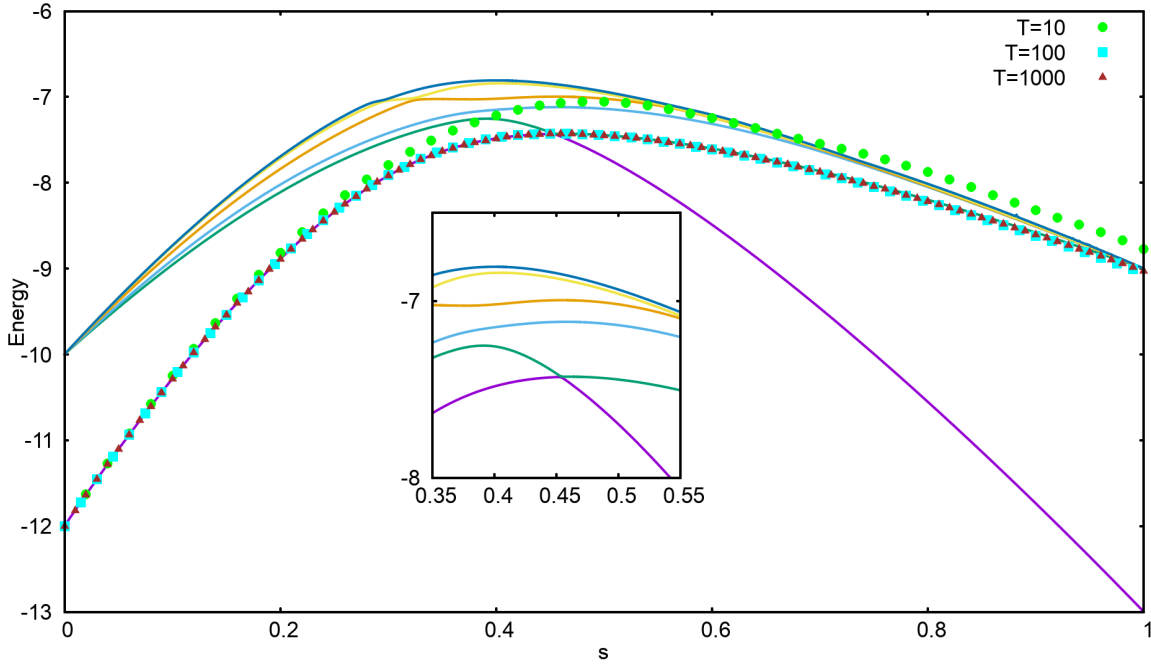


Figure 5.7: The energy spectrum for the third problem, with instantaneous energy values corresponding to three annealing times, with Anti-ferromagnetic trigger, and $g=0.5$. Δ_{min} was found to be 0.0049, while $p=0.0120$ for $T_A=100$.

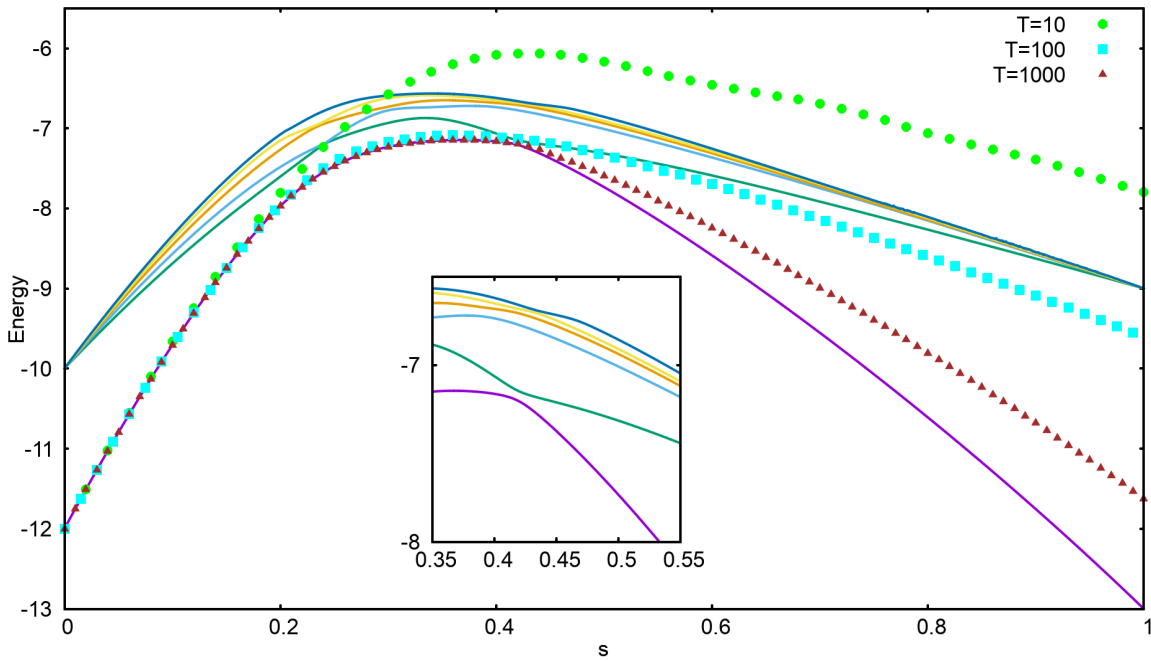


Figure 5.8: The energy spectrum for the third problem, with instantaneous energy values corresponding to three annealing times, with Anti-ferromagnetic trigger, and $g=1$. Δ_{min} was found to be 0.0562, while $p=0.1517$ for $T_A=100$.

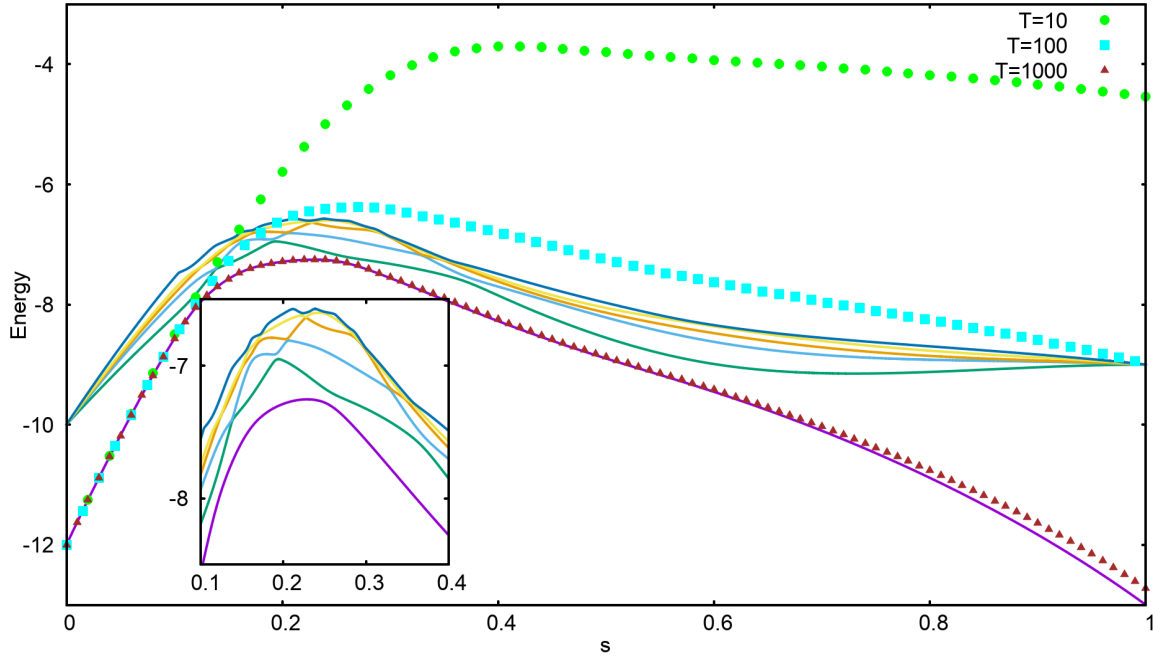


Figure 5.9: The energy spectrum for the third problem, with instantaneous energy values corresponding to three annealing times, with Anti-ferromagnetic trigger, and $g=2$. Δ_{min} was found to be 0.1008, while $p=0.0480$ for $T_A=100$.

Table (5.3) shows a comparison of the minimum energy gaps, and success probabilities (corresponding to different annealing times) between the original Hamiltonian and the Hamiltonian upon adding the anti-ferromagnetic trigger with different strengths.

CASE 3	Original Hamiltonian	Trigger=A, g=0.5	Trigger=A, g=1	Trigger=A, g=2
Δ_{min}	0.1573	0.0049	0.0562	0.1008
$p(T_A=10)$	0.1577	0.0573	0.0368	4.21×10^{-5}
$p(T_A=100)$	0.5199	0.0120	0.1517	0.0480
$p(T_A=1000)$	0.9992	0.0071	0.6565	0.9313
s value at Δ_{min}	0.514	0.454	0.418	0.256
Number of anti-crossings	1	1	3	4

Table 5.3: A comparison of the minimum gaps and the success probabilities for the third chosen case, between the original Hamiltonian and the Hamiltonian with anti-ferromagnetic trigger (A) of different strengths. The minimum energy gaps after adding the trigger are smaller than the original minimum gap, for all the values of g . They however become large upon increasing the strength of the anti-ferromagnetic trigger. The value of s corresponding to the position of the minimum gap becomes smaller with increasing strength of the trigger.

For this problem, it was observed that adding the anti-ferromagnetic trigger made the minimum energy gaps smaller than the original gap, for all the three values of the strength chosen. The gaps however increased with increasing the strength of the trigger. The original success probabilities, for all annealing times, are therefore larger than the resulting success probabilities upon adding the triggers with different g . Additionally, for all annealing times but $T_A=10$, the success probabilities become larger when the anti-ferromagnetic trigger is added with strength 1 compared to when added with strength 0.5, as the minimum energy gap for the former is larger. For $T_A=10$, and both $g=0.5$ and $g=1$ cases, the system state transitions to the first excited state prior to the first energy anti-crossing. This is followed by the state shifting to higher energy levels soon after. Since the energy spectrum becomes more complex (in terms of the number of anti-crossings between the higher energy states and their proximity,) as

the strength of the trigger is increased, the system state shifts farther away from the ground state. Consequently, the success probability decreases in the case with $g=0.5$.

Although the gap becomes even larger with $g=2$, the success probability is smaller compared the case with $g=1$. This can be explained by observing that adding the anti-ferromagnetic trigger with $g=2$ changes the energy spectrum of the Hamiltonian even more drastically. Not only do the number of anti-crossings between the ground and the first excited state increase to 4, the higher lying energy levels also become more involved and have larger number of anti-crossings. Hence, as annealing times $T_A=10$ and $T_A=100$ are not large enough for the state to stay close to the ground state upon reaching the first energy anti-crossing, the system state settles even farther away from the ground state as compared to the $g=1$ case. Hence, the success probability for $T_A=10$ and $g=2$ case is negligible. As the annealing time is increased further to $T_A=1000$, the minimum energy gap becomes large enough to keep the state of the system close to the ground state, and the success probability becomes comparable to the original success probability.

g=0.5

This section will focus on the performance of the quantum annealing algorithm upon adding the anti-ferromagnetic trigger to each of the original Hamiltonian from 12-spin SAT problems, with strength 0.5. For each problem, annealing time was chosen to be 10, 100 and 1000.

As a measure of quantifying the performance with respect to the original Hamiltonian, a metrics Relative success probability was defined as the ratio of the success probability upon adding the anti-ferromagnetic trigger (p^A) to the original success probability (p^O). Figures (5.10), (5.11) and (5.12) show the distribution of the relative success probability for annealing times of 10, 100 and 1000 respectively, with the strength of the trigger Hamiltonian chosen to be 0.5.

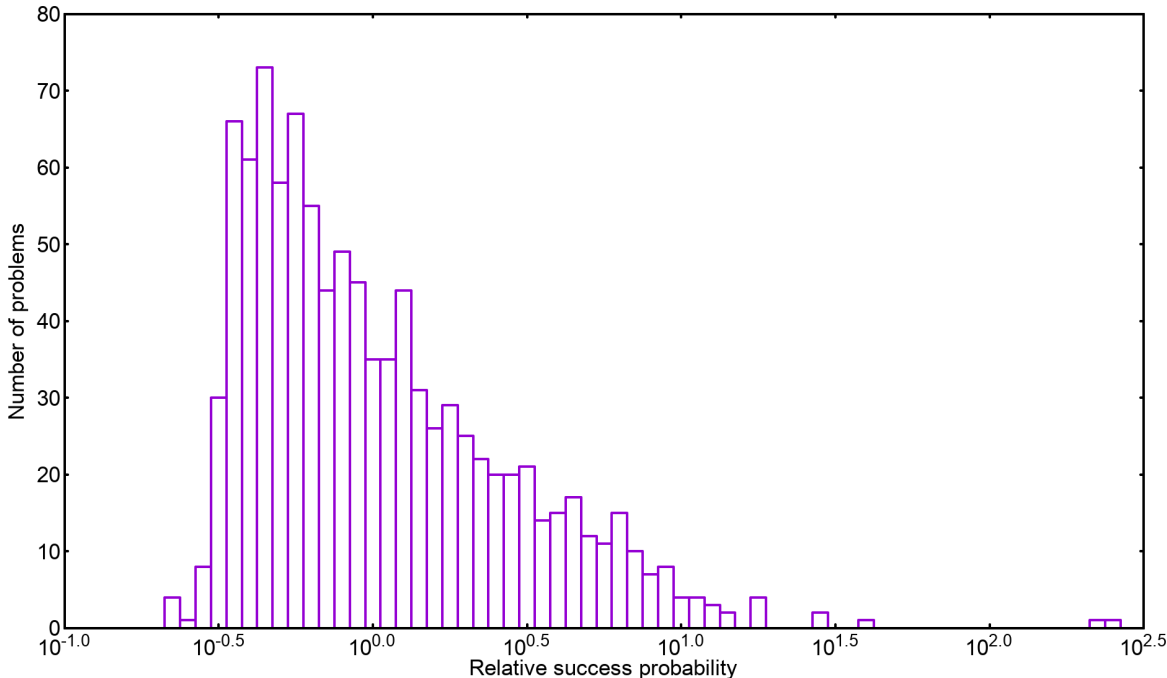


Figure 5.10: The distribution of relative success probability $\frac{p^A}{p^O}$ for $g=0.5$ and $T_A=10$. 43.9% of the cases were found to have a higher success probability after adding the trigger.

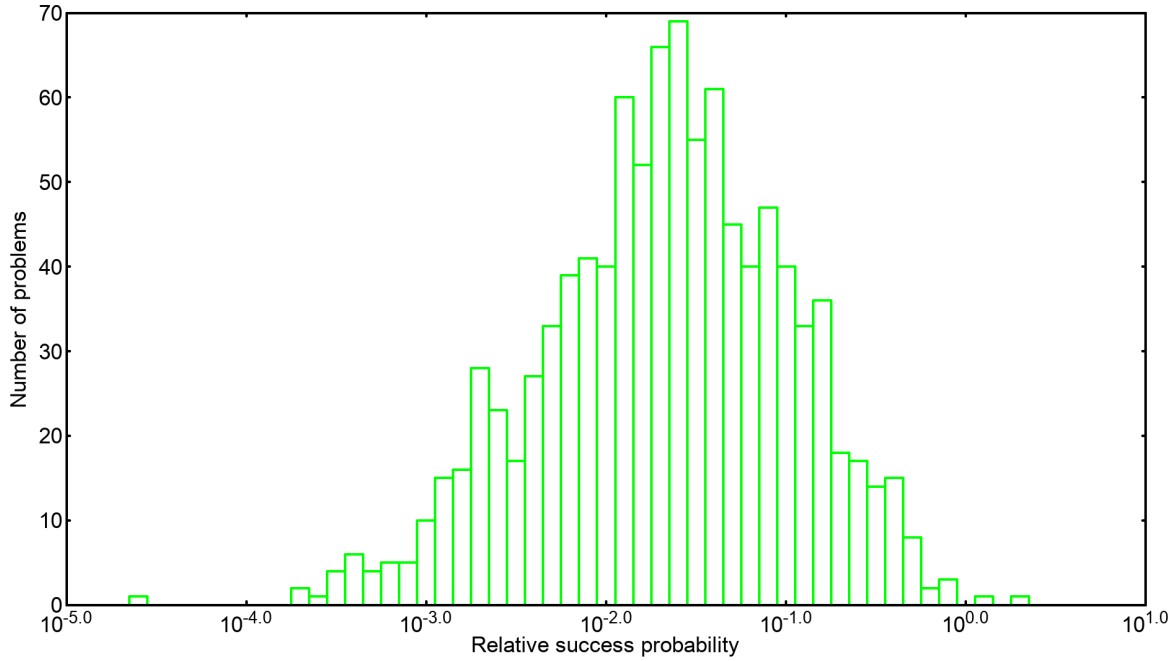


Figure 5.11: The distribution of relative success probability $\frac{p^A}{p^O}$ for $T_A=100$. 0.2% of the cases were found to have a higher success probability after adding the trigger.

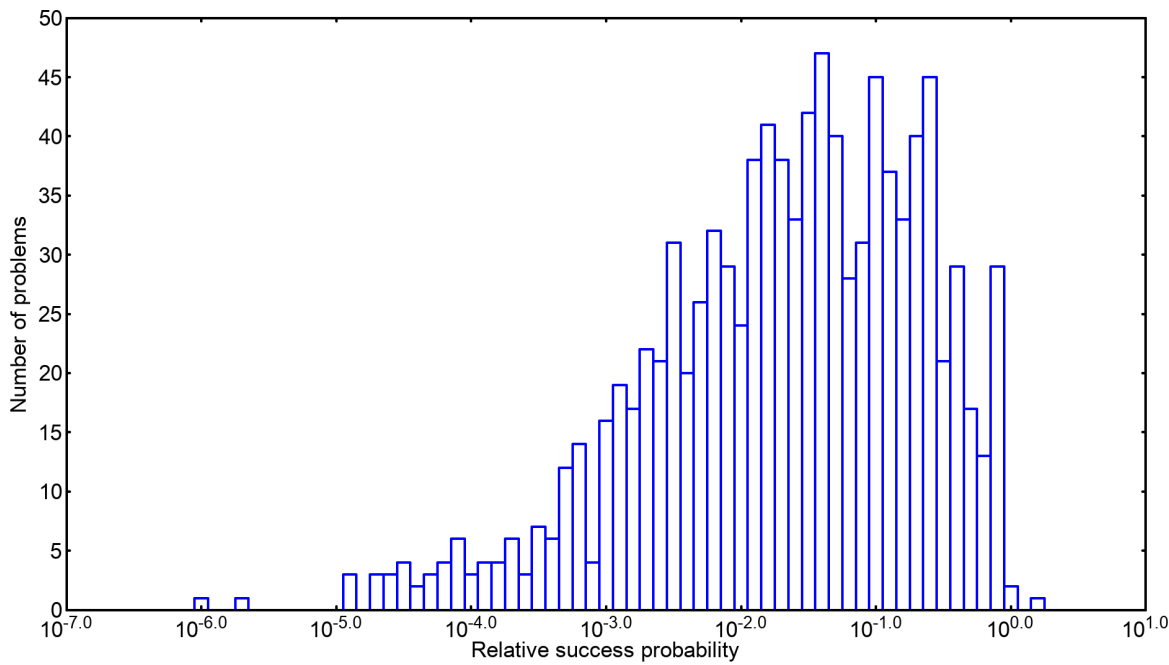


Figure 5.12: The distribution of relative success probability $\frac{p^A}{p^O}$ for $T_A=1000$. 0.2% of the cases were found to have a higher success probability after adding the trigger.

For an annealing time $T_A=10$, it was found that 43.9% of the problems of the set were improved after the anti-ferromagnetic trigger with $g=0.5$. On increasing the annealing time to 100 and 1000, the percentage of cases with improved success probability dropped to 0.2% for both the cases. Furthermore, the largest value of the relative success ratio is a little more than 250 for $T_A=10$, while it reduces to 1.995 for $T_A=100$, and to 1.585 for $T_A=1000$. In

order to understand the reasons for this decrease in the performance on increasing the annealing time, the minimum energy gaps of all the problems were calculated after adding the trigger. Figure (5.13) shows a plot of the minimum energy gaps after adding the anti-ferromagnetic trigger (Δ_{min}^A) with the original minimum energy gaps (Δ_{min}^O).

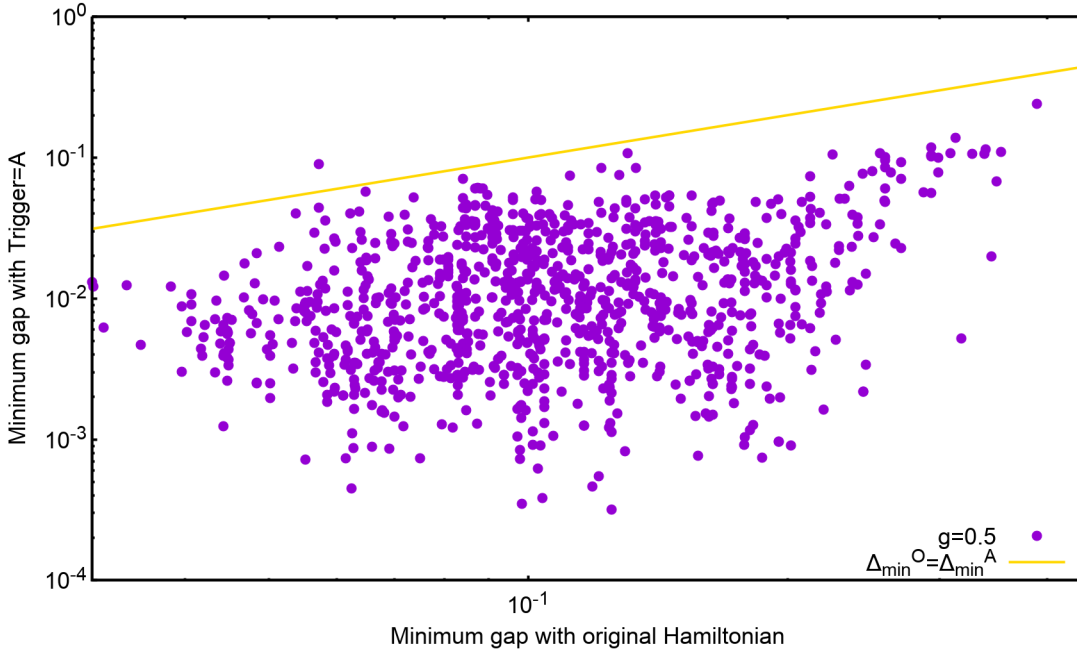


Figure 5.13: A plot of the minimum energy gaps after adding the anti-ferromagnetic trigger with $g=0.5$ (Δ_{min}^A), with the original minimum energy gaps (Δ_{min}^O). For 99.9% of the minimum energy gap was found to have decreased after adding the trigger.

As is clear from figure (5.13), for 99.9% of the cases, the minimum energy gaps reduce after adding the anti-ferromagnetic trigger with strength 0.5. Additionally, it was found that 92.3% of all the cases still had a single anti-crossing between the ground and the first excited state, while for the other 7.7% of the cases, it increased to 2.

For shorter annealing times, like $T_A=10$, the success probability can benefit because of two reasons. As seen in the second chosen problem in the previous section, for small minimum energy gaps, and smaller annealing times, the state of the system can shift to the first excited state prior to the minimum gap anti-crossing. The overlap with the ground state can then increase because of the following non-adiabatic processes:

- If there are no higher energy states close to the state of the system, the wave function of the state can transfer some amplitude back to the ground state, at one of the anti-crossings.
- If the higher energy states come close to the system state, before it approaches the energy anti-crossing, the system state can further transit to a superposition state of the higher energy levels. This might increase the overlap of the state with the ground state compared to the case where the state closely follows the first excited state after crossing the energy anti-crossing.

Thus, when the annealing time is increased to 100 or 1000, the state of the system stays close to the ground state till it reaches the energy anti-crossing, and transitions to the first excited state afterwards. This explains the drop in the percentage of improved cases upon increasing the annealing time and adding the anti-ferromagnetic trigger.

To get an estimate of the difficulty of the affected problems, figure (5.14) shows the scatter plot of the success probabilities after adding the trigger with the original success probabilities, for the three annealing times. It should be noted that the 43.9% of the problems improved upon by adding anti-ferromagnetic trigger for $T_A=10$, are the ones that had relatively smaller original success probabilities (harder problems with smaller minimum energy gaps). Adding the anti-ferromagnetic trigger reduces the minimum energy gap, thereby increasing the success probability by either of the two mechanisms listed above.

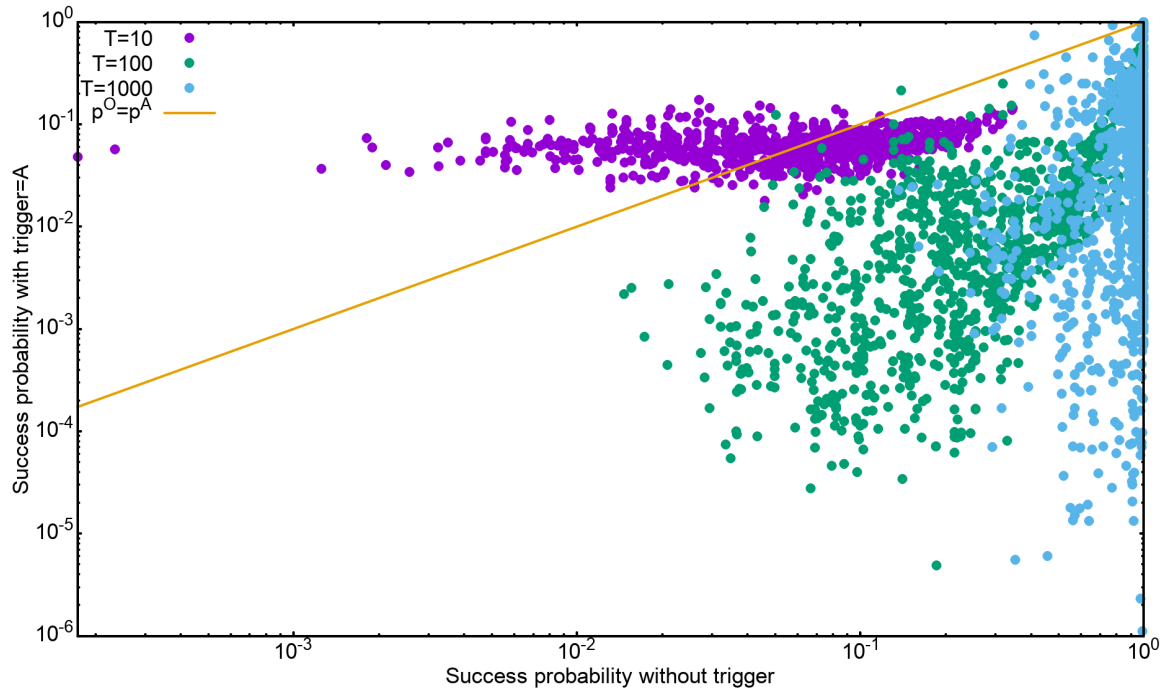


Figure 5.14: A plot of the success probabilities after adding the anti-ferromagnetic trigger with $g=0.5$ (p^A), with the original success probabilities(p^O) for annealing time 10, 100 and 1000.

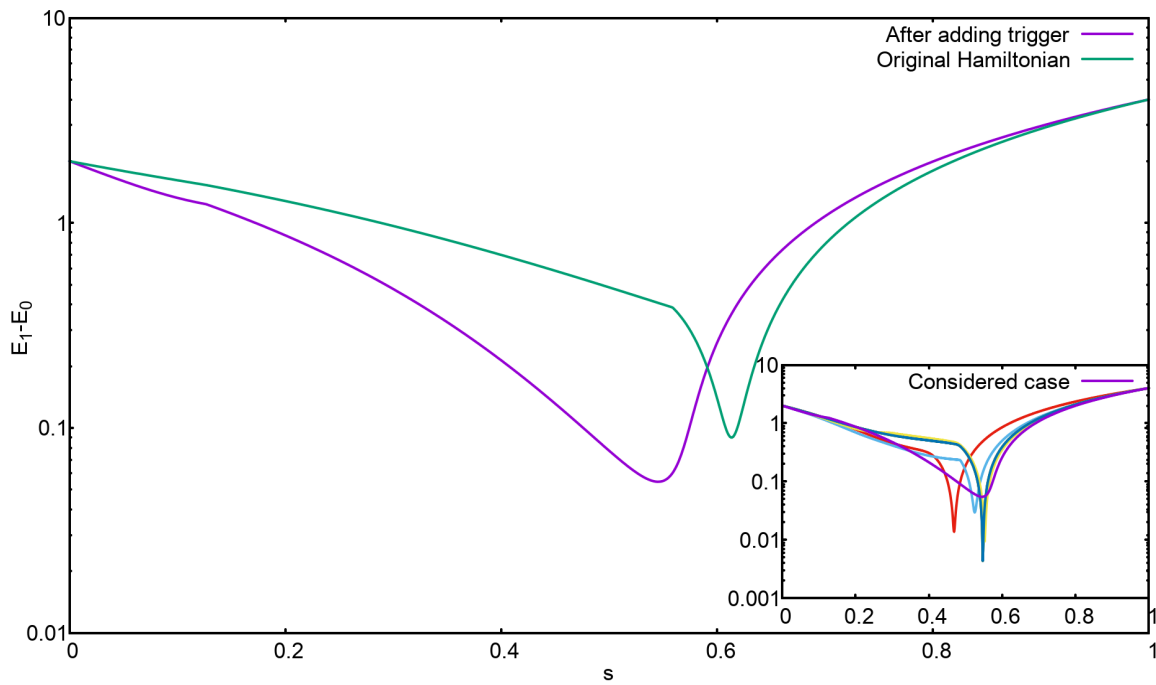


Figure 5.15: Considered here is the case with increased success probability in spite of a decrease in the minimum energy gap. The energy gap between the two lowest energy levels is compared for this case with that in the original case. The inset shows a comparison with some other problems after adding the trigger. The key difference for the considered case is that the slope of the curve is not symmetric about the point of minimum gap, unlike all other cases.

It should also be noted that for $T_A=100$ and $T_A=1000$, the original success probabilities are already quite high,

giving way to another reason for the decrease in the relative success probability with increasing annealing time.

For both $T_A=100$ and $T_A=1000$ the two problems that had a higher success probability after adding the anti-ferromagnetic trigger, were indeed the same. One of these problem happened to be the only problem that had a larger minimum energy gap upon adding the anti-ferromagnetic trigger, and hence the increase in the success probability.

For the other problem, figure (5.15) shows the energy gap between the ground energy level and the first excited state of the Hamiltonian (as a function of the annealing parameter), before and after adding the anti-ferromagnetic trigger. The inset of the figure also shows the energy gaps for some other problems after adding the trigger. As can be observed in the figure, the shape of the curve for the case with larger success probability (in spite of the decrease in the minimum energy gap) is different from both the original Hamiltonian and the other problems. The slope in this case, unlike the other cases, is not symmetric about the minimum gap value. While comparing the

success probabilities across different problems (and assuming $p = 1 - e^{-\frac{-T\Delta^2}{c}}$), the slope (c) for each problem was supposed to have a similar structure and only changes in the minimum gaps were accounted for. Since this assumption breaks down for this case, the success probability deviates from the expected value.

Finally, for checking if the dynamics during the evolution of the state under the action of the anti-ferromagnetic trigger is adiabatic, equation (2.4) should be verified, as was done in the last chapter. We plotted the success probability against the minimum energy gaps for all the problems of the set, before and after adding the ferromagnetic trigger, for all the three annealing times. The resulting plot is shown in figure (5.16).

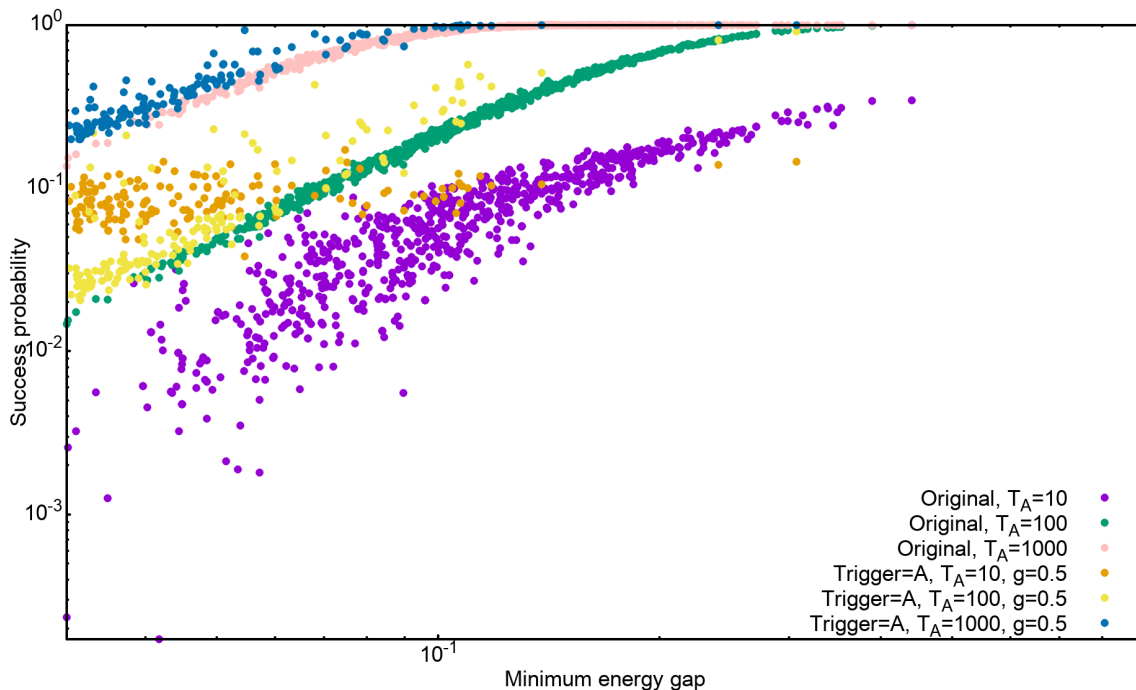


Figure 5.16: Success probability versus minimum energy plot for all the problems belonging to the set of 12-spin SAT problems, for annealing times 10, 100 and 1000, in the absence and presence of ferromagnetic trigger.

It can be noted from figure (5.16) that the original success probabilities mostly follow the exponential dependence on minimum energy gaps, although the scattering for $T_A=10$ is comparatively large. As the annealing time is increased, the curve becomes more defined. However, upon adding the trigger, the scattering becomes even larger, so that the points corresponding to $T_A=10$ appear rather flat. Also, for smaller gaps, these points have a higher success probability than the points corresponding to $T_A=100$, due to non-adiabatic evolution. Although in this case too the curves become successively more defined by increasing the annealing time, the general effect of adding the trigger with strength $g=0.5$ is to shift the data points leftwards by reducing the minimum energy gaps, and thus limiting the performance.

g=1

In this section, the same analysis will be shown as in the last section but with the value of the strength parameter set to 1. We begin by showing the distribution of the relative success probability after adding the anti-ferromagnetic trigger with g=1, for annealing times 10, 100 and 1000, in figures (5.17), (5.18) and (5.19) respectively.

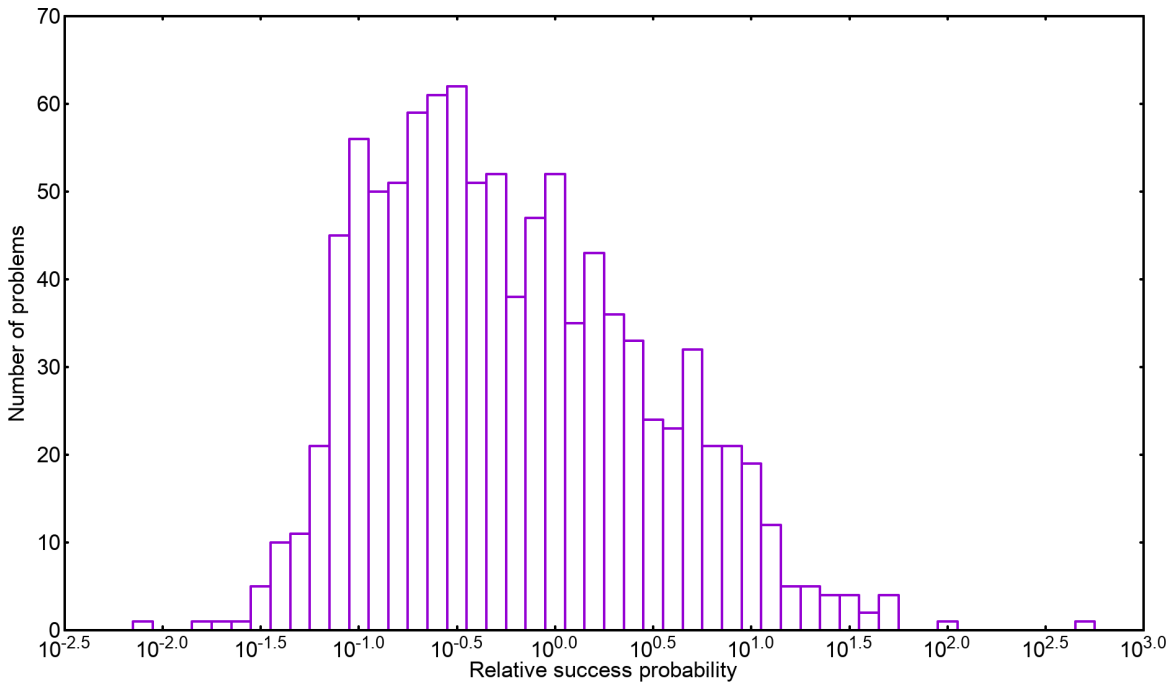


Figure 5.17: The distribution of relative success probability $\frac{p^A}{p^O}$ for $T_A=10$. 37.7% of the cases were found to have a higher success probability after adding the trigger.

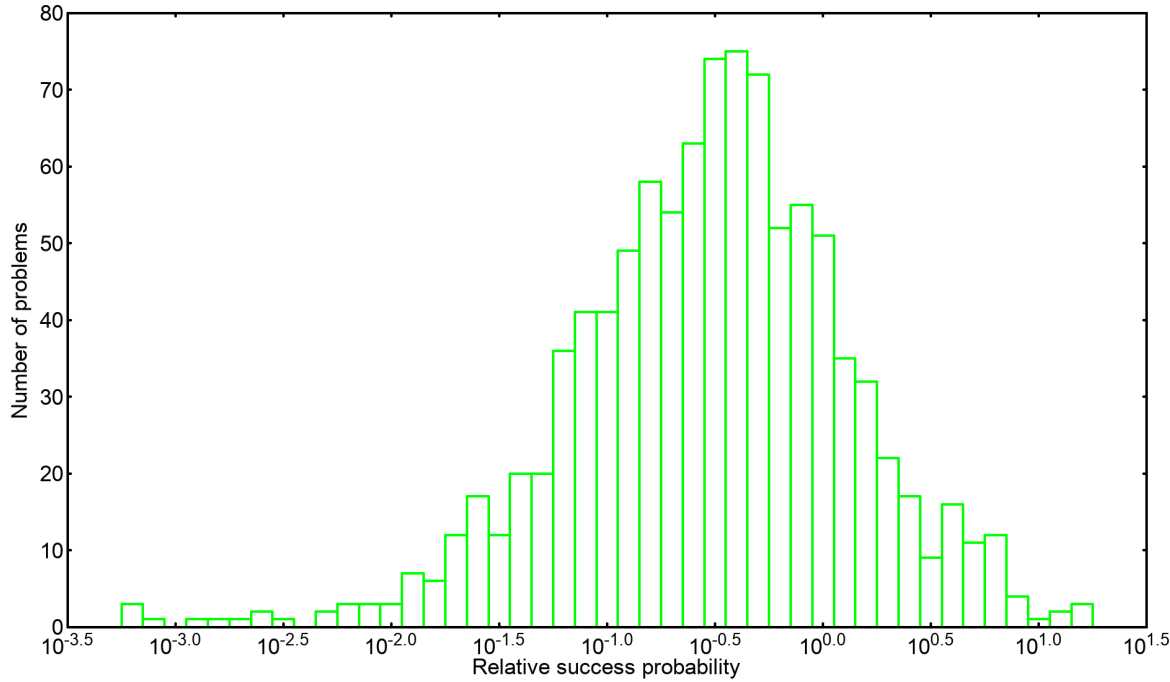


Figure 5.18: The distribution of relative success probability $\frac{p^A}{p^O}$ for $T_A=100$. 21.5% of the cases were found to have a higher success probability after adding the trigger.

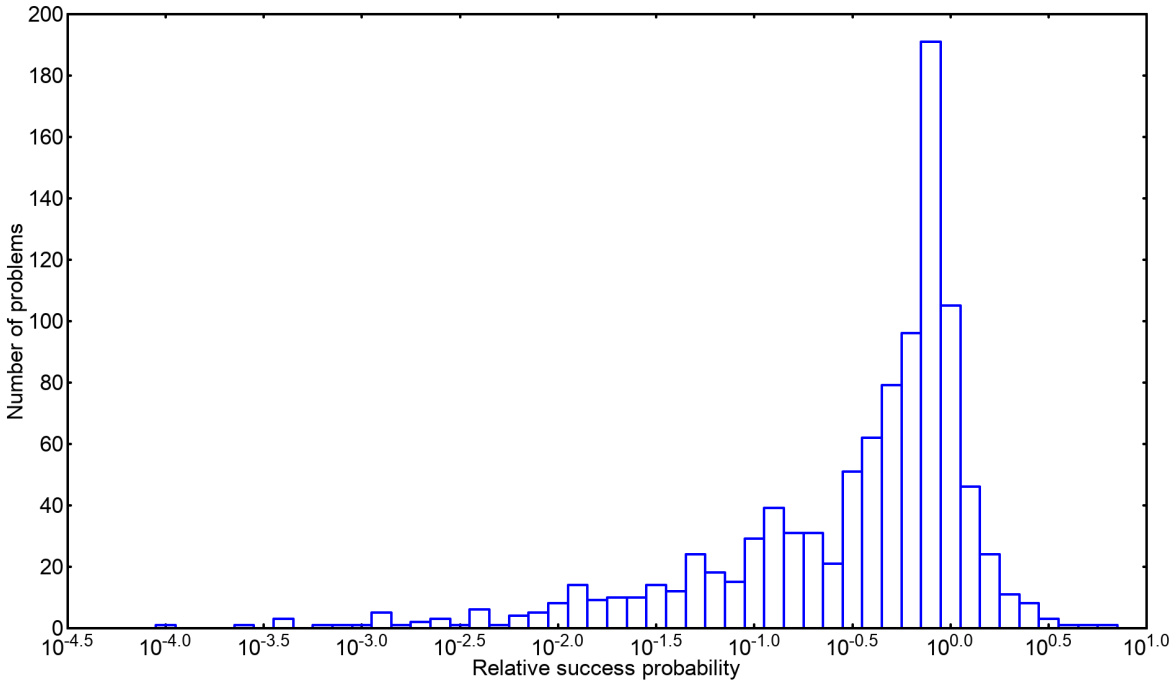


Figure 5.19: The distribution of relative success probability $\frac{p^A}{p^O}$ for $T_A=1000$. 20% of the cases were found to have a higher success probability after adding the trigger.

37.7% of the cases had an improved success probability after adding the anti-ferromagnetic trigger for $T_A=10$. This percentage reduced to 21.5% and 20% respectively upon increasing the annealing time to 100 and 1000 respectively. Moreover, as the annealing time was increased, the largest value of the relative success probability

dropped from 501 at $T_A=10$, to 15.85 at $T_A=100$, to 6.31 at $T_A=1000$. Again, for obtaining more insights about the effects of adding the anti-ferromagnetic trigger with $g=1$, the minimum energy gaps were computed for all the problems of the set after adding the trigger. Figure (5.20) shows the resulting scatter plot between the original minimum energy gaps and the gaps after adding the trigger.

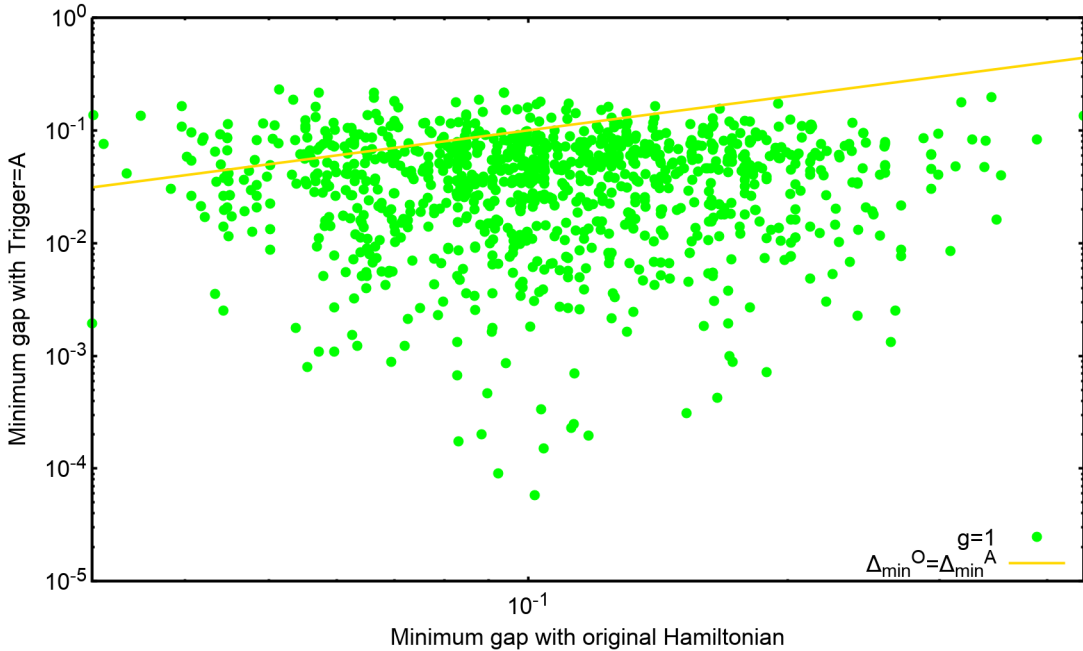


Figure 5.20: A plot of the minimum energy gaps after adding the anti-ferromagnetic trigger with $g=1$ (Δ_{min}^A), with the original minimum energy gaps (Δ_{min}^O). For 87.9% of the minimum energy gap was found to have decreased after adding the trigger.

In this case 87.9% of the cases were found to have smaller minimum energy gaps upon the addition of the trigger. Thus, a decrease in the success probability for most of the cases compared to the original seems to be plausible.

Furthermore, for most of the cases the number of energy anti-crossings between the ground state and the first excited state increased to 2, while in one case it was noted to be 4. Table (5.4) shows the percentage of cases for different number of anti-crossings.

Number of anti-crossings	Number of cases (%)
1	20.2
2	70.5
3	9.2
4	0.1

Table 5.4: Number of cases with different number of anti-crossings after adding the anti-ferromagnetic trigger.

For obtaining an estimate for the difficulty of the problems which have a relative success ratio greater than one, a scatter plot of the original success probability and that after adding the anti-ferromagnetic trigger has been shown in figure (5.21).

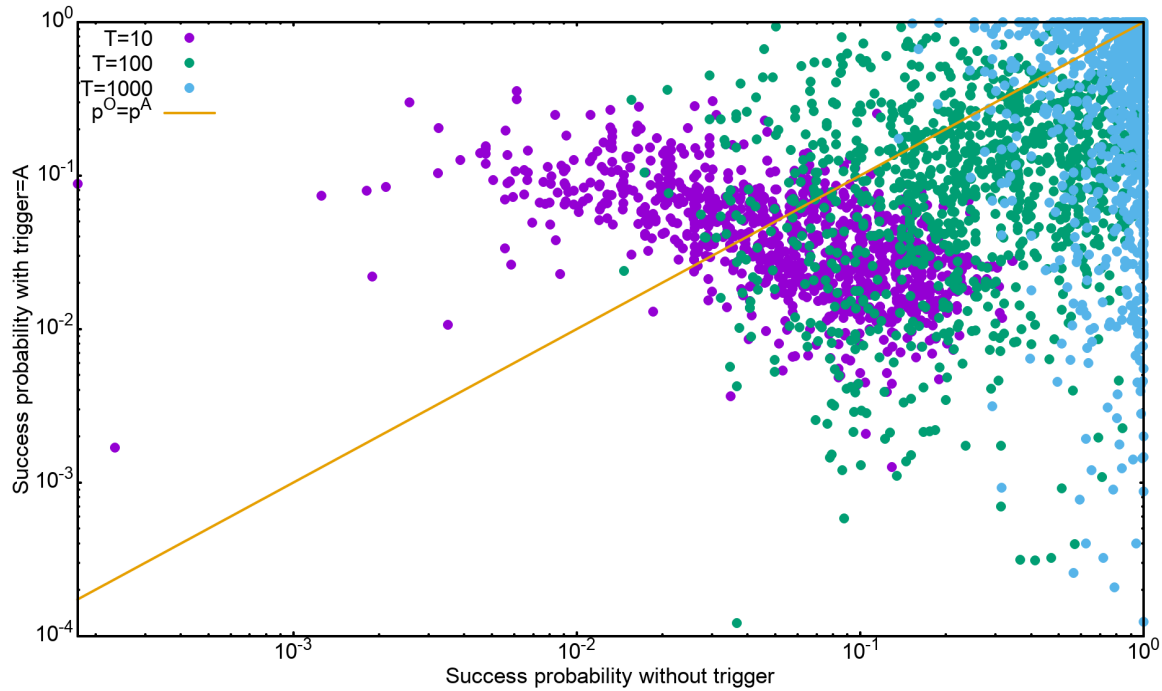


Figure 5.21: A plot of the success probabilities after adding the anti-ferromagnetic trigger with $g=1$ (p^A), with the original success probabilities(p^O) for annealing time 10, 100 and 1000.

Again, it can be noted that for $T_A=10$, the 37.7% of the problems that have a higher success probability after adding the anti-ferromagnetic trigger are limited to the cases with smaller original success probability (smaller gaps). Since adding the trigger reduces the minimum energy gap in most of the cases, the cases with smaller p^O benefit from a non-adiabatic evolution (shorter annealing time).

For understanding the role that the annealing time plays in improving the success probability, scatter plots of original and modified minimum gaps (upon adding the trigger) were plotted for the cases with relative success probability higher than 1, for the three annealing times. These plots have been shown in figure . (5.22), (5.25) and (5.26).

In the 37.7% of the cases with higher success probability after adding the trigger for $T_A=10$, 27.9% of the cases were found to have smaller minimum gaps as a result of adding the trigger. These cases can therefore be expected to have a non-adiabatic evolution at $T_A=10$, explaining the observed trend. On the other hand, for the rest 9.8% of the cases the minimum gaps were increased. It was noted that except for 2 cases with larger minimum gaps that were improved for $T_A=10$, were also improved for $T_A=100$ and $T_A=1000$. This suggests that for these cases adding the anti-ferromagnetic trigger increased the minimum energy gap, making the evolution more adiabatic even for $T_A=10$.

Additionally, for the two cases with enlarged minimum gap and higher success probability for $T_A=10$ but not for $T_A=100$, the energy spectra and instantaneous energies were studied. Same mechanics were found to be governing the trend, therefore the energy spectra for one of the problems is shown here. Figures (5.23) and (5.24) show the energy spectrum and the instantaneous energies before and after adding the trigger.

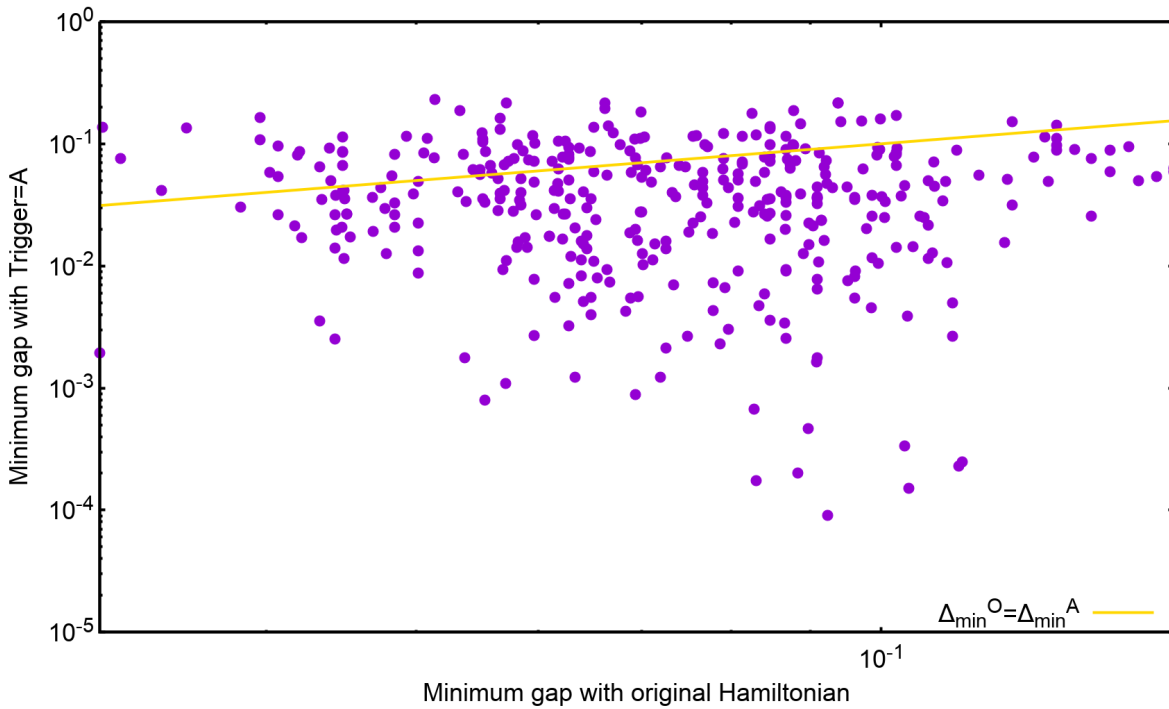


Figure 5.22: For the cases with higher success probability for $T_A=10$ after adding the anti-ferromagnetic trigger with $g=1$, the scatter plot of energy gaps Δ^A with Δ^O . 279 out of 377 of such cases were found to have smaller minimum energy gaps after adding the trigger.

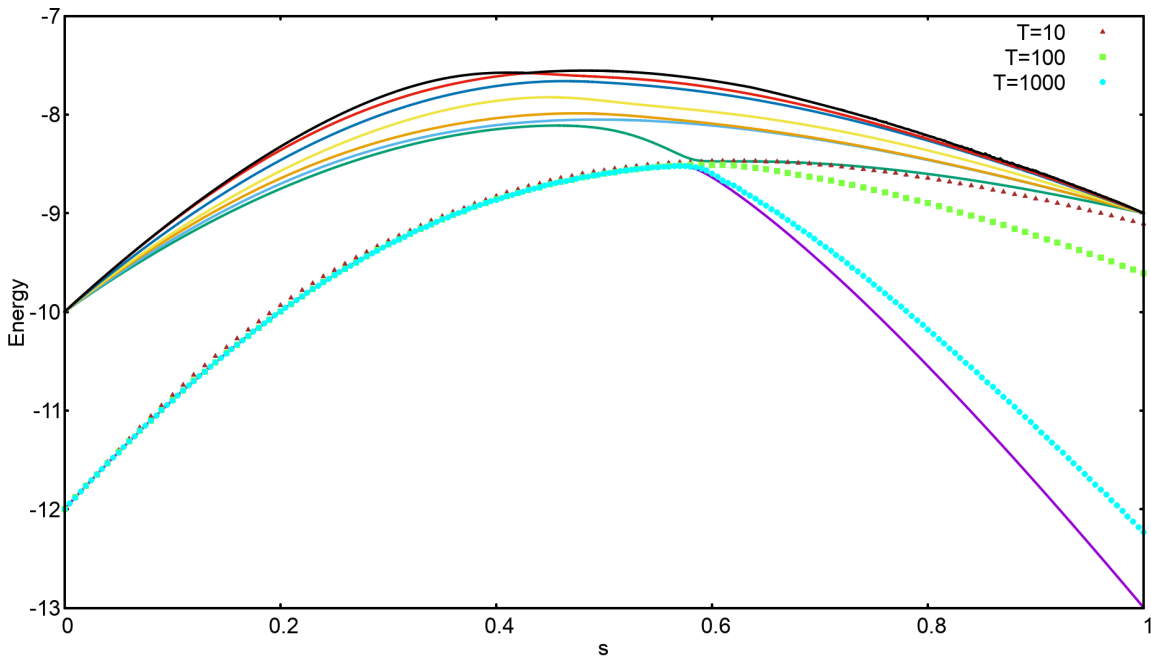


Figure 5.23: **Original** energy spectrum and instantaneous energy values for the problem with enlarged minimum energy gap, improved success probability for $T_A=10$ and $T_A=1000$, but decreased success probability for $T_A=100$, as a consequence of adding the anti-ferromagnetic trigger.

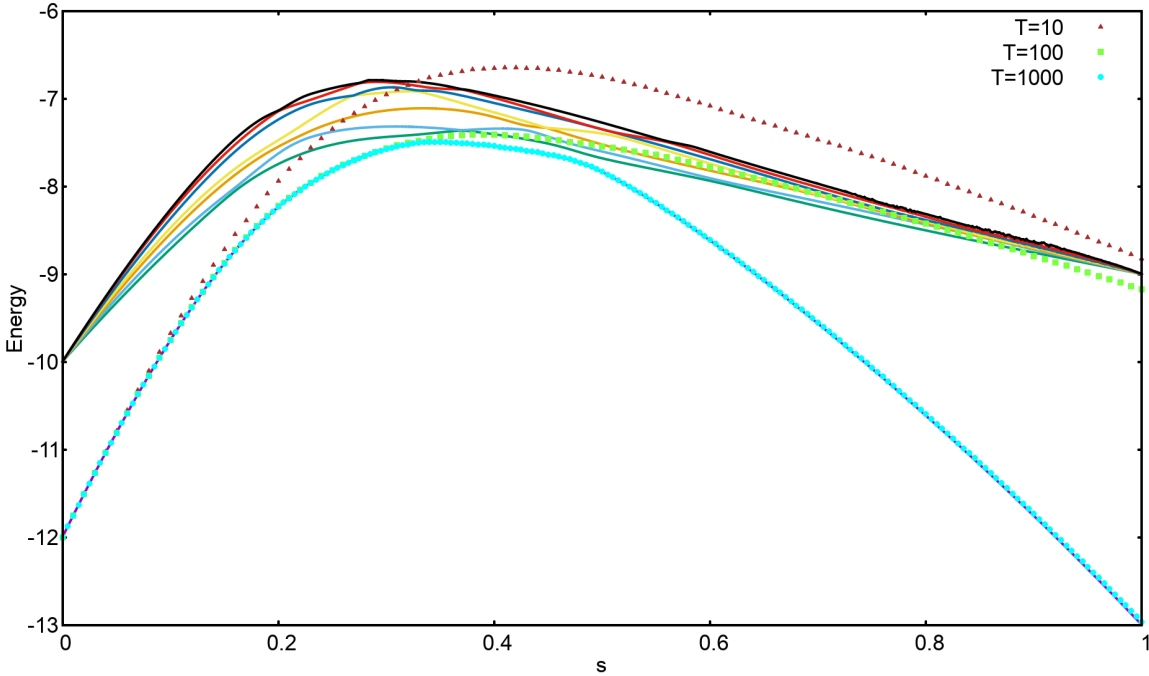


Figure 5.24: **Modified** energy spectrum and instantaneous energy values for the Hamiltonian after adding anti-ferromagnetic trigger to the problem with enlarged minimum energy gap, improved success probability for $T_A=10$ and $T_A=1000$, but decreased success probability for $T_A=100$, as a consequence of adding the anti-ferromagnetic trigger.

Although adding the trigger enlarges the minimum gap in these cases, the spectrum of the problem is changed in a way that the state has more chances of going to higher energy levels. For $T_A=10$ the system transitions to higher energy levels even before the first energy anti-crossing, and coincidentally ends in a state with larger overlap with the ground state than in the original case where it closely follows the first excited state after the anti-crossing. For $T_A=100$, and in the presence of the trigger, the state shifts to the higher excited state at the second energy anti-crossing, but this time the overlap of the final state with the ground state is smaller than that in the case of the original Hamiltonian. Finally, an annealing time of $T_A=1000$ becomes long enough for the evolution to become adiabatic, and since the minimum energy gap is increased after adding the trigger, the success probability in the presence of the trigger becomes larger.

Next, from figures (5.25) and (5.26) it can be noted that the majority of the problems improved by adding anti-ferromagnetic trigger, and choosing the annealing time to be $T_A=100$ or $T_A=1000$ correspond to the cases where the minimum energy gaps became larger upon adding the trigger. 117 of the 215 cases improved after adding the trigger for $T_A=100$, and 121 of the 200 cases for $T_A=1000$ had larger minimum gaps after including the trigger.

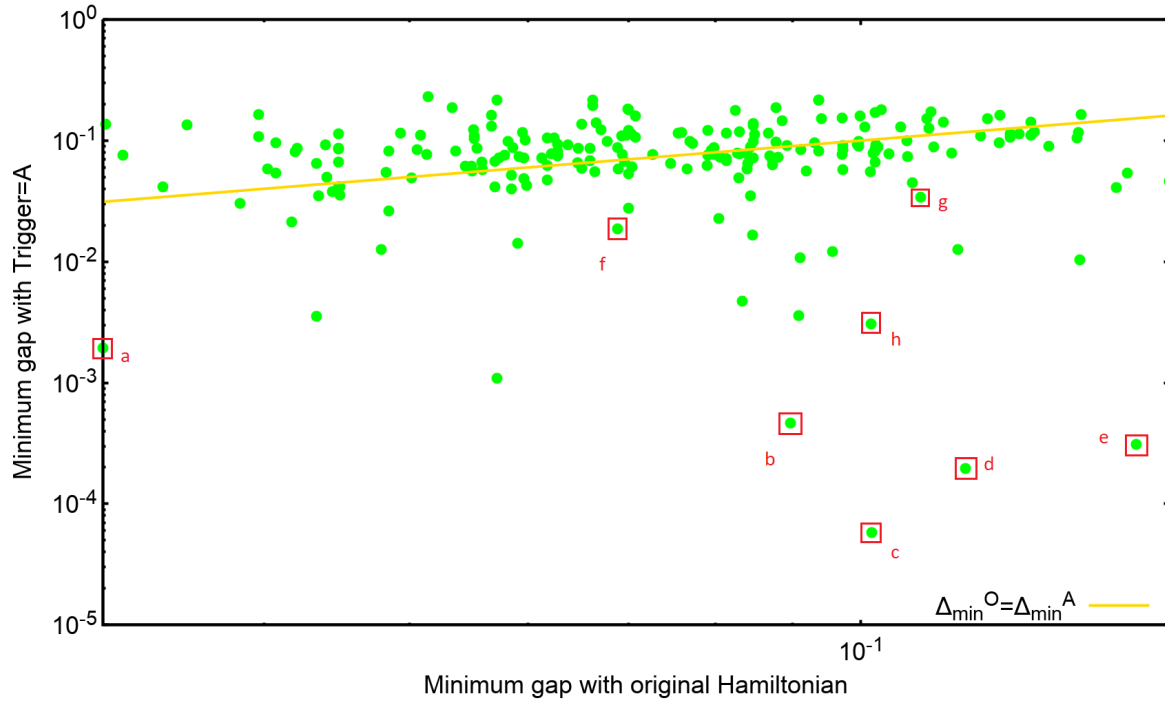


Figure 5.25: For the cases with higher success probability for $T_A=100$ after adding the anti-ferromagnetic trigger with $g=1$, the scatter plot of energy gaps Δ^A with Δ^O . 117 out of 215 of such cases were found to have larger minimum energy gaps after adding the trigger. Some of the other 98 cases studied have been marked in the figure (a-h).

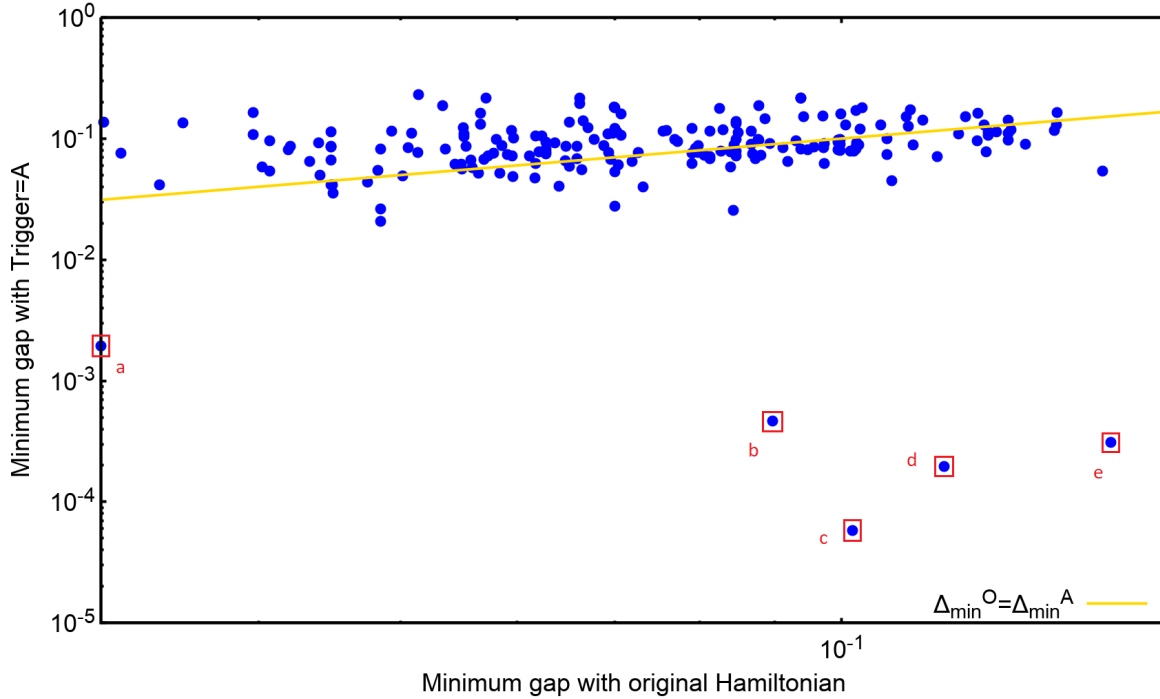


Figure 5.26: For the cases with higher success probability for $T_A=1000$ after adding the anti-ferromagnetic trigger with $g=1$, the scatter plot of energy gaps Δ^A with Δ^O . 121 out of 200 of such cases were found to have larger minimum energy gaps after adding the trigger. Some of the other 79 cases studied have been marked in the figure (a-e).

Some of the outliers from the above two plots were selected and their dynamics was studied. These have been marked in figures (5.25) and (5.26). Firstly, it should be noted that the cases (a)-(e) are the ones that appear in both the figures. Out of them, for cases (b), (c) and (d) there are exactly two anti-crossings where the energy gap is relatively small and comparable to each other. Figures (5.37) and (5.38) show the energy spectrum and the instantaneous energies for case (c), in the absence and presence of the trigger, respectively.

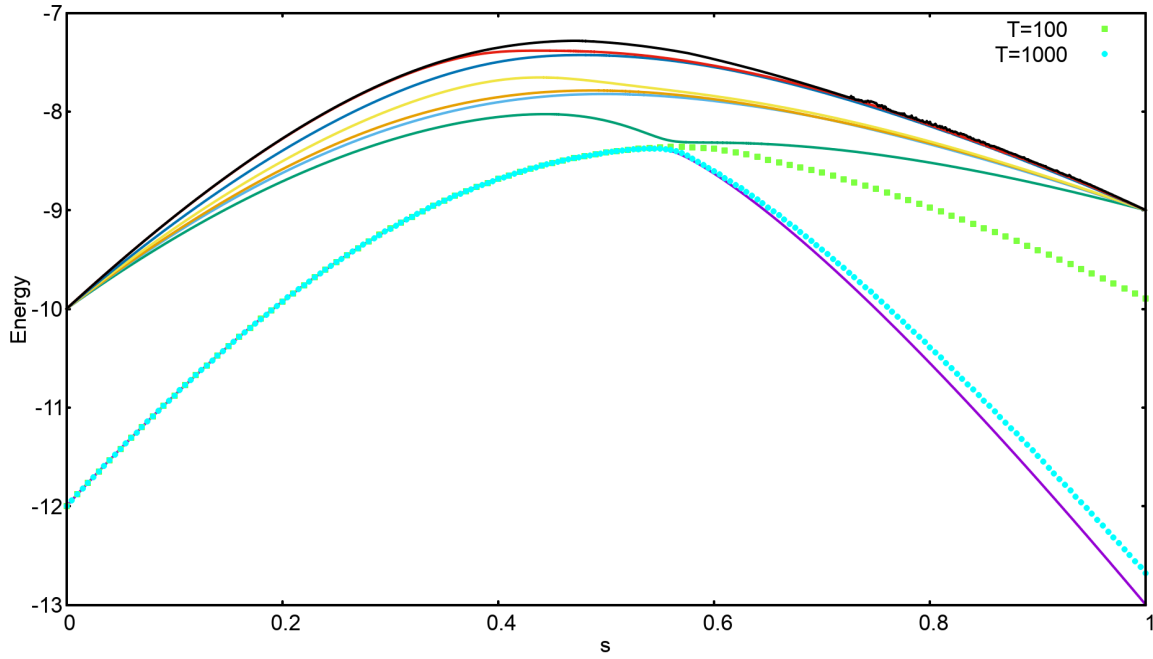


Figure 5.27: **Original** energy spectrum and instantaneous energy values for case (c) marked in figures (5.37) and (5.38).

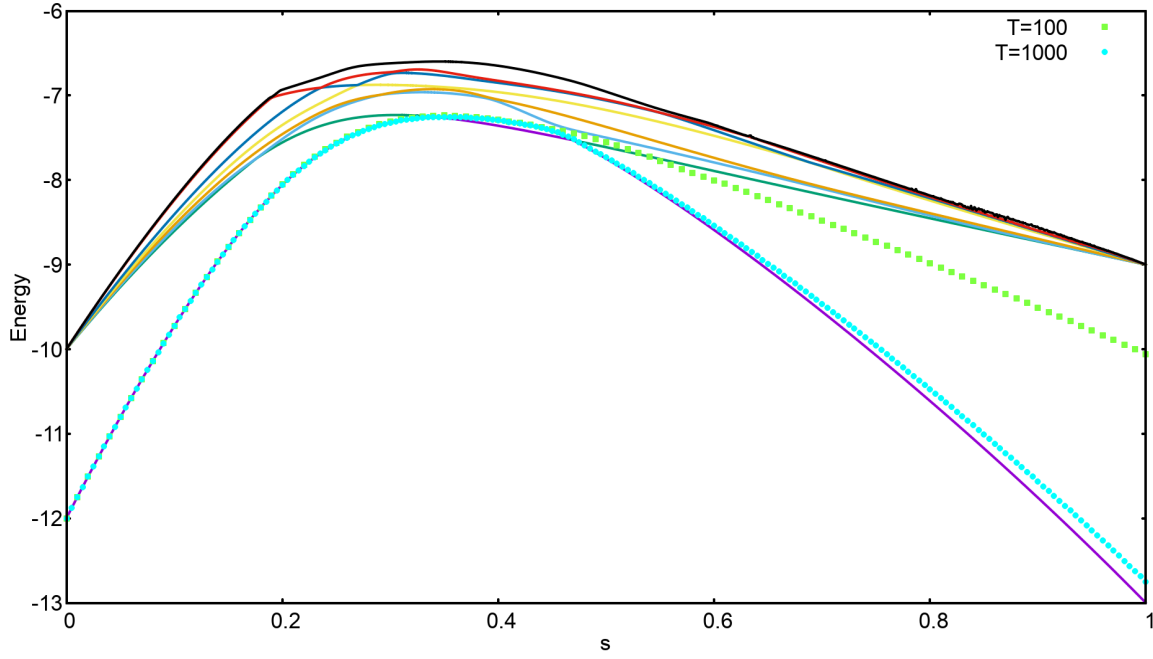


Figure 5.28: **Modified** energy spectrum and instantaneous energy values for case (c) marked in figures (5.37) and (5.38), after adding the anti-ferromagnetic trigger with $g=1$.

In this problem, the state of the system shifts to the first excited state at the first energy anti-crossing, but transits back to the ground state at the second one. Therefore, although the minimum energy gap has become smaller, the success probability after adding the trigger increases.

Moreover, for cases (a) and (e) similar kind of mechanism is at play for increasing the success probability after including the trigger, despite of a decrease in the minimum energy gap. Case (a) was found to be the same as

the second chosen problem in the first section of the chapter. It can be noted from table (5.2) that the minimum energy gap decreases by a factor of approximately 16 times upon adding the anti-ferromagnetic trigger with $g=1$. Figures (??) and (5.8) show the energy spectra for this case before and after adding the trigger. However, looking at the energy spectra alone does not make the cause of increase in the success probability apparent for this case. Therefore, the instantaneous overlaps of the system state with the three lowest lying energy states was computed at each time step. **Explain when both the files are ready.**

It was also noted that there were additional cases in the scatter plot for the minimum energy gap (Δ_{min}^A vs Δ_{min}^O) for $T_A=100$. Cases (f), (g) and (h), marked in figure (5.37) were additionally studied and were found to have similar dynamics. For cases (g) and (h) the number of anti-crossing was found to have increased to 2, where both the gaps were small enough for the state to transit at $T_A=100$, hence working in favour of the success probability.

For case (f), figures (5.29) and (5.30) show the plots for the energy spectrum and the instantaneous energy values before and after adding the trigger.

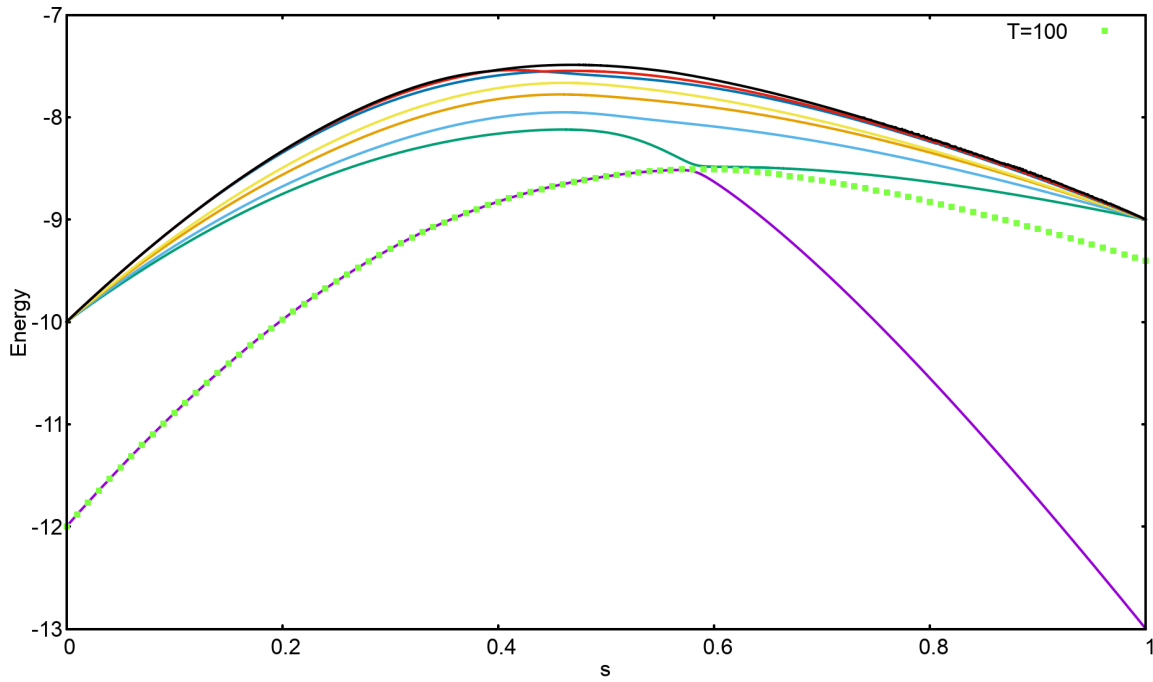


Figure 5.29: **Original** energy spectrum and instantaneous energy values for case (f) marked in figure (5.37).

In this case, adding the trigger increases the number of anti-crossings to 2, while also making the energy spectrum more involved. The energy levels come close enough for the state to shift to higher or lower levels at other points than just the anti-crossings. **(Check for the overlap. Most probably like 950.)**

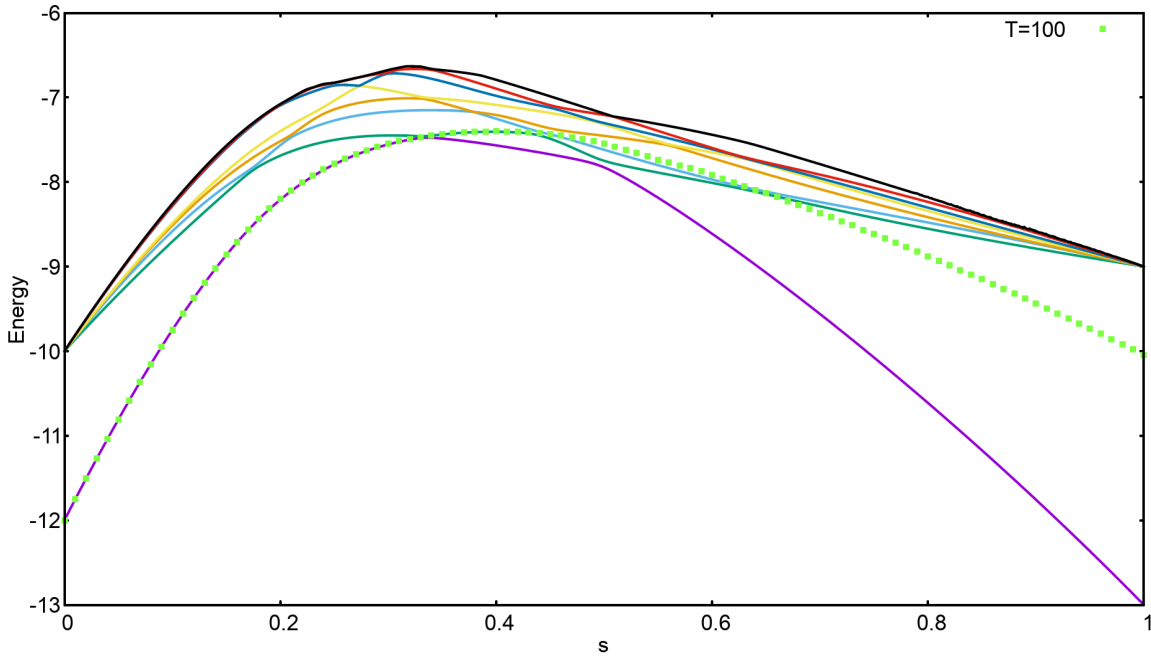


Figure 5.30: **Modified** energy spectrum and instantaneous energy values for case (f) marked in figure (5.37), after adding the anti-ferromagnetic trigger with $g=1$.

Again, for checking if the dynamics after adding the anti-ferromagnetic trigger with $g=1$ was adiabatic, the success probabilities for different problems were plotted against the corresponding minimum gaps. Figure (5.31) shows the resulting plot.

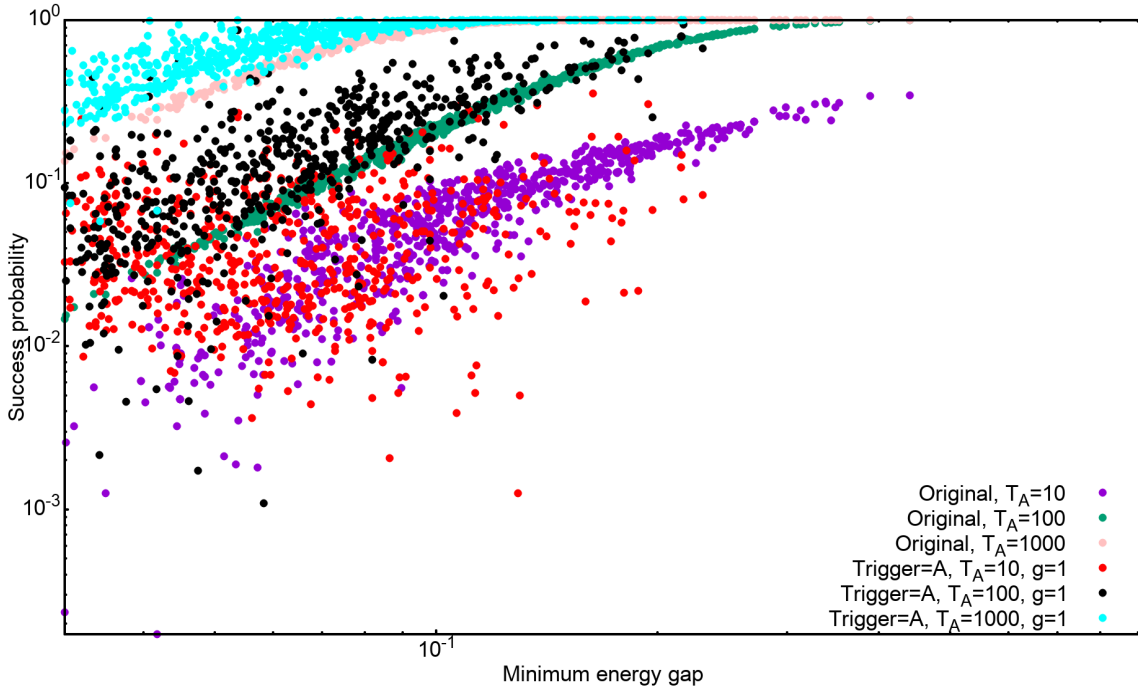


Figure 5.31: Success probability versus minimum energy plot for all the problems belonging to the set of 12-spin SAT problems, for annealing times 10, 100 and 1000, in the absence and presence of ferromagnetic trigger.

It can be noted that the scattering of the curves has increased substantially, although the form of the curves is defined better in this case compared to the last section (5.16). This suggests that the evolution becomes non-

adiabatic for more number of cases. This can be attributed to the increase in the number of anti-crossings between the ground state and the first excited state, as well as the reduced minimum energy gaps between these two levels.

g=2

Finally, in this section the effects of adding the anti-ferromagnetic with strength 2 will be discussed.

Figures (5.32) and (5.33) show the distribution of the relative success probability after adding the anti-ferromagnetic trigger for $T_A=10$ and $T_A=100$. In this case, only 1.5% were found to have an improved success probability after adding the trigger for $T_A=10$. Upon increasing the annealing time to 100, this percentage increases to 15.8%, and yet to 22.5% for $T_A=1000$. This is in contrast with the observations from the previous sections where the percentage of the cases with improved success probability is the maximum for $T_A=10$.

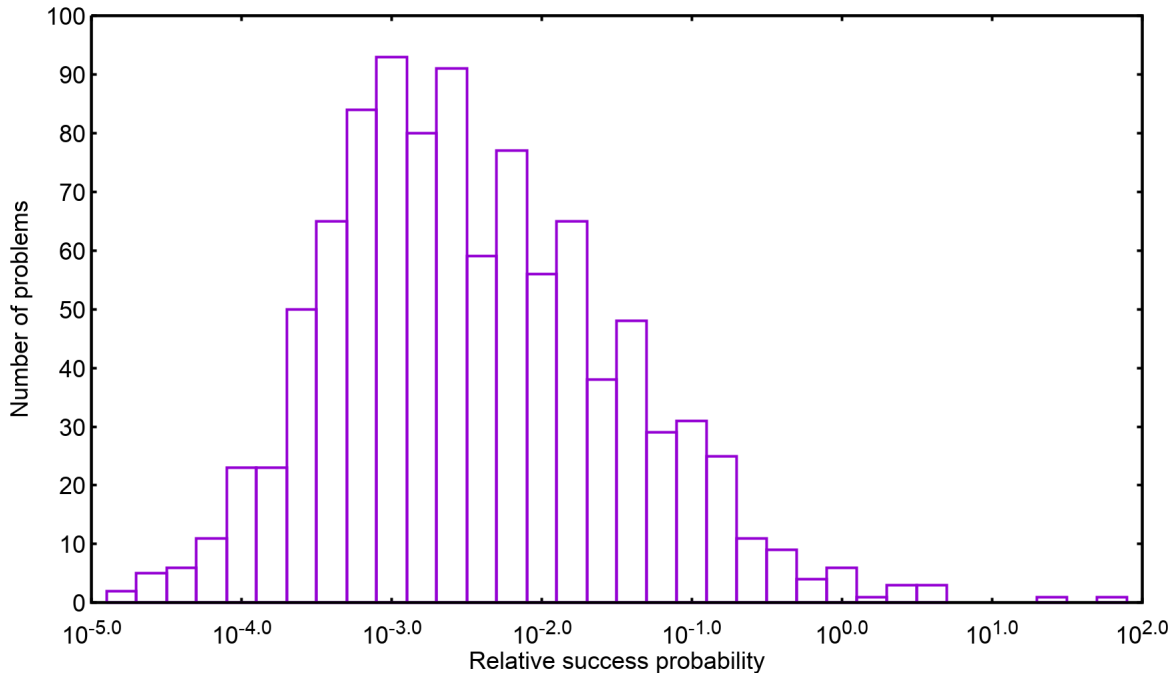


Figure 5.32: The distribution of relative success probability $\frac{p^A}{p^O}$ for $T_A=10$ and $g=2$. 1.5% of the cases were found to have a higher success probability after adding the trigger.

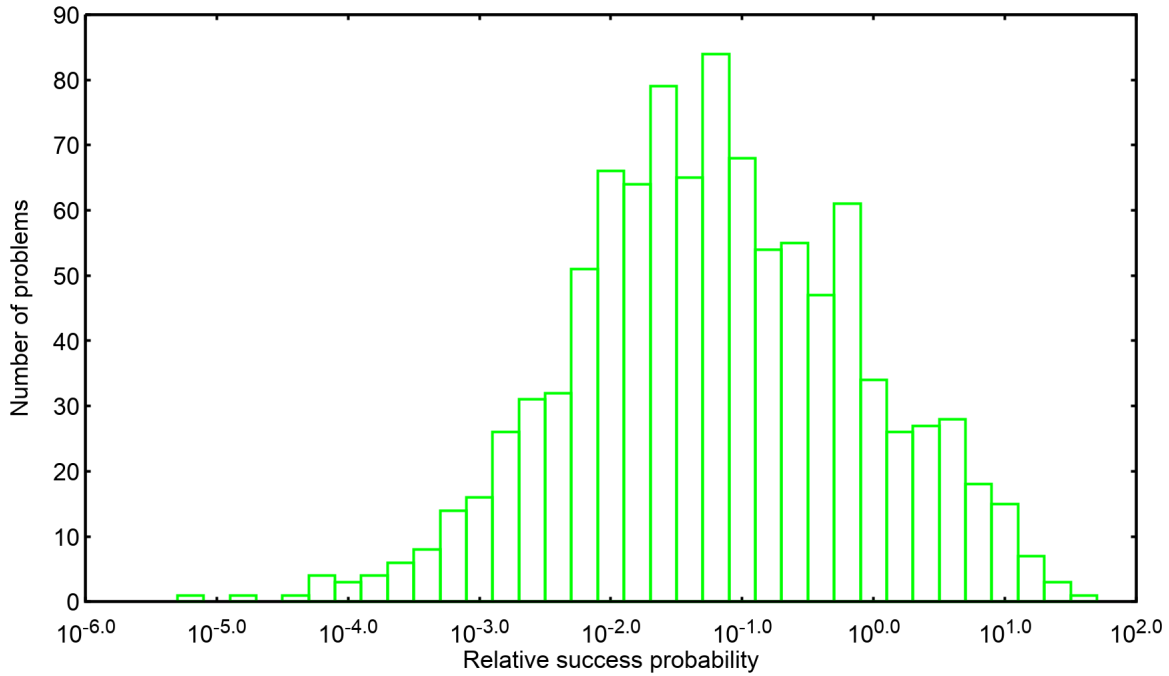


Figure 5.33: The distribution of relative success probability $\frac{p^A}{p^O}$ for $T_A=100$ and $g=2$. 15.8% of the cases were found to have a higher success probability after adding the trigger.

Furthermore, for $T_A=1000$ the spread of the relative success probability was only from 0.63 to 1.58, i.e. the effect of adding the trigger was only marginal. Additionally, for 44.8% of the cases the relative success probability was found to be 1.

Fig. (5.34) shows the scatter plot of the minimum energy gaps after adding the anti-ferromagnetic trigger (Δ^A) with the original minimum energy gap (Δ^O), for $g=2$. For this case it was observed that for 79.8% of the problems the minimum energy gaps were reduced, compared to the original minimum energy gaps, after adding the trigger. It was also noticed that with the anti-ferromagnetic trigger of strength 2 the energy spectrum significantly in terms of the number of anti-crossings between the ground and the first energy level, and the proximity of the higher energy levels. As an estimate of the same, table (5.5) shows the percentage of cases with different number of anti-crossings.

Number of anti-crossings	Number of cases (%)
1	0.1
2	13.2
3	43.9
4	36.3
5	6.5

Table 5.5: Number of cases with different number of anti-crossings after adding the anti-ferromagnetic trigger with $g=2$.

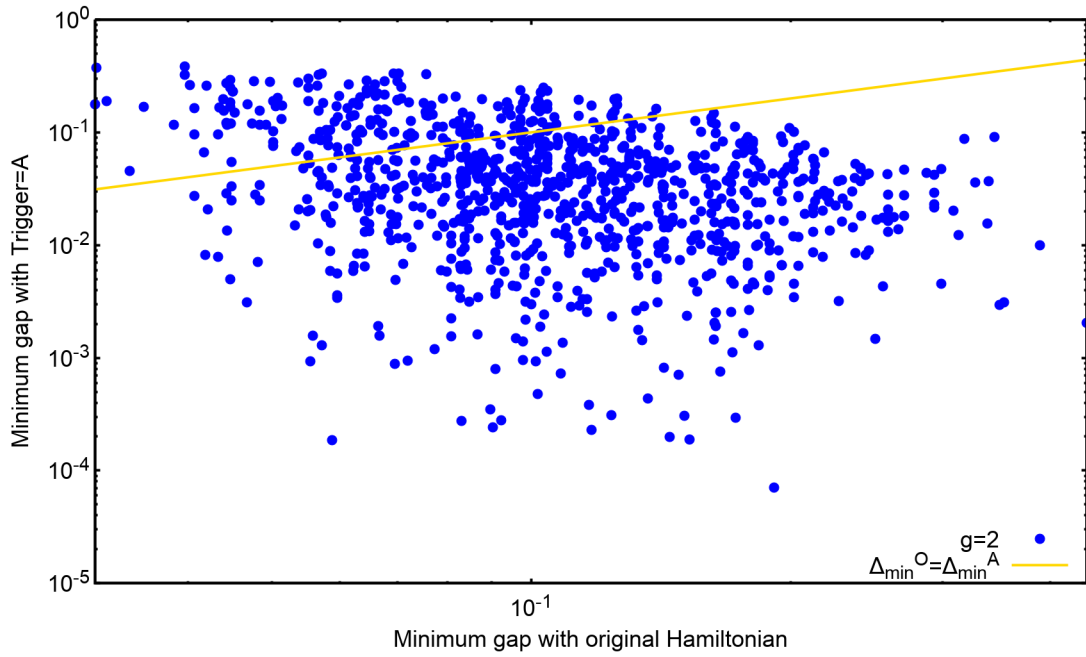


Figure 5.34: A plot of the minimum energy gaps after adding the anti-ferromagnetic trigger with $g=1$ (Δ_{\min}^A), with the original minimum energy gaps (Δ_{\min}^O). For 79.8% of the minimum energy gap was found to have decreased after adding the trigger.

Next, to obtain the range of the problems affected by the adding the trigger for different annealing times, fig. (5.35) shows the scatter plot of the success probability upon including the anti-ferromagnetic trigger (p^A) with that of the original Hamiltonian (p^O).

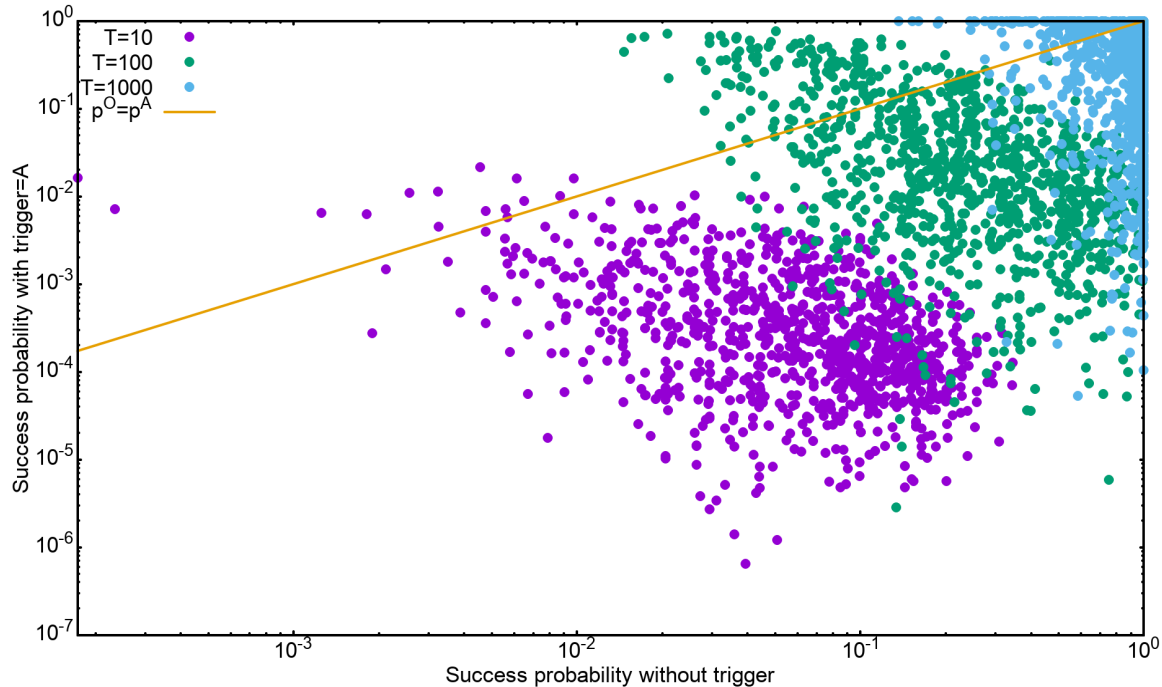


Figure 5.35: A plot of the success probabilities after adding the anti-ferromagnetic trigger with $g=2$ (p^A), with the original success probabilities(p^O) for annealing time 10, 100 and 1000.

In this case too, the spread of the problems improved by adding the trigger was the largest for annealing time of

10. This can be attributed to the small original success probability (p^o) for a small annealing time of $T_A=10$, and the non-adiabatic evolution of the state as the minimum energy gap reduces upon adding the anti-ferromagnetic trigger. Here, having the smaller original success probability was found to be the main reason for large improvements (maximum relative success ratio being 93.91). For $T_A=100$ and $T_A=1000$ the improvements become successively limited, with maximum relative success probabilities of 41.36 and 7.34 respectively. This is a consequence of increasing original success probabilities for longer annealing times. For understanding the mechanisms involved in the evolution of the state after adding the trigger, the scatter plots of the minimum energy gaps after adding the trigger (Δ^A) with the original minimum energy gaps (Δ^O) have been shown for the cases with improved success probability in figs. (5.36), (5.39), and (5.40) for annealing times of 10, 100 and 1000 respectively.

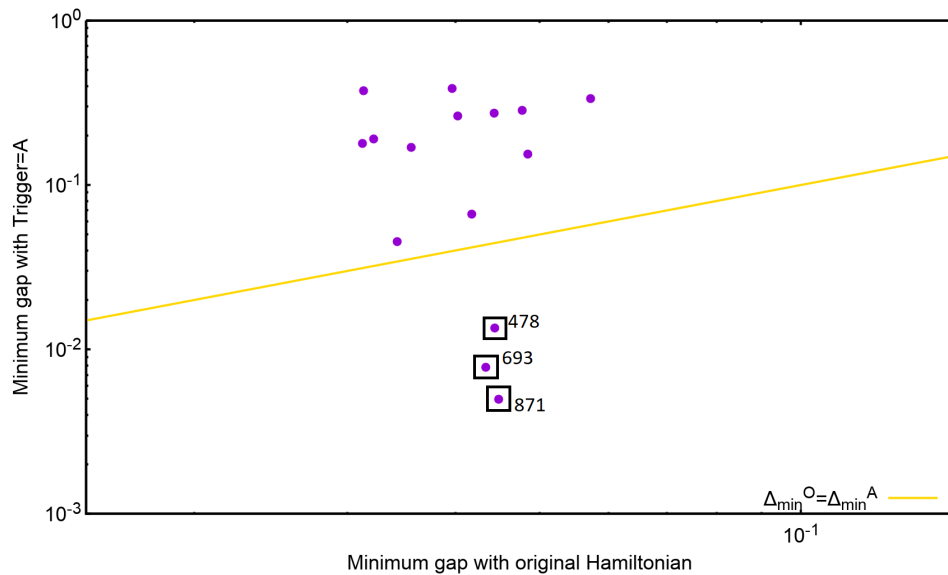


Figure 5.36: For the cases with higher success probability for $T_A=10$ after adding the anti-ferromagnetic trigger with $g=2$, the scatter plot of minimum energy gaps Δ^A with Δ^O . 3 out of 15 of such cases were found to have smaller minimum energy gaps after adding the trigger.

From figure (5.36) it can be noted that 12 out of the 15 problems with improved success probability have larger minimum energy gaps upon including the anti-ferromagnetic trigger. Furthermore, all of these problems had a larger relative success probability for longer annealing times of 100 and 1000 as well. This suggests that adding the trigger widened the minimum energy gap enough for the evolution to become more adiabatic for $T_A=10$.

However, unlike the case in the previous sections, only 3 problems had a smaller minimum energy gap after adding the anti-ferromagnetic trigger and a larger success probability. All these problems were benefited from the similar non-adiabatic evolution of the state. The energy spectrum and the instantaneous energy expectation values of the state for the original Hamiltonian and the Hamiltonian after adding the trigger have been shown in fig. (5.41) and (??) for problem 693. For the original Hamiltonian, the state of the system shifts to the first excited state on approaching the energy anti-crossing, and closely follows the first excited state thereafter. This makes the overlap of the system state with the ground state negligible. However, in the case where the anti-ferromagnetic trigger is included, the minimum energy gap reduces, making it feasible for the state to transit to the higher excited levels. Consequently, the state ends in a superposition state consisting of higher energy levels, which coincidentally has a larger overlap with the ground state of the Hamiltonian.

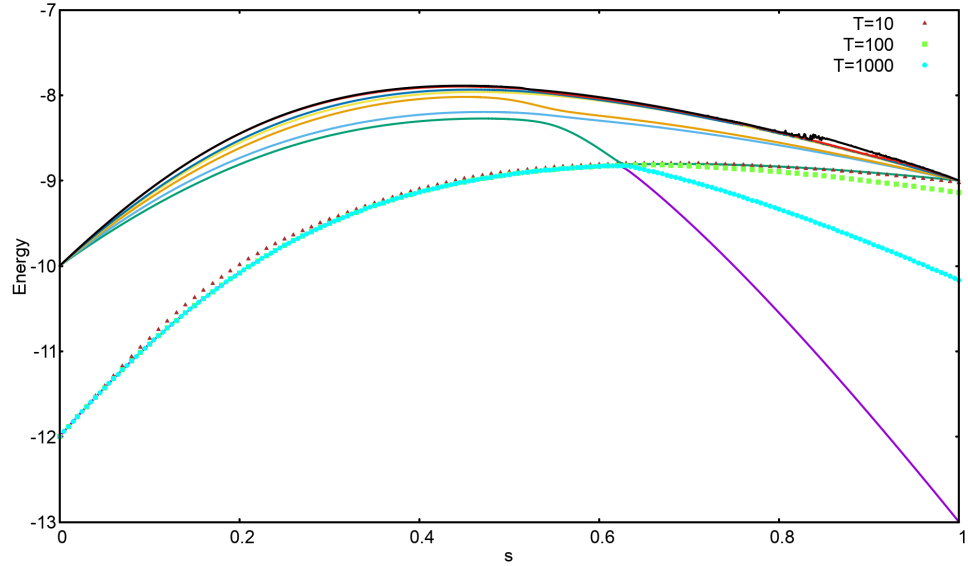


Figure 5.37: **Original** energy spectrum and instantaneous energy expectation values for problem 693 marked in fig. (5.36).

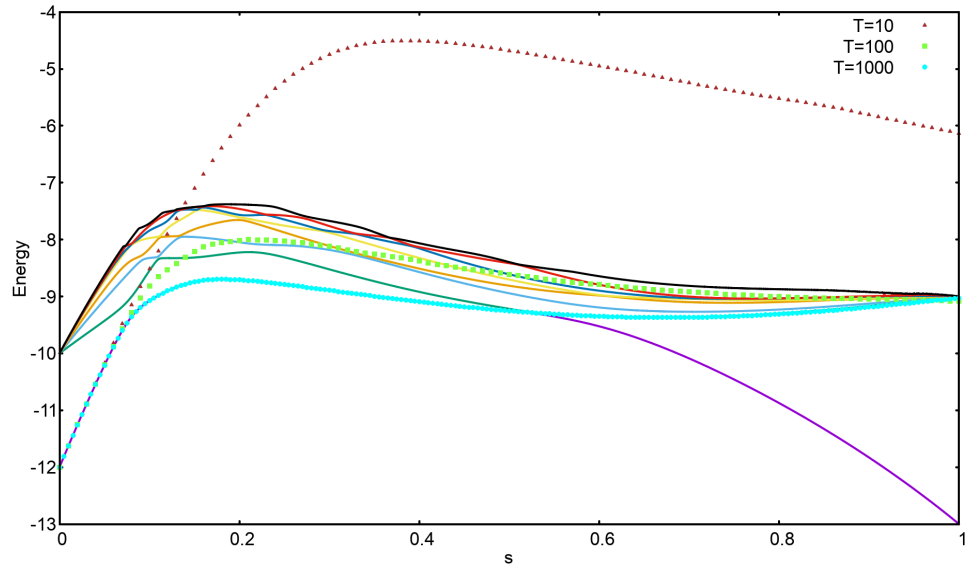


Figure 5.38: **Modified** energy spectrum and instantaneous energy expectation values for problem 693 marked in fig. (5.36), after adding the anti-ferromagnetic trigger with $g=2$.

In this problem, the success probability reduces after adding the trigger for both $T_A=100$ and $T_A=1000$. For the spectrum with the trigger and $T_A=100$, the system state shifts to the first excited state at the first anti-crossing, from where it soon shifts to the higher excited states. Unlike the case for $T_A=10$, this time the state follows them closely, resulting in a vanishing overlap with the ground state. For $T_A=1000$, on the other hand, the state shifts to the first excited state only on reaching the second anti-crossing. Since the original minimum gap is larger for this problem, the original success probability is larger for this annealing time.

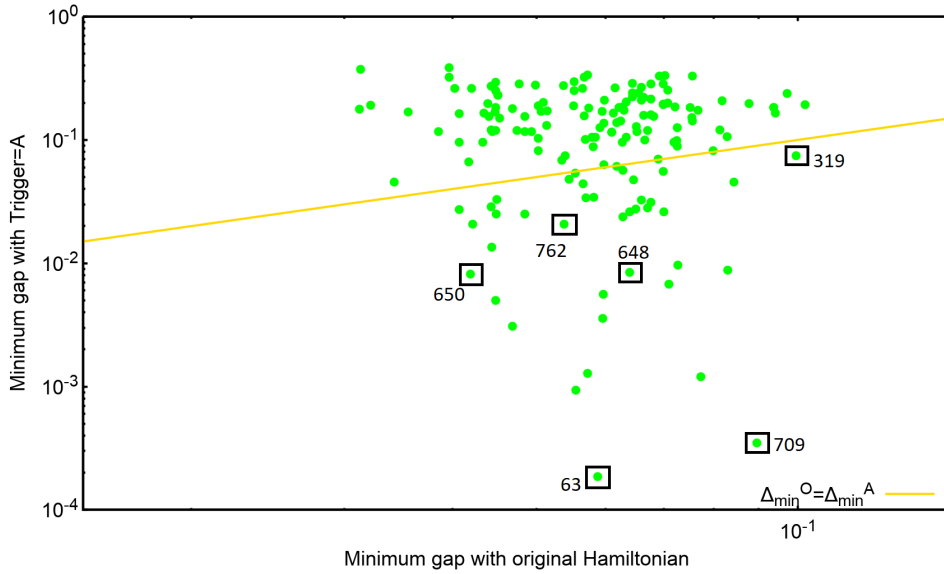


Figure 5.39: For the cases with higher success probability for $T_A=100$ after adding the anti-ferromagnetic trigger with $g=2$, the scatter plot of energy gaps Δ^A with Δ^O . 118 out of 158 of such cases were found to have larger minimum energy gaps after adding the trigger.

118 cases out of 158 cases found to have an improved success probability after adding the trigger, for $T_A=100$, also had a larger minimum energy gap as a result of adding the trigger. It was also noted that all of these cases also had a relative success probability greater than 1 for $T_A=1000$. The energy spectra for 6 of the remaining 40 cases were studied to understand the evolution of the state, leading to an improve success probability. Same mechanics was found to be governing the dynamics of the state.

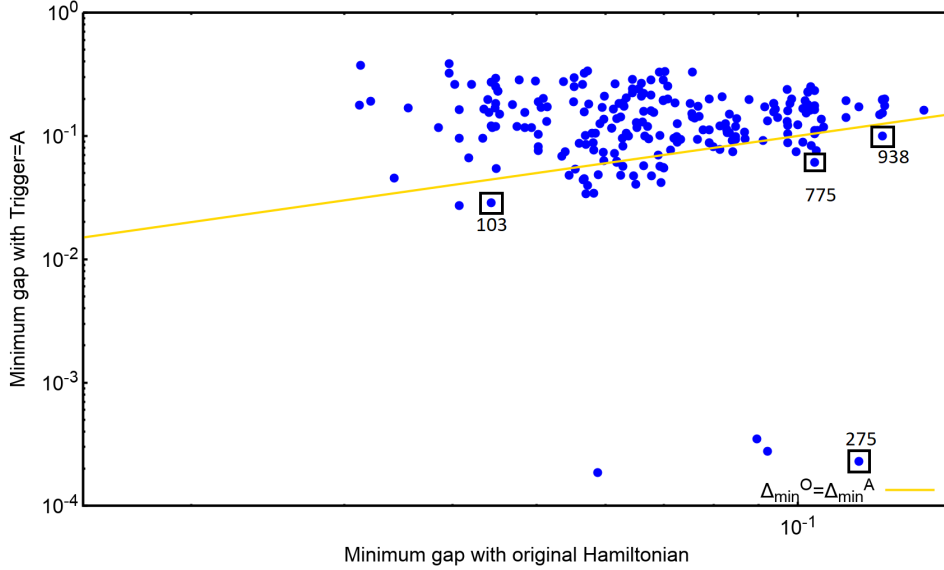


Figure 5.40: For the cases with higher success probability for $T_A=1000$ after adding the anti-ferromagnetic trigger with $g=2$, the scatter plot of energy gaps Δ^A with Δ^O . 189 out of 225 of such cases were found to have larger minimum energy gaps after adding the trigger.

For $T_A=1000$, 189 out of 225 cases where the success probability after adding the trigger was noted to be larger than the original success probability were found to have a larger minimum energy gap after adding the trigger. The energy spectra for 4 of the rest 36 cases were also studied. Furthermore, 13 of these cases were also found to have larger success probability for $T_A=100$.

Finally, fig. (5.41) shows the success probability versus minimum energy gap for all the problems of the set, for the original Hamiltonian, and the Hamiltonian after adding the trigger.

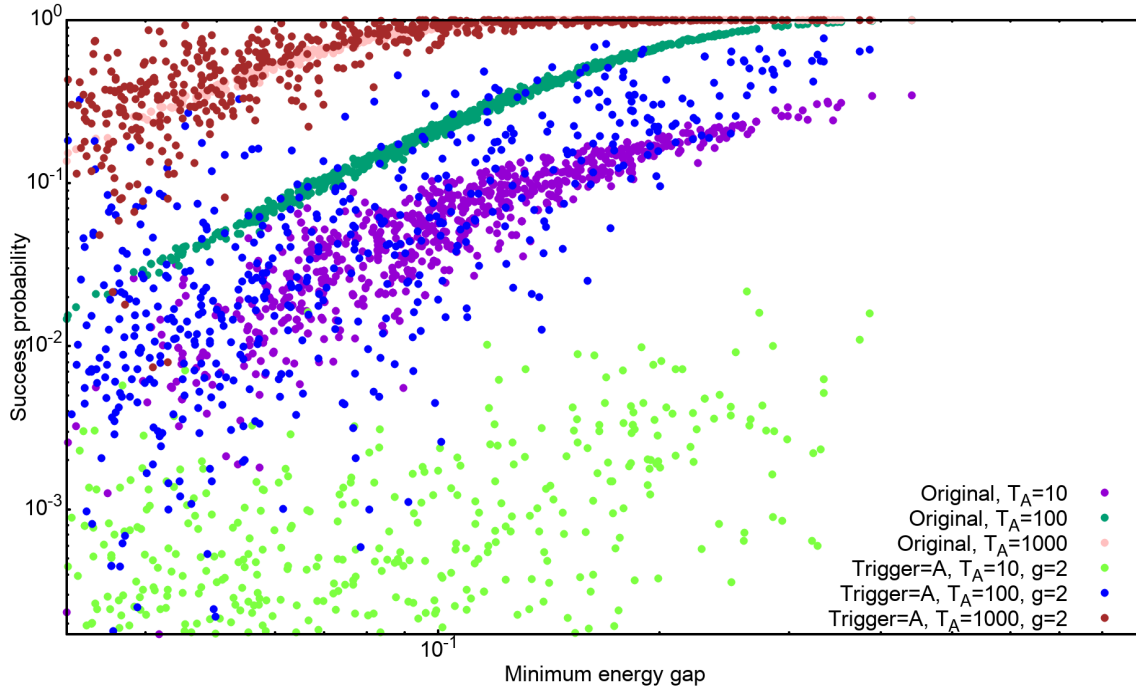


Figure 5.41: Success probability versus minimum energy plot for all the problems belonging to the set of 12-spin SAT problems, for annealing times 10, 100 and 1000, in the absence and presence of ferromagnetic trigger.

In this case, the scattering was found to have increased even more as compared to the case with $g=1$. This indicates that more problems deviated from the Landau-Zener formula in this case, suggesting a non-adiabatic evolution of the state in more number of problems.